

Computational and Analytical Methods for the Simulation of Electronic States and Transport in Semiconductor Systems

Junior Augustus Barrett

A Thesis submitted for the Degree of Doctor of Philosophy

Department of Computing and Technology

Anglia Ruskin University

May, 2014

Contents

| | |
|--|-------------|
| List of Symbols | v |
| List of Figures | viii |
| List of Tables | xiii |
| 1 Introduction | 1 |
| 1.1 Background | 1 |
| 1.2 Research Aims and Objectives | 3 |
| 1.3 Methodology | 5 |
| 1.4 Original Contribution to Knowledge | 7 |
| 1.5 Outline of the Thesis | 8 |
| 2 Background Review | 11 |
| 2.1 Introduction to Electronic Devices | 11 |
| 2.1.1 The MOSFET | 13 |
| 2.2 Review of Literature - solutions of nonlinear differential equations | 15 |
| 2.2.1 Example 1 - the Sine-Gordon equation | 16 |

| | | |
|----------|--|-----------|
| 2.2.2 | Example 2 - the scalar reaction-diffusion equation . . . | 18 |
| 2.2.3 | Example 3 - the Helmholtz equation | 20 |
| 2.2.4 | Example 4 - Laplace's and Poisson's equations in two and three dimensions | 21 |
| 3 | Overview of Modelling Electron Transport in Semiconductor | |
| | Devices | 25 |
| 3.1 | Review of existing relevant methods to solve coupled PDEs . . | 26 |
| 3.2 | Reviews of four key references | 35 |
| 3.2.1 | Review of Trellakis' computational issues in the simu- lation of semiconductor quantum wires [91] | 36 |
| 3.2.2 | Review of the accelerated algorithm for 2D simulations of the quantum ballistic transport in nanoscale MOS- FETs [6] | 40 |
| 3.2.3 | Review of efficient solution of the Schroedinger-Poisson equations in layered semiconductor devices [12] | 44 |
| 3.2.4 | Review of the fast convergent Schroedinger-Poisson solver for the static and dynamic analysis of carbon nanotube field effect transistors by Pourfath et al [74] | 49 |
| 3.3 | Summary | 51 |
| 4 | Semi-Analytical Solutions of Poisson's Equation | 53 |
| 4.1 | Semi-analytical solution to 3D Poisson's model | 56 |
| 4.2 | Semi-analytical solution to 2D Poisson's model | 60 |
| 4.3 | Semi-analytical solution to 1D Poisson's model | 61 |
| 4.4 | Application to 2D Poisson equation | 62 |

| | | |
|----------|---|-----------|
| 4.5 | Application to 3D Schroedinger-Poisson equations for device modelling | 64 |
| 5 | Semi-Analytical Solutions of Schroedinger's Equation | 69 |
| 5.1 | Example: Calculating the eigenvalues and eigenfunctions of Klein-Gordon equation in one dimension | 71 |
| 5.2 | Two-dimensional Schroedinger's equation | 73 |
| 5.3 | Three-dimensional Schroedinger's equation | 87 |
| 6 | Proposed semi-analytical method for the coupled Schroedinger and Poisson's equations | 90 |
| 6.1 | Convergence of the coupled solutions of Schroedinger-Poisson's equations using the semi-analytical method | 93 |
| 7 | Simulation results and validation of the method | 98 |
| 7.1 | Device 1: A GaAs - GaAlAs device | 100 |
| 7.2 | Device 2: A Si- SiO_2 based quantum device with a T-shaped gate | 105 |
| 7.2.1 | Eigenvalues for simulated structure | 107 |
| 7.3 | Device 3: A double well quantum device | 115 |
| 7.4 | Device 4: Analysis of the double gate 10 nm by 10 nm MOSFET | 121 |
| 7.5 | Device 5: A single walled carbon nanotube device | 129 |
| 7.6 | Validation of the semi-analytical method and comparison with experimental data | 132 |
| 7.7 | Discussion of simulation time performance | 134 |
| 7.8 | Summary | 135 |

| | | |
|----------|---|------------|
| 8 | Conclusions and Further Work | 143 |
| 8.1 | Conclusions | 143 |
| 8.2 | Further Work | 146 |
| | References | 149 |
| | Appendix A Energy band diagram - MOS diode | 162 |
| | Appendix B MOSFET characteristics | 167 |
| B.1 | Operating regions of the n-channel MOSFET | 167 |
| B.2 | Saturation region | 168 |
| | Appendix C The Wronskian | 171 |
| C.1 | Definition of the Wronskian | 173 |
| | Appendix D The Evans Function | 174 |
| D.1 | Definition of Evans function in one-dimension | 176 |
| | Appendix E Derivation of 3D Eigenfunctions | 178 |
| | Appendix F Matlab Code | 182 |

List of Symbols

| | | |
|----------------|---|-----|
| u_t | First derivative of the function u with respect to the variable t | 18 |
| u_{xx} | Second derivative of the function u with respect to the variable x | 18 |
| h_x | First derivative of the function h with respect to the variable x | 19 |
| h_{xx} | Second derivative of the function h with respect to the variable x | 19 |
| h_m | First derivative of the function h with respect to the variable m | 77 |
| h_{mm} | Second derivative of the function h with respect to the variable m | 77 |
| h_ρ | First derivative of the function h with respect to the variable ρ | 81 |
| $h_{\rho\rho}$ | Second derivative of the function h with respect to the variable ρ | 81 |
| λ | Represents an eigenvalue, sometimes given as E (energy). | 17 |
| ψ | The wave function. | 65 |
| m^* | The tensor describing the effective mass. | 23 |
| $m_x(z)$ | z-dependent effective mass. | 125 |
| m_t | The transverse effective mass. | 127 |
| m_ℓ | The longitudinal effective mass. | 127 |
| m_0 | The electron rest mass. | 101 |
| ϕ | The electrostatic potential. | 54 |
| $D(\lambda)$ | The Evans function with respect to the energy level λ | 19 |
| ∇ | Laplace's operator. | 20 |

| | | |
|-----------------|---|-----|
| L_x | The upper limit of the closed interval $[0, L_x]$ for which $x \in [0, L_x]$. Similarly for L_y and L_z | 20 |
| ϕ_{xx} | Second derivative of the function ϕ with respect to the variable x . | 54 |
| ϕ_{yy} | Second derivative of the function ϕ with respect to the variable y . | 54 |
| ϕ_{zz} | Second derivative of the function ϕ with respect to the variable z . | 54 |
| ψ_{xx} | Second derivative of the function ψ with respect to the variable x . | 76 |
| w_{xx} | Second derivative of the function w with respect to the variable x . | 55 |
| ∂_{xx} | Second order partial derivative with respect to x | 20 |
| $\wp_j(x)$ | Fermi-Dirac integral of order j | 56 |
| $V_s(\cdot, 1)$ | Gate voltage where \cdot represents a place holder in $V_s(\cdot, 1)$ | 74 |
| V | voltage | 74 |
| V_g | voltage applied to the gate electrode. | 168 |
| V_{th} | Threshold voltage. | 168 |
| V_h | The heterojunction step potential. | 23 |
| V_{xc} | The exchange correlation potential in the local density approximation. 23 | |
| V_{ds} | voltage applied to drain contact. | 167 |
| d | The thickness of the oxide (insulator). | 12 |
| Φ_m | The metal work function. | 162 |
| Φ_B | The metal metal-semiconductor barrier height. | 163 |
| Φ_s | The semiconductor work function. | 163 |
| χ | The semiconductor electron affinity. | 163 |
| E_G | The semiconductor energy band gap. | 56 |
| q | This is the electronic charge. | 56 |
| E_c | The conduction band edge. | 163 |

| | | |
|---------------|--|-----|
| E_v | The valence band edge. | 163 |
| E_F | Fermi level, sometimes given as E_f | 163 |
| E_i | Intrinsic level. | 163 |
| $\epsilon(z)$ | The dielectric constant. | 57 |
| $\beta(z)$ | The vector of effective mass coefficients in the z direction. | 23 |
| ΔE_c | The piecewise constant pseudopotential energy in the vertical direction. 23 | |
| N_D^+ | The ionised donor concentration. | 56 |
| N_A^- | The ionised acceptor concentration. | 56 |
| N_D | The donor concentration. | 56 |
| N_A | The acceptor concentration. | 56 |
| m_{dh} | The density of state mass of the valence band. | 56 |
| m_{de} | The density of state mass of the conduction band. | 57 |
| \hbar | Planck's constant divided by 2π | 131 |

List of Figures

List of Figures

| | | |
|-----|---|-----|
| 2.1 | The cross-section of a metal oxide semiconductor diode, [86]. . . . | 12 |
| 2.2 | N-Channel MOSFET diagram. | 14 |
| 6.1 | Flowchart of the Schroedinger-Poisson iteration process. | 94 |
| 7.1 | [91]. Architecture of Device 1: A model GaAs-GaAlAs device structure. | 100 |
| 7.2 | Gate voltage vs. Energy-subband (meV) for Device 1. | 103 |
| 7.3 | Occupation numbers N_ℓ of states E_ℓ for Device 1 shown in Figure 7.1. | 104 |
| 7.4 | [91]. Device 2: A $Si - SiO_2$ based quantum device with a T-shaped gate. | 105 |
| 7.5 | Device 2: Gate voltage vs. energy (meV) for quantum wire. | 109 |
| 7.6 | Device 2: Gate voltage vs. energy (meV) for quantum wire for ladder 2. | 111 |
| 7.7 | Device 2: Ladder 3 gate voltage vs. energy(meV) for quantum wire. | 113 |
| 7.8 | Device 2: Energy for different effective masses vs. gate voltage. | 115 |
| 7.9 | Device 2: Occupation numbers N_ℓ of states E_ℓ for first eigenvalue ladder with $N_A = 10^{18} cm^{-3}$ | 116 |

| | | |
|------|--|-----|
| 7.10 | Device 2: Occupation numbers N_ℓ of states E_ℓ for first eigenvalue ladder $N_A = 10^{10} \text{cm}^{-3}$ | 117 |
| 7.11 | Device 2: Cross-section of quantum electron density parallel to $\text{Si} - \text{SiO}_2$ with $N_A = 10^{18} \text{cm}^{-3}$ | 118 |
| 7.12 | Device 2: Cross-section of quantum electron density parallel to $\text{Si} - \text{SiO}_2$ with $N_A = 10^{10} \text{cm}^{-3}$ | 119 |
| 7.13 | Device 2: Electron density in quantum wire as well as undoped substrate as a function of gate potential with $N_A = 10^{18} \text{cm}^{-3}$. . . | 120 |
| 7.14 | Device 2: Electron density in quantum wire as well as undoped substrate as a function of gate potential with $N_A = 10^{10} \text{cm}^{-3}$. . . | 121 |
| 7.15 | Architecture of Device 3: Lightly shaded regions on top are the locations of the applied gates The internal lightly shaded regions are InGaAs layers [12]. | 122 |
| 7.16 | Potential in Device 3 obtained by the semi-analytical method compared to that reported in Anderson [12]. | 123 |
| 7.17 | Device 3: Potential in the transverse directions in the centre of the upper quantum well as shown in [12]. This plot is obtained by the semi-analytical method. | 124 |
| 7.18 | Device 3: Upper well energy (lowest state) as a function of gate voltage obtained by the semi-analytical method. Comparison with the simulation results reported in Anderson [12]. | 125 |
| 7.19 | Device 3: Computation times for the results shown in Figure 7.18. | 126 |
| 7.20 | Architecture of Device 4: Double-gate NMOSFET. | 128 |

| | | |
|------|--|-----|
| 7.21 | Device 4: Double-gate NMOSFET-conduction energy subbands for three different effective masses with $V_{DS} = 0 \cdot 2V$ and $V_{GS} = 0V$. The red and blue continuous lines are the energy subband for m_t , the green line is the energy subband for m_ℓ and the broken red line is the energy subband for m_t which is extracted from [6]. | 137 |
| 7.22 | Device 4: Double-gate NMOSFET-energy subbands for different drain-source voltages. | 138 |
| 7.23 | Device 4: Double-gate NMOSFET- I-V characteristics, current vs. drain-source potential V_{DS} | 139 |
| 7.24 | Architecture of Device 5: a single walled carbon nanotube field effect transistor (SWNT-FET) device structure. | 139 |
| 7.25 | [56] Sketch of CNTFET. This cylindrical structure is an approximation to the real Device 5. Simulations for this structure are carried out using the semi-analytical method. The same parameters for the SWNT are used in the simulation of the CNTFET. | 140 |
| 7.26 | Device 5: current-voltage characteristics. Comparisons of simulation for adaptive integration method (AIM) (red curve) [74], semi-analytical method (blue curve) and experimental results (extracted from [74])(green circle) with $V_G = 1.3V$, where drain current $[\mu, A]$ is plotted against drain voltage (v) for CNTFET reported in [74]. | 141 |

| | | |
|------|--|-----|
| 7.27 | Device 5: current-voltage characteristics. Comparisons of simulation for adaptive integration method (AIM) (yellow curve) [74], semi-analytical method (magenta curve) and experimental results (extracted from [74]) (blue dots) with $V_G = 1.0V$, where drain current $[\mu, A]$ is plotted against drain voltage (v) for CNTFET reported in [74]. | 142 |
| A.1 | Metal, oxide and semiconductor energy band diagrams are separately shown. | 163 |
| A.2 | Energy-band diagram of an ideal MOS at $V = 0$ for a p-type semiconductor. | 164 |
| A.3 | Energy-band diagram of an ideal MOS at $V \neq 0$ for a p-type semiconductor. The accumulation case. | 165 |
| A.4 | Energy-band diagram of an ideal MOS at $V \neq 0$ for a p-type semiconductor. The depletion case. | 166 |
| A.5 | Energy-band diagram of an ideal MOS at $V \neq 0$ for a p-type semiconductor. The inversion case. | 166 |
| B.1 | The cross-section of n-channel MOSFET. | 168 |
| B.2 | The linear operating region in the n-channel MOSFET. | 169 |
| B.3 | The pinch-off point operating region in the n-channel MOSFET. | 169 |
| B.4 | The saturation operating region in the n-channel MOSFET. | 170 |

List of Tables

List of Tables

| | | |
|------|---|-----|
| 7.1 | Eigenvalues (meV) for Device 1, obtained via the semi-analytical method. | 102 |
| 7.2 | Parameters for modelled Device 2 which is displayed in Figure 7.4. | 106 |
| 7.3 | Device 2 - Eigenvalues (meV) for Ladder 1 obtained via Semi-analytical method and Trellakis [91]. | 108 |
| 7.4 | Device 2: Relative errors (meV) of the Semi-analytical method-Ladder 1. | 108 |
| 7.5 | Device 2: Eigenvalues (meV) for ladder 2. | 110 |
| 7.6 | Device 2: Relative errors (meV) of the semi-analytical method for Ladder 2. | 110 |
| 7.7 | Device 2: Ladder 3 eigenvalues (meV). | 112 |
| 7.8 | Device 2: Relative errors (meV) of the semi-analytical method for ladder 3. | 112 |
| 7.9 | Device 2: Computational times (seconds) for $Si - SiO_2$ Device 2 by the semi-analytical method. | 114 |
| 7.10 | Device 3: Eigenvalues for modelled device with relative error given in percentage. | 127 |

| | |
|---|-----|
| 7.11 Device 4: eigenvalues (eV). These results are obtained by the semi-analytical method. | 129 |
| 7.12 Device 4: Parameters for the modelled device [6]. | 130 |
| 7.13 Device 5: Parameters for the modelled device [51,74]. | 134 |
| 7.14 Comparison of simulation times of the semi-analytical, SDM/WKB [6], predictor-corrector [91] reduced basis [12] and the adaptive integration [74] methods. | 135 |

Acknowledgements

I would like to thank almighty God for his direction and care throughout the past six glorious years in giving me the strength and health to complete this work. Furthermore, I would like to thank my supervisors Dr. Silvia Cirstea, Professor Maria DeSousa and Professor Marcian Cirstea for the guidance and unmatched support. Moreover, a special thanks to my first supervisor Dr. Silvia Cirstea whose direction in this work is instrumental and deeply appreciated, undeniably without her direction this work would not be possible. I would also like to thank Helen, who is my wife, for her full support which assists in the completion of this work.

Moreover, I would like to acknowledge the former Principal of Bacon's Academy, Mr Tony Perry for sponsoring this project. In addition, I would like to thank the current Principal and Vice Principal at Bacon's for their continued support for this thesis. A warm thank you to the staff at Bacon's for covering my lessons during my absence, especially members of the Mathematics Faculty. Also I thank my friend Munkanta Daka for his assistance with LaTeX. In addition, I would like to thank Tanya Mestry for her kind and thoughtful contribution in drawing some of the devices. Lastly, but by no means least, I would like to thank my children for the kind support they

have given me to accomplish this work, consequently, I can spend more time at the park playing football and rounders.

My time in the department of Computing and Technology at Anglia has been exceedingly rewarding and would like to extend my thanks to the head of the department, Professor Marcian Cirstea for his invaluable advice. Furthermore, the experience gained through giving presentation at the department's seminar has been vital in the preparation of this thesis. I wish also to thank the members of the Department of Computing and Technology for their useful suggestions given in order to improve my work, I am most grateful.

Abstract

The work in this thesis is focussed on obtaining fast, efficient solutions to the Schroedinger-Poisson model of electron states in microelectronic devices. The self-consistent solution of the coupled system of Schroedinger-Poisson equations poses many challenges. In particular, the three-dimensional solution is computationally intensive resulting in long simulation time, prohibitive memory requirements and considerable computer resources such as parallel processing and multi-core machines.

Consequently, an approximate analytical solution for the coupled system of Schroedinger-Poisson equations is investigated. Details of the analytical techniques for the approximate solution are developed and the original approach is outlined. By introducing the hyperbolic secant and tangent functions with complex arguments, the coupled system of equations is transformed into one for which an approximate solution is much simpler to obtain. The method solves Schroedinger's equation first by approximating the electrostatic potential in Poisson's equation and subsequently uses this solution to solve Poisson's equation. The complete iterative solution for the coupled system is obtained through implementation into Matlab.

The semi-analytical method is robust and is applicable to one, two and three dimensional device architectures. It has been validated against alternative methods and experimental results reported in the literature and it shows improved simulation times for the class of coupled partial differential equations and devices for which it was developed.

Chapter 1

Introduction

1.1 Background

Undeniably, over the past decades, the electronic industry has witnessed rapid progress in its quest to deliver high quality products to consumers, businesses and organisations. Currently, there are lucrative markets for products ranging from netbooks and smartphones whilst in the past this industry witnessed booms in the demand for MP3 players and digital versatile discs (DVDs). Consumer and industrial electronic products' core design is based on microelectronic semiconductor devices, whose continuously improved performance, reliability and cost-effectiveness have facilitated the rapid growth of this economy sector.

The reduction in the components of semiconductor devices to the sub-100 nanometric scale is currently a reality [6,7,72]. Reducing device architecture to this scale and beyond serves several important purposes, namely enhanced device functionality, faster processing speed and less consumption of power.

Given such desirable features, it is important to be able to efficiently model electronic transport in such structures in order to understand and optimize semiconductor electron systems. Electron transport becomes almost ballistic, i.e. the electrical resistivity due to scattering is negligible, [6, 57, 63, 87, 93] and quantum effects such as tunnelling, interference and confinements must be incorporated in any model.

Classical motion of charged particles can be described by kinetic equations (for example, Boltzmann) coupled to the Poisson equation for the electrostatic forces. In partially confined electron systems like nanotubes or nanowires, both quantum and classical effects are present. For example, the mechanism by which a particle penetrates a barrier that it could not surmount in the classical mechanical case is called tunnelling, which may be described as a quantum effect. Importantly, tunnelling becomes significant over small dimensions. For very small electron systems, like nanostructures, quantum effects are important and are well described by the Schroedinger-Poisson model [66].

Much work has been done on numerical methods for the self-consistent solution of Schroedinger-Poisson model. In previous work [6, 7, 12], the three-dimensional computation presents many challenges:

- prohibitive memory requirements;
- long simulation time;
- considerable computer resources, for example, parallel processing and multicore machines.

Naturally, it is important to address the above issues and offer solutions for improvement. Many authors are concerned with this problem [6, 12], i.e. the need to solve fast this coupled system of equations. Poisson's equation is a boundary value problem and Schroedinger's equation is an initial value problem [91], hence, analytic or semi-analytic solutions are quite difficult to find. Full analytical solutions are prevented, for example, by the form of the Poisson equation, which involves a Fermi-Dirac integral, for which a closed form does not exist and which has to be solved by series approximation. A further challenge is the discontinuous nature of the dielectric constant and of the effective mass coefficients. These issues are such that a complete analytical solution is not possible at present. Therefore, given this background, if semi-analytical solutions can be found, then the problem of electron transport may be simulated faster and more efficiently. It is this question with which this thesis is concerned. Therefore, in this thesis, the research addresses this gap in knowledge by deriving an accurate and efficient semi-analytical solution to the electron transport model in three dimensions and applies it to the prediction of performance of semiconductor devices.

1.2 Research Aims and Objectives

The overarching aim of this thesis is to develop new and robust analytical and computational techniques for the simulation of electronic states and transport in semiconductor systems, which go beyond the performance of current methods of numerical and computational solutions for the coupled system of Schroedinger-Poisson's equations in one, two and three dimensions. This

aim is achieved through four specific objectives of the research, which are:

- Overview of existing methods which are used to solve the coupled system of Schroedinger-Poisson's equation;
- The conceptual development of a new and efficient semi-analytical procedure which solves the coupled system of Schroedinger-Poisson's equations;
- The original design of a Matlab model supporting the implementation of the new semi-analytical procedure in order to simulate accurately electron transport in semiconductor systems;
- The validation of the proposed method by comparisons with reported computational [6, 12, 91] and experimental results [51, 74].

It is common practice to solve the original coupled system of Schroedinger-Poisson equations on a fine grid using the standard finite element approach. Although the process of obtaining the solution using this method is usually slow, nevertheless, it is seen as a benchmark to which other methods of solutions can be compared and validated. Solutions obtained via other methods are verified against finite element solutions in order to check accuracy rather than speed [6, 12, 91]. In addition to the finite element approach, when available, one also uses experimental data [51, 74], against which one's results can be verified. Given this background, the simulation results of semi-analytical method will be compared with reported finite element method solutions and experimental data where available.

1.3 Methodology

The purpose of this section of the thesis is to set out the strategies which underpin this research commencing with the literature review and ending with the thesis production. This work has used a range of research methodologies to achieve these above specific objectives. These are:

- literature review of current methods employed in the simulation of electronic device;
- investigation of analytical and computational solutions of coupled system of partial differential equations and then definition of new method;
- development of original code in Matlab. Then testing by simulation of elements and then of the overall model;
- comprehensive testing of the solution, evaluate performance by critical comparison with other methods reported in literature and benchmarked against known finite element and experimental results which are reported in literature.

A review of the relevant literature of general partial differential equations (PDEs) and those PDEs which are specifically used for device modelling is conducted. Here specific attention is given to the numerical, computational and, where possible, analytical solutions. Regarding analytical solutions, it was noticeable that these were difficult to find and hence the standard approach to solving the electron transport problem is mainly through computational means. Against this background, it was necessary to take a closer

look at a semi-analytical approach. The semi-analytical approach is defined as a combination of analytical and numerical techniques for the solution of a system of equations.

Development of a semi-analytical approach demanded the construction of an approximate initial electrostatic potential, enabling the consequential reduction of the Schroedinger-Poisson's model to a conventional eigenvalue problem for which bound states and wave functions were determined. The determination of the bound states was achieved via the application of the Evans function approach. To construct this function, it has been necessary to extend the Wronskian of solutions for the homogeneous equation to two and three dimensions.

Given a successful initial solution of Schroedinger's equation, the electron density was constructed and substituted into Poisson's equation, thus enabling an initial solution to Poisson's equation. The challenging task of finding an initial solution to Poisson's equation involved applications of the methods of variation of parameters and power series. Using this successful solution to Poisson's equation, an iterative procedure was developed in order to simulate the solution technique and implemented in Matlab.

The difference between the previous and new electrostatic potentials was compared in order to check convergence of the procedure. Comparisons were made against published data and improved simulations times have been achieved. This testing was done for one, two and three dimensional devices previously reported in literature.

1.4 Original Contribution to Knowledge

The original contributions to knowledge brought by this work are:

- A new generalised semi-analytical method is developed to efficiently solve the coupled system of Schroedinger-Poisson's equations. The method is applicable to one, two and three dimensions;
- The Evans function techniques which were previously applied only to one dimensional Schroedinger's equations are extended in a new way to find bound states from two and three dimensional Schroedinger's equations. This enables wave functions to be easily calculated. Furthermore, since the Evans function is a complex analytical function whose zeros correspond to the discrete spectrum of the differential operator, it is found in this research that the problem of finding the energies (eigenvalues) of devices is effectively the study of complex analytical functions;
- The new semi-analytical method is shown to be accurate and produces results which compare favourably in terms of speed with those reported in literature. Particularly, improved simulation times have been achieved using this new method for 3D structures, which are generally very hard to simulate.
- The original design of a Matlab model supporting the implementation of the semi-analytical procedure. This model computes simulation results in faster times compared to those reported in [6, 12, 91].

1.5 Outline of the Thesis

This thesis is organised as follows:

Chapter 2 presents a background review on one, two and three dimensional electronic devices, including operational principles and architectures. Included in the discussion is a brief overview of the well known Metal Oxide Field Effect Transistor (MOSFET). Further details on the MOSFET are found in Appendix B. In addition, as nonlinear differential equations are effective tools in scientifically modelling physical problems, an overview of analytical and numerical methods for solving them is briefly presented. In particular, the discussion focuses on those equations which are used to model the solutions of electronic devices.

Chapter 3 reviews the analytical and numerical methods used to solve the Schroedinger-Poisson model with application to electron transport. Particular attention is given to methods which are found in [6, 8, 12, 13, 55, 60, 68, 80, 91]. Moreover, reviews of well known Schroedinger-Poisson solvers [17, 22, 23, 94] and NEMO-3D developed by [54, 84] and the Device modelling group at the University of Glasgow [42, 64, 95] are presented. Finally, in this chapter, special reviews of four key references, [6, 12, 74, 91] are presented.

Chapter 4 develops a new semi-analytical method for the solution of the Schroedinger-Poisson equation in one, two and three dimensions. It is shown that by considering the solution of the homogeneous operator of the Schroedinger-Poisson model, one can effectively reduce this model to a simplified model where the electrostatic potential is easier to obtain and therefore this allows one to establish a semi-analytical solution.

In Chapter 5, the new semi-analytical method found in Chapter 4 is extended to Schroedinger equation. It is shown that the eigenvalues of Schroedinger's equation can be obtained via the Evans function techniques. Having found the eigenvalues, the associated eigenfunctions are established. As far as known by the author of this thesis, the Evans function techniques had not been applied before in capturing the discrete spectrum of the coupled system of Schroedinger-Poisson's equations which is used to determine electron transport in semiconductor systems.

In Chapter 6, it is shown that using the semi-analytical method discussed in Chapters 4 and 5, the successive approximations of the solutions of Schroedinger's equations are bounded, hence will always lead to local convergence. This is very important as it is not always the case that convergence happens in practice when Schroedinger and Poisson's equations are coupled. A proof of this convergence is detailed in this chapter.

Chapter 7 presents simulation results which are obtained using the semi-analytical method. It is shown that this method gives excellent results which compare well with published results. Moreover, it will be emphasised that the method is competent through two aspects, namely, speed and accuracy. It will be shown that, for the applications considered and analysed, the results are in good agreement with those published in literature and the method is computationally faster compared to other known methods employed in [6, 12, 91].

Finally, chapter 8 concludes the research and suggests how this work may be taken forward in the future. In particular, from the findings, the effectiveness of the semi-analytical method is discussed. Furthermore, the

application of the Evans function technique is highlighted. It is also suggested how this technique may be included in state-of-the-art device simulators such that speed, accuracy and computer memory are optimised when analysing semiconductor and other devices. Moreover, further implementation of the semi-analytical procedure in C⁺⁺ language may result in faster and improved simulation times. This is because Matlab, though versatile and powerful in executing complex calculations, is restricted in its processing speed. On the other hand, C⁺⁺ presents the user with a more versatile environment such that the performance of the code can be improved. In addition, by definition, the Evans function is a complex analytic function whose zeros correspond to point eigenvalues. Therefore, one must understand the properties of complex analytic functions which clearly suggests one may study complex analysis for future exploration in device analysis.

Chapter 2

Background Review

2.1 Introduction to Electronic Devices

This section of the thesis is concerned with a brief introduction to the operational principles and architecture of one of the most widely used microelectronic devices, the Metal Oxide Semiconductor Field Effect Transistor (MOSFET). The electron states and transport theory that is developed in Chapters 4 and 5 will be demonstrated on Metal-Oxide-Semiconductor (MOS) devices, therefore it is necessary to describe the principles of this architecture. Technological advances and market demand for electronic devices brought about unprecedented miniaturisation of electronic components, which are now part of everyday life, with applications that range from complex industrial processes to domestic appliances and to entertainment.

A review of the solutions of the relevant nonlinear coupled partial differential equations which concern this thesis is outlined. Attention is devoted to the numerical and analytical methods of solutions for these differential equa-

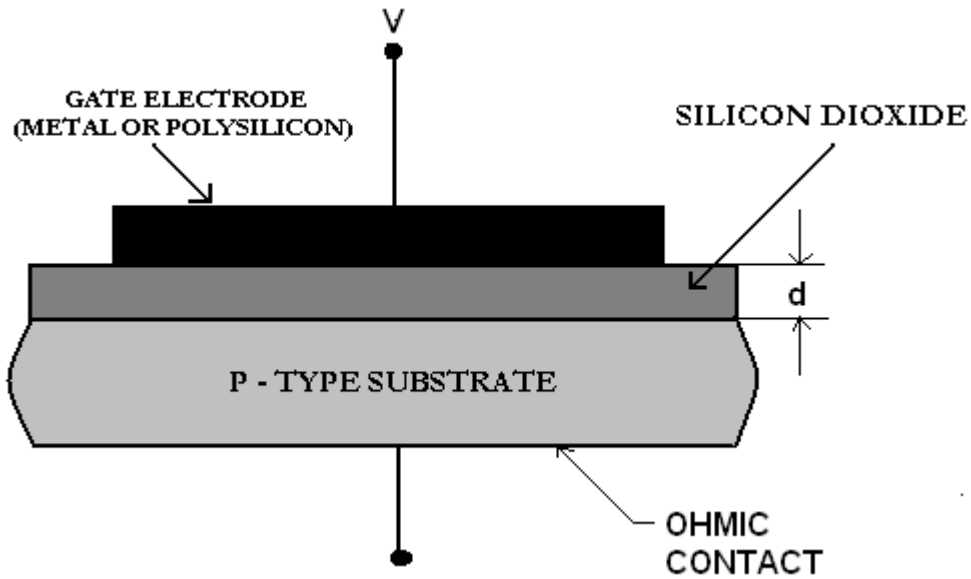


Figure 2.1: The cross-section of a metal oxide semiconductor diode, [86].

tions. The theory of the method of solution of the important Sine-Gordon equation [24, 80] is presented. Particularly, in this section of the thesis the coupled system of Schroedinger-Poisson equations which is frequently used to model the electron transport in electronic devices is introduced.

2.1.0.1 Introduction-The MOS Structure

Figure 2.1 shows a Metal Oxide Semiconductor (MOS) diode which is a structure consisting of a thin layer of oxide which is grown on top of a semiconductor substrate followed by a metal layer which is deposited on the oxide. V is the applied voltage on the metal and d is the thickness of the oxide (insulator).

Applying voltage to the gate of this MOS structure will control the state of the silicon surface underneath. The MOS diode comprises of two states,

namely, the *accumulation* and *inversion* which are used to make a voltage-controlled switch. In the case of the *accumulation* state, negative voltage is applied thus attracting holes from the p-type silicon to the surface, whilst in the *inversion* state a positive voltage which is larger than the threshold voltage is applied resulting in the creation of an inverted layer of electrons at the surface [86].

The voltage-controlled switch is in two modes, namely, *on* and *off*. These correspond to the existence or absence of the electron channel through which current flows. In the case when the gate voltage is lower than the threshold voltage there is no conducting channel and the source and drain regions are isolated by the p-type substrate. Thus the switch is in the *off-mode* state. On the other hand, the *on-mode* occurs when the gate voltage is higher than the threshold voltage resulting in the flow of current through the surface and the electron channel appearing [31, 86]. The operational details of the three separate components (metal, oxide and semiconductor) of the MOS structure are outlined in Appendix A.

2.1.1 The MOSFET

The Metal Oxide Semiconductor Field Effect Transistor (MOSFET) as shown in Figure 2.2 is based on the MOS diode illustrated in Figure 2.1. On the top of the oxide, a gate electrode, which is a conducting layer of metal, is attached. Just underneath the oxide and inside the substrate there are two heavily doped regions called the *source* and *drain*. The source to drain electrodes are equivalent to two p-n junctions that are situated back-to-back.

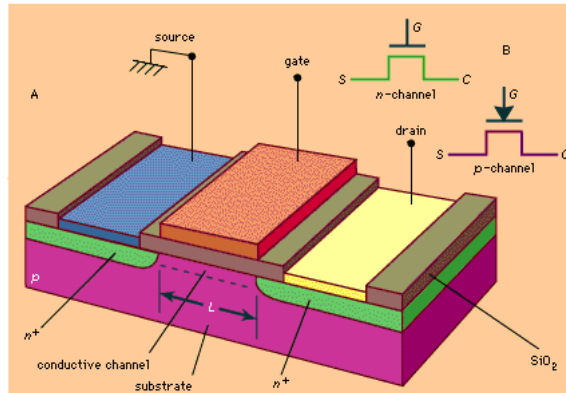


Figure 2.2: N-Channel MOSFET diagram.

The central MOS diode with the inverted channel region between the source and the drain is controlled by an electric field, hence the name MOSFET, created by a voltage V_g applied to the gate electrode.

The MOSFET may be n-channel or p-channel depending on the type of carriers in the channel region. For the MOSFET model, the channel contains electrons (n-channel), the source to drain regions are heavily n^+ doped and the substrate is p-type. When there is no voltage applied to the gate and there is no conduction channel between the drain and the source regions, the MOSFET is referred to as a normally-off device. A certain minimum voltage (e.g. $0.3V$), called the threshold voltage should be applied to the gate to induce a conduction channel.

If a conduction channel exists between the source and the drain regions even at zero gate voltage, then it is called a depletion mode device. In this case, the current flow is not exactly at the surface, some carriers are in the bulk of the silicon. Details of the MOSFET characteristics and operating

region of the n-channel MOSFET are given in Appendix B.

2.2 Review of Literature - solutions of non-linear differential equations

Many physical phenomena in physics and engineering are well modelled by non-linear differential equations. Electron states and transport in semiconductor devices are well described by the coupled non-linear Schroedinger-Poisson equations.

The differential equations used to model layered electronic devices are relatively easy to develop. What is challenging is the efficient (speed and accuracy) solution of these models. It is well known that one does not have a general method to solve nonlinear partial differential equations. Therefore, solutions are found through analytical, numerical and computational means. Numerical and computational methods are two separate classes [24]: numerical methods form a branch of Applied Mathematics which analyses the problem from the view point of finite dimensional spaces and present a rigorous mathematical treatment of error bounds and clearly set out the criteria under which convergence is achieved. On the other hand, the computational approach uses computer models to analyse the problem. As a result convergence is not proven, but comes from the speed of the machine and accuracy is achieved with a large number of iterations. Consequently, combination of these techniques with analytical solutions is powerful in finding solutions to difficult partial differential equations. Therefore, semi-analytical

solutions are those which combine numerical and analytical methods in finding solutions to differential equations.

For the purposes of this thesis, the task is to find simplified models which are much easier to solve through the application of computational, analytical and numerical methods or through combinations of these different methods. In the following, some general differential equations which are of interest and whose solution methods are in part relevant to this work are considered. These solution methods are interesting in that one can easily apply the hyperbolic tangent and secant functions (which are used in the examples below) to the coupled system of Schroedinger-Poisson equations. When this is done, the original coupled system of equations is transformed to a simplified system of equations for which semi-analytical solutions can be found, as will be shown in Chapters 4 and 5.

2.2.1 Example 1 - the Sine-Gordon equation

The Sine-Gordon equation [24] is given by:

$$\frac{\partial^2 u(t, x)}{\partial t^2} - \frac{\partial^2 u(x, t)}{\partial x^2} + \sin(u(x, t)) + \epsilon g(u(x, t)) = 0. \quad (2.1)$$

$u(x, t)$ is a smooth function. When $g(u) = \sin(2u)$, equation (2.1) is called the *double sine - Gordon* equation. From [24] it has been shown that with $\epsilon = 0$ one has an exact time independent solution

$$u_0(x) = 4\arctan(e^x). \quad (2.2)$$

Equation (2.2) satisfies

$$\frac{d^2}{dx^2} u_0(x) = \sin(u_0(x)), \quad (2.3)$$

$$\frac{d}{dx}u_0(x) = 2\operatorname{sech}^2(x) \text{ and} \quad (2.4)$$

$$\cos(u_0(x)) = 1 - 2\operatorname{sech}^2(x). \quad (2.5)$$

To find an approximate solution to the perturbed time-independent problem, let

$$\hat{u}(x, \epsilon) = u_0(x) + \epsilon u_1(x) + O(\epsilon^2) \quad (2.6)$$

and substitute it into (2.1) to obtain the governing equation for $u_1(x)$, which is given as

$$\frac{d^2}{dx^2}u_1(x) + (2\operatorname{sech}^2 - 1)u_1(x) = \sin(2u_0(x)) \quad (2.7)$$

which has a particular solution

$$u_1(x) = 2(x\operatorname{sech}(x) - \operatorname{sech}(x)\tanh(x)). \quad (2.8)$$

When interest is in the spectral problem, the spectral Ansatz is employed and a linearised spectral operator is obtained in the conventional form $L\xi = \lambda\xi$.

In order to find the spectrum of this operator one requires the use of the techniques of variation of parameters, a change of variable and application of power series. Using these techniques the problem reduces to the study of the general solution of second order differential equation with variable coefficients of the form

$$\frac{d^2u(x)}{dx^2} + 2\operatorname{sech}^2(x)u(x) = t(x). \quad (2.9)$$

This equation has general solution

$$u(x) = a\phi_1(x) + b\phi_2(x) + \int_{x_0}^x k(x, s)t(s) ds, \quad (2.10)$$

where $k(x, s)$ is the Wronskian [40] of the two linearly independent solutions $\phi_1(x)$ and $\phi_2(x)$. With an application of the Evans function techniques [25, 71, 77], one gets the eigenvalues which are of interest. Therefore, it has been seen that given a suitable non-linear perturbed differential equation in one-dimension, one can linearise it about its stationary solution and obtain an eigenvalue problem to which the Evans function techniques can be applied in order to find the discrete spectrum of the differential operator, hence, the eigenfunctions can be calculated.

2.2.2 Example 2 - the scalar reaction-diffusion equation

As a second example, let $\frac{d^2}{dx^2}u(x) = u_{xx}$ and consider the scalar partial differential equation [24], where $u_t = \frac{d}{dt}u(t)$.

$$u_t = u_{xx} - u(x) + u^3(x), \quad u(x) \in R, \quad x \in R. \quad (2.11)$$

Equation (2.11) admits a stationary time independent solution

$$u(x, t) = q(x) \quad (2.12)$$

$$= \sqrt{2}\operatorname{sech}(x). \quad (2.13)$$

Linearising about this stationary solution results in the linear partial differential equation

$$u_t = u_{xx} - u(x) + 6\operatorname{sech}^2(x)u(x). \quad (2.14)$$

As above, applying the spectral Ansatz to (2.14) results in the time-independent spectral problem

$$u_{xx} - u(x) + u^3(x) + 6\operatorname{sech}^2(x)u(x) = \lambda u(x). \quad (2.15)$$

Now $\lim_{x \rightarrow \pm\infty} (6\operatorname{sech}^2(x) - 1) \rightarrow -1$. Therefore, (2.15) reduces to

$$u_{xx} - (1 + \lambda)u(x) = 0. \quad (2.16)$$

The idea is to write a solution to (2.15) in the form $e^{\mu x}h(x)$ where $\mu = \pm\sqrt{1 + \lambda}$ and assume $\operatorname{Real}(1 + \lambda) > 0$. Substitute this into (2.15), then the function $h(x)$ satisfies

$$h_{xx}(x) + 2\mu h_x(x) + 6\operatorname{sech}^2(x)h(x) = 0. \quad (2.17)$$

Solutions to (2.17) which decay as $x \rightarrow \pm\infty$ can be found by using hypergeometric series [83], or power series method, [69]. These bounded solutions are found to be

$$u^-(x, \lambda) = e^{\sqrt{1+\lambda}x} \left(1 + \frac{\lambda}{3} - \sqrt{1+\lambda} \tanh(x) - \operatorname{sech}^2(x) \right) \quad (2.18)$$

$$u^+(x, \lambda) = e^{-\sqrt{1+\lambda}x} \left(1 + \frac{\lambda}{3} + \sqrt{1+\lambda} \tanh(x) - \operatorname{sech}^2(x) \right). \quad (2.19)$$

The Evans function $D(\lambda)$ is defined to be the Wronskian

$$D(\lambda) = \begin{pmatrix} u^+(x; \lambda) & u^-(x; \lambda) \\ u_x^+(x; \lambda) & u_x^-(x; \lambda) \end{pmatrix} \quad (2.20)$$

of the two solutions $u^\pm(x; \lambda)$. The zeros of the constructed Evans function are $\lambda = 0$ and $\lambda = 3$.

Naturally, one would like to extend the methods to the two dimensional case and also investigate various techniques used to obtain solutions to partial differential equations (PDEs). In [43, 47] one can use Fourier decomposition to reduce two-dimensional PDEs to one-dimensional differential equation. For example, consider the equation

$$B(U_{xx}(x, y) + U_{yy}(x, y)) + cU_x + DF(\hat{U}(x, y))U(x, y) = \lambda U(x, y).$$

To analyse this equation it is assumed the functions $U(x, y)$ and $DF(\hat{U}(x, y))$ are L-periodic and expand

$$U(x, y) = \sum_k \hat{U}_k(x) e^{\frac{2\pi i k y}{L}} \quad (2.21)$$

and

$$DF(\hat{U}(x, y)) = \sum_k \hat{D}_k(x) e^{\frac{2\pi i k y}{L}}. \quad (2.22)$$

Substituting (2.21) and (2.22) into the PDE results in the eigenvalue problem [43]

$$B\partial_{xx}\hat{U}_k - \left(\frac{2\pi k}{L}\right)^2 B\hat{U}_k + c\partial_x\hat{U}_k + \sum_v \hat{D}_{k-v}(x)\hat{U}_v = \lambda\hat{U}_k. \quad (2.23)$$

This produces a system of ordinary differential equations to which one can apply the known Evans function technique.

2.2.3 Example 3 - the Helmholtz equation

As another example of interest in this thesis, one is concerned with the solution of the Helmholtz equation in two and three dimensional rectangular domains with piecewise constant coefficients $a(z)$ and $b(z)$ [13] is

$$\nabla \cdot (a(z)\nabla\phi) + b(z)\phi = f(x, y, z) \quad (2.24)$$

$$(x, y, z) \in [0, L_x] \times [0, L_y] \times [0, L_z]$$

with Dirichlet boundary conditions at $z = 0$,

$$\phi(x, y, 0) = g(x, y), \quad (x, y) \in [0, L_x] \times [0, L_y],$$

Neumann, Dirichlet, or "infinite" boundary conditions at $z = L_z$, $\phi(x, y, z)$ periodic in x and y for all $z \in [0, L_z]$.

This equation arises in various areas of Applied Mathematics, particularly in the area of modelling layered semiconductor devices. The solution method in [13] is to apply Fourier basis method in the (x, y) dependent directions thus

$$\phi(x, y, z) = \sum_{k_1, k_2} e^{2\pi i k_1 \frac{x}{L_x}} e^{2\pi i k_2 \frac{y}{L_y}} \gamma_{k_1, k_2}(z) \quad (2.25)$$

which, when substituted into (2.25) is a solution to the resulting equation

$$\frac{d}{dz} \left(a(z) \frac{d}{dz} \gamma_{k_1, k_2}(z) \right) + \left(b(z) - 4\pi^2 k_1^2 \left(\frac{x}{L_x} \right)^2 - 4\pi^2 k_2^2 \left(\frac{y}{L_y} \right)^2 \right) \gamma_{k_1, k_2}(z) = \hat{f}(k_1, k_2)(z)$$

where

$$\hat{f}(k_1, k_2)(z) = \int_0^{L_x} \int_0^{L_y} f(x, y, z) e^{-2\pi i k_1 \frac{x}{L_x}} e^{-2\pi i k_2 \frac{y}{L_y}} dx dy.$$

Solutions to this equation are much easier to obtain through the application of numerical and computational techniques [13, 33].

2.2.4 Example 4 - Laplace's and Poisson's equations in two and three dimensions

In [75], Laplace's equations in rectangular coordinates are given in two and three dimensions respectively. One has

$$\frac{\partial^2 \psi(x, y)}{\partial x^2} + \frac{\partial^2 \psi(x, y)}{\partial y^2} = 0, \quad (2.26)$$

and

$$\frac{\partial^2 \psi(x, y, z)}{\partial x^2} + \frac{\partial^2 \psi(x, y, z)}{\partial y^2} + \frac{\partial^2 \psi(x, y, z)}{\partial z^2} = 0, \quad (2.27)$$

with appropriate boundary conditions. One famous method which is widely used to solve this equation is the well known separation of variables method.

If the right hand sides of equations (2.26) and (2.27) are functions $f(x, y)$ and $f(x, y, z)$ respectively, equations (2.26) and (2.27) are called Poisson's equations.

In order to obtain general solutions to equations (2.26) and (2.27), the following definition and theorem are necessary. From [75] one has

Definition 1

Let $r = \sqrt{x^2 + y^2 + z^2}$.

Let the function $u(x, y, z)$ be defined for sufficiently large r , then it is said to vanish at infinity if for every $\epsilon > 0$ there exists a real number R such that $|u(x, y, z)| < \epsilon$ whenever the point (x, y, z) is such that $r > R$.

Theorem 2.1 Assume the function $f(x, y, z)$ is continuously differentiable in the entire three dimensional space and if for large r the inequality

$$|f(x, y, z)| < \frac{A}{r^{2+\alpha}}$$

holds, for positive constants A and α , then two and three dimensional solutions to (2.26) and (2.27) are thus given respectively as

$$u(x, y) = \int_{-\infty}^{\infty} \int_{-\infty}^{\infty} f(\xi, \eta) \ln \frac{1}{\sqrt{((x - \xi)^2 + (y - \eta)^2)}} d\xi d\eta \quad (2.28)$$

and

$$u(x, y, z) = \int_{-\infty}^{\infty} \int_{-\infty}^{\infty} \int_{-\infty}^{\infty} \frac{f(\xi, \eta, \zeta)}{\sqrt{((x - \xi)^2 + (y - \eta)^2 + (z - \zeta)^2)}} d\xi d\eta d\zeta.$$

For the purposes of this thesis, one considers nanoscale layered semiconductor devices. For a comprehensive overview one may refer to [6, 7, 12, 59, 91, 94]. Hitherto, references are made to PDEs which are used directly in

modelling these layered structures. It has been shown in Trellakis et al [91] that the coupled Schroedinger-Poisson equations may be analysed and solved by various numerical means. For example, in [91] we have the equations

$$-\frac{\hbar^2}{2}\nabla \cdot \left(\frac{1}{m^*}\nabla\psi_\ell \right) + [V_h - e\phi + V_{xc}(n) - E_\ell]\psi_\ell = 0 \quad (2.29)$$

$$\nabla \cdot [\epsilon\nabla\phi] = -\rho(\phi), \quad (2.30)$$

where the various energy terms and charge density terms are defined in Chapter 4. This system is in three dimensions and the tasks are to find solutions $\psi_\ell(x, y, z)$ and $\phi(x, y, z)$. This system is not easy to solve. In fact, no closed solution exists. However, over the years researchers have developed various computational methods to successfully tackle these coupled differential equations. For example, in [91] a predictor-corrector approach which successfully describes efficiently the electron transport in semiconductor devices has been presented.

Furthermore, Anderson [12] analyses a slightly different version of the coupled system of Schroedinger-Poisson equations, that is

$$\nabla \cdot (\kappa(z) \cdot \nabla\phi(\vec{x})) = q\rho(\vec{x}) \quad (2.31)$$

$$-\frac{\hbar^2}{2}\nabla \cdot (\beta(z)\nabla\psi(\vec{x})) + [\phi(\vec{x}) + \Delta E_c(z)]\psi(\vec{x}) = E\psi(\vec{x}) \quad (2.32)$$

in light of developing efficient simulation of semiconductor devices. This three dimensional system of PDEs can be reduced to one dimensional and two dimensional systems, thus reducing the computational task in the simulation process. For example, it is noted that if the potential, the dielectric constant and the vector of effective mass are functions of the vertical coordinate only, for example, $\phi(x, y, z) = \phi(z)$, then equations (2.31) and (2.32)

can be reduced to a one dimensional system which is less computationally demanding to solve.

To conclude, the technique of creating approximate mathematical models in this thesis shows semi-analytical solution to the coupled system of Schroedinger-Poisson equations can be computed. As will be seen in the next chapter of this thesis, if closed form solutions do not exist (they rarely do), then one has to consider computational and numerical methods which are powerful techniques in analysing electron transport in electronic devices. In the next chapter of this thesis, a review of the numerical solutions to differential equations will be discussed.

Chapter 3

Overview of Modelling Electron Transport in Semiconductor Devices

The previous chapter demonstrates that whilst it is sometimes possible to find closed solutions to partial differential equations (PDEs), in the majority of cases this is not possible, therefore one has to seek numerical and computational solutions. A central theme in this thesis is the modelling of electron transport in semiconductor systems which is important in device analysis. Accurately analysing the electron transport requires the computational, numerical and analytical solutions of the coupled system of Schroedinger-Poisson's equations.

Therefore, this chapter reviews the literature covering the relevant work in the field of numerical and analytical methods for ordinary and partial differential equations. The chapter contains numerical and analytical techniques

that are employed to solve the coupled system of Schroedinger-Poisson equations. Furthermore, it reviews the literature of computationally less expensive alternatives to the Schroedinger-Poisson model from the class of quantum diffusion models (quantum hydrodynamic and quantum drift-diffusion models). Finally, a special review of four key references which are discussed in this work is presented.

3.1 Review of existing relevant methods to solve coupled PDEs

Much work has been done on the solution of the coupled system of Schroedinger-Poisson's equations. A great deal of previous work has been focussed on numerical and computational methods. Excellent reviews of the numerical and computational methods can be found in [7, 14, 21, 36, 39, 62, 85, 87, 89–91, 95]. In addition, in [6] an accelerated algorithm in 2D is presented which provides a fast solution to the above system of equations. In [6], it is shown that the accelerated algorithm improves upon the previous subband decomposition method (SDM) previously reported in [7].

In general it is not possible to obtain closed-form (analytical) solutions which describe sufficiently and satisfactorily the operation of layered semiconductor devices. Whilst analytical solutions are desirable and should be obtained where possible, in most of the research to date, numerical solutions are often sought because these solutions are usually achievable and they provide useful and quick insights into the equations being studied. Other cou-

pled systems of equations which are widely used to model various phenomena in other important fields such as biology, engineering and electrostatic are outlined in [18,21,24,37,82]. In electrostatics, Poisson's equation is used to compute the electrostatic potential. Schroedinger's equation is used for modelling wave functions as well as for finding appropriate energy states. Therefore, it is necessary to develop robust numerical algorithms to solve the above system of equations efficiently, although the demand on computer resources can be quite formidable, especially in 3D simulation problems.

Two powerful numerical techniques which are employed to solve the above system of partial differential equations are the finite-element and finite-difference methods. In both methods, the equations are discretised using specified grids for the domain of the device. Other successful techniques that have been successfully used to solve problems of this kind are reported in [32]. These include boundary integral methods and finite volume methods. An account of the meshless Finite Point (FP) method used to solve the nonlinear semiconductor Poisson's equation is reported in [21].

The finite difference method is very simple to implement and is particularly suited to simple device geometries. Given this advantage, it is widely used in modelling one-dimensional and two-dimensional rectangular devices [21,45]. It is also known that three-dimensional models have been developed using finite difference methods [89]. The application of finite-difference techniques is well established and there is considerable information in literature dealing with stability and convergence properties of this method. Details of the criteria for convergence and stability are found in [2,30].

Matrices obtained from the discretisation process are usually large in the

order of 10^4 by 10^4 . Therefore, solving the resulting linear system becomes computationally intensive. Many authors are conducting extensive research in this area and have reported techniques for efficient solution of the resulting system of equations obtained from the discretisation of the Schroedinger-Poisson model, as detailed in [6, 12, 45, 89–91, 95].

Similarly, the finite-element method [18, 41] is used to solve many partial differential equations. Therefore, this method requires the discretisation of the whole domain. The method still results in a large matrix. The consequential linear system then has to be solved using preconditioners [91]. However, a clear advantage of the finite-element method over the finite difference method is that it can be used to model complex-shaped and inhomogeneous structures. Elements can be chosen to closely conform to the original geometry of material boundaries.

The goal is to solve the resulting linear system fast whilst simultaneously utilising minimum computer resources. From here on, the main focus is on numerical techniques which are found in literature dealing with numerical solution to coupled system of equations. In [48], a comprehensive review of both classical linear and nonlinear techniques is presented for solving the coupled system of Poisson-Boltzmann equations. The main aim in this work is the development of a robust and efficient inexact-Newton multigrid numerical method which is used to solve the set of equations obtained from discretisation. In this work it is shown that this method is superior to all other methods considered, particularly it is shown to converge in cases where other methods fail.

In addition to the above numerical techniques, the work in [97] focuses

on using hybrid techniques in the electrostatic analysis of a nanowire. The authors propose an efficient approach called the hybrid boundary integral equation (BIE)-Poisson-Schroedinger approach. With this approach, a solution to Laplace's equation in the exterior domain of the nanowire structure is obtained. This is achieved through boundary integral formulation. Subsequently, analysis of the semiconductor structures is achieved by a combination of Poisson-Schroedinger equation with the boundary integral equations for the interior domain. Furthermore, a meshless Finite Cloud method and a Boundary Cloud method are employed in order to self-consistently solve the coupled system of equations. This approach appears to achieve a significant reduction in computational cost and provide higher degree of accuracy, however, the author analyses the problem only in two-dimensions.

Further analysis of the numerical techniques employed to obtain self-consistent solution to the coupled system of Schroedinger-Poisson equations is detailed in [62]. The main interest here is the three dimensional self-consistent solution of Poisson-Schroedinger for electrostatically formed quantum dots. Quantum dots are nanoscale devices which can be used in various nanoelectronic applications. In this work, it is reported that quantum dots may be treated as the memory cells which can be arranged into matrices and form the whole memory circuits. As a result, accurate analysis of these structures must be carried out. The analysis can be done by numerical simulation.

The method used in [62] in solving the above problem is to check if the approach in which the electron gas is treated separately in a plane ($x - y$ plane) of 2D electron gas (2DEG) and separately in the z direction which

is perpendicular to a heterojunction, can provide accurately acceptable results. To this aim, the one-dimensional Schroedinger equation is solved for part of the potential distribution corresponding to the z -direction. Consequently, the authors obtained the ground state of 2DEG together with the electron gas density distribution. Superposition of the results obtained for one-dimensional and two-dimensional problems gave final information which could be compared with results obtained in fully three-dimensional simulations. It is expedient to declare here that analysis of the 2D and 1D calculations have to be analysed with great care, particularly with regard to the positions of energy levels which determine the number of electrons in quantum dots for a given electrode potential. In addition, the time taken in the simulation process is a key aspect of any research one which will be addressed later in this thesis.

The Schroedinger-Poisson equations have far reaching applicability in various areas of technological industry. As semiconductor technology advances, this technology can be applied to optics and biology. In [61], the nanowire core-shell structure with a radial variation in material characteristics, such as semiconductor composition, is among the various structures currently under investigation. This core shell structure is popular because it provides great versatility for use in many devices such as field effect transistors, photodetectors and photoemitters.

So far, one has not addressed the commercial implications of semiconductor devices. It is now usual practice to scale aggressively semiconductor devices in order to meet the demands of reduced cost per function on a chip used in modern integrated circuits. It has been noticed that quantum effects

have played an indispensable role in the operation of these microelectronic devices. A typical method to simulate these effects is to simultaneously and self-consistently solve the coupled system of Schroedinger-Poisson's equations in both two and three dimensions. It is expedient to investigate alternative ways or models (for example, spectral element method and quantum drift-diffusion models) to solve the electron transport problem quickly and accurately.

The work in [27] investigates alternative models other than the Poisson-Schroedinger model to describe quantum effects, suggesting the use of the recently developed effective potential approach which accounts for the natural non-zero size of an electron wave packet in the quantised system. The work illustrates application to a proposed silicon-on-insulator (SOI) structure in order to quantify these quantum effects. Furthermore, the authors used a formalism known as Landauer-Buttiker formalism [35] to calculate the on-state current quantum-mechanically and estimate the increase in device threshold voltage [92]. Whilst this work is confined only to analysing the problem in two-dimensions, it highlights the need to consider other appropriate "less expensive" models.

Indeed, quantum corrected drift-diffusion models can be used to carry out numerical simulation of tunnelling effects in nanoscale semiconductor devices [27, 44]. In these studies the authors focus on a novel mathematical reformulation of the quantum drift-diffusion transport model. The aim of this reformulation is to devise an efficient and stable simulation procedure based on a suitable generalisation of the Gummel's decoupled algorithm [53], a widely adopted iterative technique in the context of semiconductor device

simulation based on the drift-diffusion (DD) model. The study analyses the problem in one dimension only, however, it indicates that one of the goals of the computation is to accurately estimate the current flowing through the oxide and the carrier densities at the semiconductor-oxide interface, in order to provide appropriate boundary conditions to multidimensional simulations using quantum drift diffusion model (QDD).

Furthermore, another alternative to the Poisson-Schroedinger model is the spectral element method. The work done in [26, 52] demonstrates significantly lower computer memory and computational time compared to other conventional methods when the spectral method is applied and the results analysed. In addition, the spectral element method divides the computational domain into non-overlapping subdomains and Chebyshev polynomials are used to represent the wave function in each subdomain. Analysis of the method reveals that it is suitable for large scale problems and is highly accurate. Compared to the second order finite difference method, it appears to be significantly faster. Although it is not known how well the method compares with higher order finite difference method, the method seems to be validated by the results obtained by other methods, namely, the Airy function [49], finite element [18] and the Nemerov's methods [16]. Section 3.2 discusses various computational methods).

Therefore, as an initial conclusion, it is clear that the implementation of numerical techniques has equipped the research community with invaluable insights into the nature of the problem being investigated. Moreover, numerical methods assist researchers to better understand and obtain vital information regarding the behaviour and simulation of semiconductor de-

vices. Indeed, in many instances only numerical techniques are possible if one wishes to understand the electronic behaviour of semiconductor devices. Some common issues highlighted by various authors are those posed by the strong nonlinearity of the problem and by intermediate approximations which have to be made in the solution process [89]. For example, the closed form of the Dirac-Fermi integral [29,67], which plays a significant role in semiconductor physics, is not known. As such, various approximations have to be made. Some useful approximations are reported in literature, particularly the work in [15] gives rational function approximations for the complete Fermi-Dirac integrals of orders $\frac{1}{2}$ and $-\frac{1}{2}$. Furthermore, the work in [67] derives two new series expressions for this integral which are useful in the quest to find approximate analytical solutions to the system of Schrodinger-Poisson's equations. With these limitations, as well as the already mentioned drawbacks of speed and computer resources experience during the simulation process, it is natural to investigate new approaches in order to solve the problem of electron transport in semiconductor systems. One way to achieve this is to investigate analytical methods which are reported in literature.

Two efficient analytical methods are derived in [78], namely the homotopy-perturbation method (HPT) and the Adomain decomposition method (ADM) to find exact analytical solutions to Laplace's equation in two dimensions with Dirichlet boundary conditions. In addition, the work in [19] shows further development of the homotopy perturbation method as a useful analytical tool for solving differential equations. Comparing the results of the HPT and the ADM methods with the variational iterative method (VIM) reported in [78] suggests that the HPT is much easier and more convenient

than the methods of VIM and ADM. However, the analysis in [3] suggests that although the HPT and ADM give the same results when applied to study the generalised Hirota-Satsuma coupled Korteweg-de Vries (KdV) equation, an improved method known as the homotopy analysis method (HAM) is proposed. Additional details of the variational method for exact solution of Laplace's equation can be found in [9, 70].

Further analytical techniques to solve coupled systems of differential equations are given in [20, 28, 65, 82]. This work shows how to find analytical solutions by applying the Jacobi elliptic expansion method. Moreover, in [76] new exact solutions for three nonlinear evolution equations are proposed. In this work, analytical solutions are derived based on the Ansatz of combination of solutions to the Riccati equations. Consequently, closed form travelling wave solutions of three systems of nonlinear partial differential equations are derived. In achieving these analytical solutions, some of the work employed symbolic computing to arrive at the desired results.

A careful study of the above methods which are employed by various authors to find analytical solutions suggests that no single analytical method exists as far as it is reported in literature that solves efficiently the coupled nonlinear system of partial differential equations. Indeed, the degree of precision and operational parameters associated with analytical models make it difficult to find closed form solutions to the coupled system of Schroedinger-Poisson's equations. However, this does not prevent the need to search for approximate analytical solutions which will improve the two and three dimensional numerical processes which are used to analyse the above system of equations, which are currently time consuming and memory intensive.

Therefore, the goal of the next two chapters of this thesis is to admit ideas from several sources then propose an original semi-analytical method which will accurately predict the transport of electrons in semiconductor systems.

As is indicated in this thesis, there are four key references which are essential in this work. Therefore, in the following section, reviews of these are presented [6, 12, 74, 91].

3.2 Reviews of four key references

The four key references reported in this thesis are entitled:

- Computational issues in the simulation of semiconductor quantum wires by Trellakis et al [91],
- An accelerated algorithm for 2D simulations of quantum ballistic transport in nanoscale MOSFETs by Abdallah et al [6],
- Efficient solution of the Schroedinger-Poisson equations in layered semiconductor devices by Anderson [12] and
- Fast convergent Schroedinger-Poisson solver for the static and dynamic analysis of carbon nanotube field effect transistors by Pourfath et al [74].

3.2.1 Review of Trellakis' computational issues in the simulation of semiconductor quantum wires [91]

Trellakis et al [91] describe a number of efficient computational methods which are used in the simulation of electronic states in quantum wires formed as a result of quantum confinement in two directions. The physical model used to describe the bound states in the cross-section of a quantum wire is the coupled system of Schroedinger-Poisson equations. Schroedinger's equation is

$$-\frac{\hbar^2}{2}\nabla \cdot \left[\frac{1}{m^*}\nabla\psi_n \right] + [V_h - e\phi + V_{xc}(n) - E_n]\psi_n = 0. \quad (3.1)$$

ψ_n is the wave function corresponding to the eigenvalue E_n . The electrostatic potential is ϕ . V_h is the heterojunction step potential. n is the quantum electron density. V_{xc} is the exchange correlation potential and m^* is the tensor describing the effective mass. The nonlinear Poisson equation:

$$\nabla \cdot (\epsilon\nabla\phi) = -q [-n + p(\phi) + N_D^+(\phi) - N_A^-(\phi)] \quad (3.2)$$

determines the electrostatic potential ϕ . Here ϵ is the dielectric constant, q is the electric charge. p is the hole density and N_D^+ and N_A^- are the ionized and donor and acceptor concentrations. In addition,

$$p(\phi) = 2 \left(\frac{m_{dh}k_B T}{2\pi\hbar^2} \right)^{\frac{3}{2}} \wp_{\frac{1}{2}} \left(\frac{-e\phi + V_h - E_G - E_F}{k_B T} \right), \quad (3.3)$$

$$N_D^+(\phi) = N_D \left[1 + g_D \exp \left(\frac{E_F + e\phi - V_h + E_d}{k_B T} \right) \right]^{-1}, \quad (3.4)$$

and

$$N_A^-(\phi) = N_A \left[1 + g_A \exp \left(\frac{-E_F - e\phi + V_h - E_G + E_a}{k_B T} \right) \right]^{-1}. \quad (3.5)$$

N_D and N_A are the donor and acceptor concentrations. E_a and E_d are the donor atom ionisation energies, g_D and g_A their respective ground state level degeneracies. The band gap is E_G and m_{dh} is the density-of-state mass of the valence band. The electron density is given as

$$n = \sum_n g_v \left(\frac{2m_w k_B T}{\pi^2 \hbar^2} \right)^{\frac{1}{2}} \wp_{-\frac{1}{2}} \left(\frac{E_F - E_n}{k_B T} \right) |\psi_n|^2.$$

Here g_v represents the number of equivalent conduction band valleys. The electron mass along the wire is m_w , the temperature is T , the Boltzmann's constant is k_B , the Fermi level is represented by E_F and the Fermi-Dirac integral of order $-\frac{1}{2}$ is denoted by $\wp_{-\frac{1}{2}}$.

3.2.1.1 Solution by Underrelaxation

The coupled system of equations (3.1) and (3.2) is normally solved by iteration between Poisson's and Schroedinger's equations. However, plain iteration by itself does not necessarily lead to convergence, therefore, one has to underrelax in the electron density n by using an adaptively determined relaxation parameter ω^k . The underrelaxation approach is outlined below:

- Solve nonlinear Poisson equation using the old electron density $n^{(k-1)}$ to obtain electrostatic potential $\phi^{(k)}$,
- Use $\phi^{(k)}$ and $V_{xc}(n^{(k-1)})$ to solve Schroedinger's equation in order to obtain a new set of eigenfunctions and corresponding eigenvalues, $(E_n^k, \psi_n^{(k)})$,

- Calculate an intermediate electron density, $n_{int}^{(k)}$,
- Determine an appropriate relaxation parameter $\omega^{(k)}$ in order to obtain new electron density $n^{(k)}$,
- Repeat outer iteration until n becomes stationary.

This method has a major weakness, which is the inherent instability of the outer iteration which is controlled only by the underrelaxation procedure. One does not know in advance the precise value of the relaxation parameter $\omega^{(k)}$ and thus it has to be dynamically re-adjusted during the iteration process. The choice of this parameter has consequences; if it is chosen too large then it results in oscillations from one iteration step to the next in the total quantized charge $\int n dx$; on the other hand, if $\omega^{(k)}$ is too small, then convergence is achieved in too many iteration steps. Therefore, this problem has to be addressed, hence the predictor-corrector type approach is proposed [91].

3.2.1.2 Solution by a Predictor-Corrector Type Approach.

With this approach, fast convergence can be achieved by modification in the underrelaxation algorithm by partial decoupling of both partial differential equations and damping the oscillations in the total electric charge. To this end, one substitutes into Poisson's equation a modified expression for the quantum electron density $\tilde{n}(\phi)$, which approximates the implicit dependence of the electron density n on the electrostatic potential ϕ due to Schrodinger's equation.

By using quantum mechanical perturbation theory, a suitable expression

for the electron density n is given as

$$\tilde{n}(\phi) = \sum_{\ell} \tilde{N}_{\ell}(\phi - \phi_{old}) |\psi_{\ell}^{(k-1)}|^2, \quad (3.6)$$

$$\tilde{N}_{\ell}(\phi - \phi_{old}) = \left(\frac{2m_q k_B T}{\pi^2 \hbar^2} \right)^{\frac{1}{2}} \wp_{-\frac{1}{2}} \left(\frac{E_F - E_{\ell} + e(\phi - \phi_{old})}{k_B T} \right). \quad (3.7)$$

Therefore, the original approach starts by solving a modified Poisson equation which contains $\tilde{n}(\phi)$ as a predictor for the electron density n . Hence, the original Poisson's equation is changed to

$$\nabla \cdot (\epsilon \nabla \phi) = -e [-\tilde{n}(\phi) + p(\phi) + N_D^+(\phi) - N_A^-(\phi)], \quad (3.8)$$

which is solved for ϕ . Using this value of ϕ along with the predicted electron density \tilde{n} enables the potentials in modified Schroedinger's equation

$$-\frac{\hbar^2}{2} \nabla \cdot \left[\frac{1}{m^*} \nabla \psi_n \right] + [V_h - e\phi + V_{xc}(\tilde{n}) - E_n] \psi_n = 0 \quad (3.9)$$

to be determined and a corrected update of the electron density is calculated.

3.2.1.3 Validation of Results in [91]

The Schroedinger and Poisson equations are both discretised by box integration finite difference method in order to take into account discontinuities in the material properties. As the quantum wire covers only a small part of the whole computational domain, a non-uniform rectangular mesh is used around the wire region in order to minimise computational cost, while retaining high accuracy within the region of interest.

Discretisation of Schroedinger's equation results in a large eigenvalue problem which demands a solution by the Chebyshev-Arnoldi iteration, since

this method is well suited to compute the relevant lowest energy states. Poisson's equation is solved by Newton-Raphson method with inexact line search. Solving this sparse linear system at each iteration step is accomplished by a version of the preconditioned conjugate gradient method.

In order to validate the results obtained by the predictor-corrector method, comparison of the method was done with the well known fast adaptive underrelaxation scheme, which is an adaptive nonlinear version of the standard Gauss-Seidel algorithm. The comparison which is validated against the standard Gauss-Seidel method shows faster convergence using the predictor-corrector method. The numerical experiments carried out in this review are for two dimensional devices.

3.2.2 Review of the accelerated algorithm for 2D simulations of the quantum ballistic transport in nanoscale MOSFETs [6]

Abdallah et al.'s work develops a new and powerful model which is described as Sub-band Decomposition Method/Wentzel, Kramers and Brillouin (SDM/WKB) which is an extension of the WKB method [6]. This new method has shown considerable gain in computation time over the SDM through the use of WKB techniques and thus reducing the numerical cost of computation. Here SDM refers to the subband decomposition method and WKB is a method of finding approximate solutions to linear partial differential equations with spatially varying coefficients.

In the SDM method a two-dimensional solution of the self-consistent

Schroedinger equation with open boundary conditions (current carrying) is sought. In modern devices, electron gas is confined in one or more directions thus reducing the dimensions of the propagation space. It is assumed that the electron gas is confined in the z direction and a decomposition of the wave function is considered:

$$\psi_\epsilon(x, z) = \sum_i \varphi_\epsilon^i(x) \chi_i(z; x), \quad (3.10)$$

where φ_ϵ^i represents the longitudinal wave functions and X_i are the transversal wave functions.

In the 2D domain, Schroedinger's equation is

$$-\frac{\hbar^2}{2} \frac{1}{m_z(z)} \Delta_x \psi_\epsilon(x, z) - \frac{\hbar^2}{2} \frac{\partial}{\partial z} \left(\frac{1}{m_z(z)} \frac{\partial}{\partial z} \psi_\epsilon(x, z) \right) + V(x, z) \psi_\epsilon(x, z) = \epsilon \psi_\epsilon(x, z) \quad (3.11)$$

Using equation (3.10), the solution of equation (3.11) is replaced by the solution of 1D eigenvalue problems in the confined direction z :

$$\begin{aligned} \frac{\hbar^2}{2} \frac{\partial}{\partial z} \left(\frac{1}{m_z(z)} \frac{\partial}{\partial z} X_i(z; x) \right) + V(x, z) X_i(z; x) &= \\ &= E_i(x) X_i(z; x), \end{aligned} \quad (3.12)$$

$\int_0^1 |X_i(z; x)|^2 dz = 1$ and the other resulting coupled one-dimensional Schroedinger equations are projected on the transport direction x :

$$\begin{aligned} -\frac{d}{dx^2} \varphi_\epsilon^i(x) - 2 \sum_{j=1}^{\infty} a_{ij}(x) \frac{d}{dx} \varphi_\epsilon^j(x) - \\ - \sum_{j=1}^{\infty} \left(b_{ij}(x) + \frac{2}{\hbar^2} c_{ij}(x) (\epsilon - E_j(x)) \right) \varphi_\epsilon^j(x) = 0. \end{aligned} \quad (3.13)$$

As a result the size of the linear system which one needs to solve is reduced from $N_x \times N_z$ for the original two-dimensional model to one of the form

$N_x \times M$ for the subband decomposition method. Here N_x and N_z are the number of grid points respectively in the transport and confined directions. M represents the number of transverse modes which are taken into consideration.

The new SDM/WKB is essentially an improvement in the SDM through the use of WKB techniques, thus a reduction in the numerical cost of simulating the Schroedinger-Poisson model. The SDM/WKB method uses oscillating interpolation functions instead of polynomial (which are used in the SDM) functions for the solution of the 1D Schroedinger's equation, resulting in significant reduction in the number of grid points in the x direction. Using the coupled one-dimensional Schroedinger equations (3.13) with a finite number of subbands which are denoted by M and define $\Phi := (\varphi_\epsilon^i)_{i=1}^M$, $A := (a_{ij})_{i,j=1}^M$, $B := (b_{ij})_{i,j=1}^M$ and $C := (2c_{ij}(\epsilon - E_j))_{i,j=1}^M$, equation (3.13) is

$$-\hbar^2 \Phi_{xx}(x) - 2\hbar^2 A(x) \Phi_x(x) - \hbar^2 B(x) \Phi(x) - C(x) \Phi(x) = 0, \quad (3.14)$$

where $x \in [a, b]$. In order to solve equation (3.14), an approximate solution is of the form

$$\Phi(x) = e^{\frac{i}{\hbar} S(x)} \vec{e}(x), \quad (3.15)$$

with $\vec{e}(x) = \alpha(x) \vec{u}(x)$ where $|\vec{u}(x)| = 1, \forall x, \forall \hbar$. Substituting (3.15) into (3.14) and neglecting terms in \hbar^2 , results in the equation

$$-2i\hbar S_x \vec{u}_x - 2i\hbar S_x \alpha \vec{u}_x - i\hbar S_{xx} \alpha \vec{u} + (S_x)^2 \alpha \vec{u} - 2i\hbar S_x \alpha A \vec{u} - \alpha C \vec{u} = 0.$$

A close examination of this equation suggests that it can be solved if it is decomposed into two equations, namely

$$-2i\hbar S_x \vec{u}_x + (S_x)^2 \vec{u} - 2i\hbar S_x A \vec{u} - C \vec{u} = 0 \quad (3.16)$$

and

$$2S_x\alpha_x + S_{xx}\alpha = 0. \quad (3.17)$$

Now both S and \vec{e} depend on \hbar , then rewrite equation (3.17) as

$$((S_{\hbar})_x(\alpha_{\hbar})^2)_x = 0,$$

which suggests that $(S_{\hbar})_x \neq 0$ and $\alpha_{\hbar}(x) = \frac{c}{\sqrt{|(S_{\hbar})_x|}}$, $c \in C$. Expand \vec{u}_{\hbar} and S_{\hbar} in powers of \hbar , substitute these into equation (3.16), compare terms of the same order in \hbar and take zeroth and first order terms give the equations

$$\left(\frac{d}{dx}S^0\right)^2(x)u^0(x) = C(x)u^0(x), \quad (3.18)$$

$$S(x) = 0, \quad (3.19)$$

where

$$S(x) = -2\iota(S^0)_x(u^0)_x + (S^0)_x^2 u^1 + 2(S^0)_x(S^1)_x u^0 - 2\iota(S^0)_x A u^0 - C u^1.$$

It is reported in [6] that the term u^1 will only increase the simulation cost and offer no significant gain in accuracy, therefore it is omitted and the contribution of the zeroth order term u^0 is only considered.

Then an approximate solution to equation (3.14) can be written in the form $\Phi(x) = T(x)\xi(x)$ where $T(x)$ and $\xi(x)$ are defined in [6]. This produces a numerical scheme such that the entire wave function can be expressed by means of the so-called WKB basis functions. The discretisation which is then employed is a finite volume method.

3.2.2.1 Validation of Results in [6]

The efficiency of the SDM/WKB method is illustrated by extensive comparisons with the SDM. The channel length of the device under consideration

in this review is 10 nm. Currently, experimental results do not exist because devices of this size are yet to be achieved in practice. Analytical solutions are not found in literature either. Therefore, in order to validate the results of the new SDM/WKB, comparisons are made with a reference solution which is obtained by the well known standard full 2D finite element method on a fine grid of mesh size $N_x = 540, n_z = 210$. Here both the SDM and the SDM/WKB methods are compared with the standard finite element method in terms of accuracy and speed. The SDM/WKB very accurately produces approximate solution to the Schroedinger-Poisson equation when checked against the finite element results and shows improved simulation times compared to the SDM method. The devices considered in this paper are 3D.

3.2.3 Review of efficient solution of the Schroedinger-Poisson equations in layered semiconductor devices [12]

Anderson [12] reviews approximation models for the coupled system of Schroedinger-Poisson equations. The system of equations considered is

$$\begin{aligned} \nabla \cdot (\vec{\kappa}(\vec{X}) \cdot \nabla \phi(\vec{X})) &= M(\vec{X}), \\ -\frac{\hbar^2}{2} \nabla \cdot (\vec{\beta}(\vec{X})) \cdot \nabla \Psi(\vec{X}) + [\phi(\vec{X}) + \Delta E_c(\vec{X})] \Psi(\vec{X}) &= E \Psi(\vec{X}) \end{aligned} \quad (3.20)$$

where

$$M(\vec{X}) = q(\sigma_b(\vec{X}) - N_D(\vec{X}) - n(\vec{X})).$$

The vector of dielectric coefficients is $\vec{\kappa}(\vec{X})$, E is the energy, $\vec{\beta}(\vec{X})$ is the vector of effective mass coefficients, in the vertical direction, piecewise constants

functions are ΔE_c , also $\sigma_b(\vec{X})$ is a background hole density and the density of bound states electrons is denoted by $n(\vec{X})$.

When the potential in a device has variation only in the vertical direction, $\phi(x, y, z) = \phi(z)$, and if there is no transverse variation in the boundary conditions, then the dielectric constants, the doping density and the background hole concentrations will be functions of the vertical z coordinate. In addition, if the effective mass coefficients takes the form $\vec{\beta}(\vec{X}) = \vec{\beta}(z) = \left(\frac{1}{m_x^*}, \frac{1}{m_y^*}, \frac{1}{m_z^*} \right)$, then the 3D eigenfunction is given as

$$\Psi(x, y, z) = \eta(z) e^{2\pi i k_x \frac{x}{D}} e^{2\pi i k_y \frac{y}{D}}, \quad (3.21)$$

where D represents the size of the periodic domain in the transverse directions. Substituting $\phi(x, y, z) = \phi(z)$ and equation (3.20) into (3.19), applying the separation of variable technique and making $D \rightarrow \infty$ result in the reduction of the 3D system (3.20) to the 1D system

$$\begin{aligned} \frac{d}{dz} \left(\kappa(z) \frac{d\phi(z)}{dz} \right) &= N(z), \\ -\frac{\hbar^2}{2} \frac{d}{dz} \left(\beta_z(z) \frac{d\eta}{dz} \right) + [\phi(z) + \Delta E_c(z)] \eta(z) &= E\eta(z), \end{aligned} \quad (3.22)$$

where $N(z) = q(\sigma_d(z) - n^1(z) - N_D(z))$, $\beta_z(z) = \frac{1}{m_z^*(z)}$ and $n^{(1)}(z) = 2 \sum_{E_k < E_F} D_k^2 \eta_k^*(z) \eta_k^*(z)$. The 2D density of states functional is

$$D_k^{(2)} = \begin{cases} \frac{(E_F - E_k) \sqrt{|m_y| |m_x|}}{2\pi \hbar^2} & E_k < E_F, \\ 0 & E_k \geq E_F. \end{cases} \quad (3.23)$$

In the case where the potential has transverse variation in one direction, then $\phi(X, y, z) = \phi(y, z)$ resulting in eigenfunctions of the form $\Psi(X, y, z) = \eta(y, z) e^{2\pi i k_x \frac{x}{D}}$. Following a similar procedure as that outlined above in the

1D case, results in the reduced 2D Schroedinger-Poisson system

$$\begin{aligned}\nabla \cdot (\kappa(y, z) \nabla \phi(y, z)) &= q\rho(y, z), \\ -\frac{\hbar^2}{2} \nabla \cdot (\vec{\beta}(y, z) \cdot \nabla \eta(y, z)) + H(y, z) \eta(y, z) &= E\eta(y, z),\end{aligned}$$

where

$$\rho(y, z) = \sigma_b(y, z) - n^{(2)}(y, z) - N_D(y, z), \quad (3.24)$$

$$H(y, z) = \phi(y, z) + \Delta E_c(y, z) \quad (3.25)$$

and

$$n^{(2)}(y, z) = 2 \sum_{E_F < E_k} D_k^{(1)} \eta_k^*(y, z) \eta_k(y, z). \quad (3.26)$$

The 1D density of states functional is given as

$$D_k^{(1)} = \begin{cases} -\frac{\sqrt{2(E_F - E_k)} \sqrt{|m_X|}}{\pi \hbar} & E_k < E_F, \\ 0 & E_k \geq E_F. \end{cases} \quad (3.27)$$

A very important feature of the system of equations (3.20) is that it is separable, thus a reduction in the dimension of the eigenvalue problem is achievable. Given this feature, additional approximation to the system can be achieved by retaining the original form of ϕ in Poisson's equation (3.20) and approximate the electrostatic potential ϕ in Schroedinger's equation (3.20). A suitable approximate potential is

$$\Phi(\vec{x}) = \tilde{\phi}_1(z) + \tilde{\phi}_2(x, y), \quad (3.28)$$

where

$$\tilde{\phi}_1(z) = \frac{1}{L_x L_y} \int \int \phi(x, y, z) dx dy - \frac{1}{2} \bar{\phi} \quad (3.29)$$

and

$$\tilde{\phi}_2(x, y) = \frac{1}{L_z} \int \phi(x, y, z) dz - \frac{1}{2} \bar{\phi}. \quad (3.30)$$

Furthermore, a rectangular domain is assumed with side lengths L_x , L_y and L_z and

$$\bar{\phi} = \frac{1}{L_x L_y L_z} \int \int \int \phi(x, y, z) dx dy dz. \quad (3.31)$$

Therefore, replacing ϕ in (3.20) with (3.28) results in the 3D separable approximation

$$\nabla \cdot (\vec{\kappa}(\vec{x}) \cdot \nabla \phi(\vec{x})) = q\rho(\vec{x}), \quad (3.32)$$

$$-\frac{\hbar^2}{2} \frac{d}{dz} (\beta_z(z) \frac{d\eta}{dz}) + [\tilde{\phi}_1(z) + \Delta E_c(z)] \eta(z) = \lambda \eta(z), \quad (3.33)$$

$$-\frac{\hbar^2}{2} \left(\frac{\partial}{\partial x} \left(\beta_x \frac{\partial \gamma}{\partial y} \right) + \frac{\partial}{\partial y} \left(\beta_y \frac{\partial \gamma}{\partial x} \right) \right) + \tilde{\phi}_2(x, y) \gamma(x, y) = \mu \gamma(x, y) \quad (3.34)$$

In a similar manner, approximation for the 2D Schroedinger-Poisson equations can be derived along with those approximations which are constructed via charge densities which do not require a numerical solution of the Schroedinger operator. For the Schroedinger's equation in the transverse directions, high order finite difference approximations are used and a finite volume discretisation method is used in the vertical direction. For the 2D and 3D cases where only a certain range of eigenvalues are required, the approach is to follow the same procedure reported in [91]. On the other hand, the method of solution of the 1D Poisson equation follows the procedure outlined in [12]. The 2D and 3D cases use basis functions in the vertical direction.

Given these simplified models, the task is to implement them using efficient algorithmic procedures in order to simulate accurately and efficiently

layered semiconductor devices. A close examination of equation (3.20) as well as the various approximations which are outlined above suggest the general structure

$$L\phi = S(\Psi), \quad (3.35)$$

$$H(\phi)\Psi = E\Psi. \quad (3.36)$$

L is the Poisson operator and the source term is given by $S(\Psi)$. The Schroedinger operator which depends on the electrostatic potential ϕ is $H(\phi)$. Now $S(\Psi)$ can be computed for any given ϕ , therefore equations (3.35) and (3.36) are combined to give

$$L\phi = S(\Psi(\phi)). \quad (3.37)$$

By using the inverse of the Poisson's operator L^{-1} equation (3.37) reduces to

$$L^{-1}S(\Psi(\phi)) - \phi = 0. \quad (3.38)$$

The form of (3.38) enables solution by evolving the partial differential equation

$$\frac{\partial \phi}{\partial t} = L^{-1}S(\Psi(\phi)) - \phi \quad (3.39)$$

to steady-state by using a "method of lines" approach as well as specially designed explicit stabilised Runge-Kutta methods to solve the resulting ordinary differential equations.

3.2.3.1 Validation of Results in [12]

The simulation results obtained with the simplified models are validated and compared with the finite element solution of the original quantum model

given in equation (3.20) for accuracy. Improved simulation time of more than an order of magnitude less than the solution obtained by solving the original system of Schroedinger-Poisson equations is achieved compared to the standard finite element method. The 3D device considered in this paper is also analysed in 1D and 2D.

3.2.4 Review of the fast convergent Schroedinger-Poisson solver for the static and dynamic analysis of carbon nanotube field effect transistors by Pourfath et al [74]

Carbon nanotubes (CNTs) have special electronic and mechanical properties making them a candidate for nanoscale field effect transistors (FETs). In order to study the static response of carbon nanotube field effect transistors (CNTFETs), the coupled system of Schroedinger-Poisson equations is solved. This system is given in [74] as

$$\frac{\partial^2 V}{\partial \rho^2} + \frac{1}{\rho} \frac{\partial V}{\partial \rho} + \frac{\partial^2 V}{\partial z^2} = -\frac{Q}{\epsilon} \quad (3.40)$$

$$-\frac{\hbar^2}{2m^*} \frac{\partial^2 \Psi_{s,d}^{n,p}}{\partial z^2} + (U^{n,p} - E) \Psi_{s,d}^{n,p} = 0. \quad (3.41)$$

Equation (3.40) is Poisson's equation in two-dimensions whilst the one-dimensional Schroedinger's equation is given by (3.41). The electrostatic potential in (3.40) is $V(\rho, z)$ and the space charge is Q . In Schroedinger's equation, m^* is the effective mass for both electrons and holes. $\Psi_{s,d}^{n,p}$ is the wave function, where the superscripts denote the type of carrier and the subscripts d and s represent the source and drain contacts. U^n is the potential energy [74].

In equation (3.40), the space charge Q is computed by the formula

$$Q = \frac{q(p - n)\delta(\rho - \rho_{cnt})}{2\pi\rho}, \quad (3.42)$$

where q is the electronic charge, n and p are total electron and hole concentrations per unit length [74], δ is the delta function in cylindrical coordinates.

And the total electron concentration in the CNT is given by

$$\begin{aligned} n &= \frac{4}{2\pi} \int f_s |\Psi_s^n|^2 dk_s + \frac{4}{2\pi} \int f_d |\Psi_d^n|^2 dk_d \\ &= \int \frac{\sqrt{2m^*}}{\pi\hbar\sqrt{E_s}} f_s |\Psi_s|^2 dE_s + \int \frac{\sqrt{2m^*}}{\pi\hbar\sqrt{E_d}} f_d |\Psi_d|^2 dE_d. \end{aligned} \quad (3.43)$$

In equation (3.43), the equilibrium Fermi functions at the source and drain contacts are $f_{s,d}$. Finally, the current in the device is calculated by the formula

$$I^{n,p} = \frac{4q}{\hbar} \int [f_s^{n,p}(E) - f_d^{n,p}(E)] T_c^{n,p}(E) dE, \quad (3.44)$$

where the transmission coefficients of electrons and holes are $T_c^{n,p}(E)$.

The system of Schroedinger-Poisson equations in (3.40) and (3.41) is solved iteratively using an appropriate numerical damping factor α [74]. Schroedinger's equation (3.41) is solved at the $(k + 1)^{th}$ iteration by using the old electrostatic potential V^k . Subsequently the charge density Q^{k+1} is computed and Poisson's equation is solved using the updated Q^{k+1} . An intermediate new electrostatic V_{int}^{k+1} is calculated. Consequently, the potential is computed as:

$$V^{k+1} = \alpha V_{int}^{k+1} + (1 - \alpha)V^k, \quad (3.45)$$

where $0 < \alpha < 1$. The process then continues until convergence is achieved.

The damping factor α is not known in advance so it has to be set at an initial value. If this value is too high, oscillations may occur. If it is set at a low

value, the simulations will take too long. However, if the carrier concentration is appropriately evaluated this problem can be avoided [74]. To achieve this, the integrals in equations (3.43) and (3.44) are computed accurately by an adaptive method. In this method, one uses the fact that in (3.43) and (3.44) the integration is computed in an energy interval $[E_{min}, E_{max}]$.

These integrals in (3.43) and (3.44) are then computed by two integration methods, I_1 and I_2 , where explicit expressions for I_1 and I_2 are given in [74]. If the absolute difference between the results of these two methods is less than some predefined tolerance, the integration is accepted. If not, $[E_{min}, E_{max}]$ is divided into two parts and I_1 and I_2 are computed separately.

3.2.4.1 Validation of Results in [74]

In order to validate the effectiveness of the adaptive integration method, [74], the results are compared with experimental data reported in [51] and there is good agreement between experimental and simulation results.

3.3 Summary

In summary, this chapter demonstrates how the coupled system of equations may be solved efficiently by employing various robust numerical techniques, such as the conjugate gradient and the incomplete Cholesky methods. Moreover, one key feature of all the solution techniques requires some computational procedure to achieve speed and minimize computer resources. As speed and computer resource are key features in any simulation process, the need for analytical solutions is a reality. To this end, analytical solutions

are known, however, only in one-dimensional cases. This thesis develops proposed models for 1D, 2D and 3D Schroedinger-Poisson's equations and presents semi-analytical solutions. It is to this analysis that the next chapters are devoted.

Chapter 4

Semi-Analytical Solutions of Poisson's Equation

Solving the coupled system of Schroedinger-Poisson's equations is a challenging task. Therefore, in order to overcome this problem, this chapter presents semi-analytical solutions to one dimensional (1D), two-dimensional (2D) and three-dimensional (3D) Poisson's equations. The goal here is to create proposed models and hence semi-analytical solutions to these models which can be used to efficiently analyse the Schroedinger-Poisson model [6, 12, 91].

In particular, this chapter analyses the theory of solutions of well known differential equations and combines this analysis with the original method developed in this thesis to reduce the coupled system of equations to a quasi-Poisson's for which semi-analytical solutions can be easily obtained. An excellent review of analytical methods for solving Poisson's equation is given in [37, 38, 58, 81, 96].

The proposed method uses the Wronskian [40] of solutions of the homo-

geneous Poisson's equation. This Wronskian is extended to two and three dimensions and has proved to be instrumental in finding semi-analytical solutions to Poisson's equation. With the successful solution of Poisson's equation, one wishes to use this to solve Schroedinger's equation. Since the system of equations is coupled, expressions for the wave functions $\psi_1(x, y, z)$ and $\psi_2(x, y, z)$ have to be found. Finding these expressions requires the application of the Evans function techniques (to be discussed in the next chapter) to the Schroedinger's equation. By substituting $\phi(0, 0, 0)$ into Schroedinger's equation, this thesis addresses in the next chapter the challenge of finding semi-analytical solutions (wave functions) for the Schroedinger's equation. The Wronskian and Evans function techniques are described in detail in Appendices C and D.

Before looking at this coupled system of equations, it is essential to develop a detailed analysis of the general Poisson's equation which is essential in device analysis. Therefore, for 3D, 2D and 1D Poisson's equations, respectively, the following notations are adapted.

$$\frac{\partial^2 \phi(x, y, z)}{\partial x^2} + \frac{\partial^2 \phi(x, y, z)}{\partial y^2} + \frac{\partial^2 \phi(x, y, z)}{\partial z^2} = \phi_{xx} + \phi_{yy} + \phi_{zz}, \quad (4.1)$$

$$\frac{\partial^2 \phi(x, y)}{\partial x^2} + \frac{\partial^2 \phi(x, y)}{\partial y^2} = \phi_{xx} + \phi_{yy} \quad (4.2)$$

and

$$\frac{\partial^2 \phi(x)}{\partial x^2} = \phi_{xx}. \quad (4.3)$$

In this thesis an effective technique based on the application of hyperbolic functions is shown to be extremely useful in obtaining semi-analytical solu-

tions to Poisson's equation. Before discussing Poisson's equation it is useful to briefly present background analysis and justification of this method.

Consider equation (2.9) which was briefly introduced in Chapter 2. This equation exhibits important features: its solution can be found by the method of variation of parameters [34, 75, 88] and it can be easily transformed into a differential equation with variable coefficients. To this transformed equation one can apply power series methods to find the general solution. This equation is of the form

$$w_{xx} + 2\operatorname{sech}^2(x)w = b(x), \quad (4.4)$$

where $w = w(x)$ is the unknown function. With $b(x) = 0$, this equation has two linearly independent solutions

$$w_1(x) = \tanh(x), \quad (4.5)$$

$$w_2(x) = \tanh(x)(x - \operatorname{coth}(x)). \quad (4.6)$$

Using the method of variation of parameters, the two linearly independent solutions and taking $b(x) \neq 0$, the general solution to equation (4.7) is given as

$$w(x) = a\phi_1(x) + b\phi_2(x) + \int_{x_0}^x k(s, x)b(s)ds, \quad (4.7)$$

where

$$k(s, x) = \phi_1(s)\phi_2(x) - \phi_1(x)\phi_2(s)$$

and a, b are arbitrary constants. This solution technique is very important and will be seen later in this work to be instrumental in developing the original semi-analytical method for the solutions to 2D and 3D Poisson's equations.

4.1 Semi-analytical solution to 3D Poisson's model

With this as background, consider the 3-D Poisson's model [91] which is given as:

$$\nabla \cdot (\epsilon \nabla \phi(x, y, z)) = \rho(\phi(x, y, z)), \quad (4.8)$$

$$\nabla \cdot (\epsilon \nabla \phi(x, y, z)) = -q[-n + p(\phi(x, y, z)) + N_D^+(\phi(x, y, z)) - N_A^-(\phi(x, y, z))],$$

where $\epsilon = \epsilon(z)$ is the dielectric constant, q is the unit electric charge, $p(x, y, z)$ is the hole density, and $N_D^+(\phi(x, y, z))$ and $N_A^-(\phi(x, y, z))$ are the ionised donor and acceptor concentrations. Furthermore, let $\phi = \phi(x, y, z)$, one has

$$p(\phi) = 2 \left(\frac{m_{dh} k_B T}{2\pi \hbar^2} \right)^{\frac{3}{2}} \wp_{\frac{1}{2}} \left(\frac{-q\phi + V_h - E_G - E_F}{k_B T} \right), \quad (4.9)$$

$$N_D^+(\phi) = N_D \left(1 + g_D \exp \left(\frac{E_F + q\phi - V_h + E_d}{k_B T} \right) \right)^{-1}, \quad (4.10)$$

$$N_A^-(\phi) = N_A \left(1 + g_A \exp \left(\frac{-q\phi + V_h - E_G + E_a - E_F}{k_B T} \right) \right)^{-1}.$$

Here N_D and N_A are the donor and acceptor concentrations, E_d and E_a are the donor and acceptor atom ionisation energies, g_D and g_A are their respective ground state level degeneracies. E_G is the band gap and m_{dh} is the density-of-state mass of the valence band and define the Fermi-Dirac integral [67] as

$$\wp_j(x) = \frac{1}{\Gamma(1+j)} \int_0^\infty \frac{t^j dt}{e^{t-x} + 1}. \quad (4.11)$$

The approximate but compact truncated series representation of the Fermi-Dirac integral is given as

$$\begin{aligned} \wp_{\frac{1}{2}}(x) &= -23.51121 + 2.8356x + 0.05585x^2 + 0.000713x^3 \quad (4.12) \\ &- 0.000022x^4 + (8\pi)^{\frac{1}{2}}[(\sqrt{P} - x)^{\frac{1}{2}} + (\sqrt{Q} - x)^{\frac{1}{2}}], \end{aligned}$$

$$\begin{aligned} \wp_{-\frac{1}{2}}(x) &= 2.8356 + 0.1117x + 0.002138x^2 - 0.000086x^3 \quad (4.13) \\ &- (2\pi)^{\frac{1}{2}}\left[\left(\frac{\sqrt{P} - x}{P}\right)^{\frac{1}{2}} + \left(\frac{\sqrt{Q} - x}{Q}\right)^{\frac{1}{2}}\right], \end{aligned}$$

where $P = (x^2 + \pi^2)$, $Q = (x^2 + 9\pi^2)$ and for $j = \frac{1}{2}$ and $j = -\frac{1}{2}$.

For the electron density n occurring in equation (4.8) one uses the semi-classical expression [91]

$$n(\phi) = 2 \left(\frac{m_{de} k_B T}{2\pi \hbar^2} \right)^{\frac{3}{2}} \wp_{\frac{1}{2}} \left(\frac{E_F + q\phi - V_h}{k_B T} \right), \quad (4.14)$$

where m_{de} is the density-of-state mass of the conduction band.

In order to obtain a semi-analytical solution for equation (4.8), write it in rectangular coordinates as

$$\begin{aligned} \epsilon(z) \left(\frac{\partial^2 \phi(x, y, z)}{\partial x^2} + \frac{\partial^2 \phi(x, y, z)}{\partial y^2} + \frac{\partial^2 \phi(x, y, z)}{\partial z^2} \right) + \frac{\partial \epsilon(z)}{\partial z} \frac{\partial \phi(x, y, z)}{\partial z} \quad (4.15) \\ = q[-n + p(\phi) + N_D^+(\phi) - N_A^-(\phi)], \end{aligned}$$

where $\phi = \phi(x, y, z)$ and consider the homogeneous equation

$$\frac{\partial^2 \phi(x, y, z)}{\partial x^2} + \frac{\partial^2 \phi(x, y, z)}{\partial y^2} + \frac{\partial^2 \phi(x, y, z)}{\partial z^2} = 0. \quad (4.16)$$

It is verified in Appendix A that a general solution to equation (4.16) is given as

$$\phi(x, y, z) = \tanh(x + i\sqrt{3}y - \sqrt{2}z). \quad (4.17)$$

Therefore, (4.16) may be recast as

$$\frac{\partial^2 \phi(x, y, z)}{\partial x^2} + 2\operatorname{sech}^2(x + \iota\sqrt{3}y - \sqrt{2}z)\phi(x, y, z) = 0. \quad (4.18)$$

Using the expression given in (4.17), a solution to equation (4.18) is given as

$$\phi(x, y, z) = \tanh(x + \iota\sqrt{3}y - \sqrt{2}z). \quad (4.19)$$

In order to find a second solution for equation (4.18), let

$$\phi(x, y, z) = \tanh(x + \iota\sqrt{3}y - \sqrt{2}z)v(x, y, z)$$

and substitute this into (4.18) to obtain

$$\frac{\partial^2 v(x, y, z)}{\partial x^2} + \frac{2\operatorname{sech}^2(x + \iota\sqrt{3}y - \sqrt{2}z)}{\tanh(x + \iota\sqrt{3}y - \sqrt{2}z)} \frac{\partial v(x, y, z)}{\partial x} = 0. \quad (4.20)$$

To solve equation (4.20), let

$$\frac{\partial v(x, y, z)}{\partial x} = r(x, y, z).$$

This implies that

$$\frac{\partial^2 v(x, y, z)}{\partial x^2} = \frac{\partial r(x, y, z)}{\partial x}.$$

Therefore, equation (4.20) reduces to the first order differential equation

$$\frac{\partial r(x, y, z)}{\partial x} + \frac{2\operatorname{sech}^2(x + \iota\sqrt{3}y - \sqrt{2}z)}{\tanh(x + \iota\sqrt{3}y - \sqrt{2}z)} r(x, y, z) = 0. \quad (4.21)$$

To solve equation (4.21), let

$$u = \tanh(x + \iota\sqrt{3}y - \sqrt{2}z).$$

Then

$$\frac{du}{dx} = \operatorname{sech}^2(x + \iota\sqrt{3}y - \sqrt{2}z)$$

and

$$dx = \frac{du}{\operatorname{sech}^2(x + \iota\sqrt{3}y - \sqrt{2}z)},$$

hence equation (4.21) becomes

$$\frac{\partial r(x, y, z)}{\partial u} + \frac{2}{u}r(x, y, z) = 0. \quad (4.22)$$

Using the integrating factor $r = e^{-\int \frac{2}{u} du}$, one obtains

$$r(x, y, z) = \frac{1}{\tanh^2(x + \iota\sqrt{3}y - \sqrt{2}z)}.$$

Integration of $r(x, y, z)$ gives

$$v(x, y, z) = x - \operatorname{coth}(x + \iota\sqrt{3}y - \sqrt{2}z),$$

resulting in the second solution one needs. Again, this second solution can be easily verified. Thus, two solutions to equation (4.18) are given as

$$\phi_1(x, y, z) = \tanh(x + \iota\sqrt{3}y - \sqrt{2}z) \quad (4.23)$$

and

$$\phi_2(x, y, z) = \tanh(x + \iota\sqrt{3}y - \sqrt{2}z)(x - \operatorname{coth}(x + \iota\sqrt{3}y - \sqrt{2}z)). \quad (4.24)$$

Therefore, the approximate semi-analytical solution to (4.15) is given as

$$\phi(x, y, z) = \alpha_1\phi_1 + \alpha_2\phi_2 + \int_{x_0}^x \int_{z_0}^z \int_{y_0}^y K(x, y, z, a, b, c)\varphi(a, b, c) da db dc,$$

where

$$K(x, y, z, a, b, c) = \phi_1(a, b, c)\phi_2(x, y, z) - \phi_1(x, y, z)\phi_2(a, b, c),$$

$$\varphi(a, b, c) = \frac{q}{\epsilon(c)} (-n + p(\phi(a, b, c)) + N_D^+(\phi(a, b, c)) - N_A^-(\phi(a, b, c))) - V(a, b, c),$$

$$V(a, b, c) = \frac{1}{\epsilon(c)} \frac{\partial \epsilon(c)}{\partial c} \frac{\partial \phi(a, b, c)}{\partial c},$$

$$\phi_1 = \phi_1(x, y, z),$$

$\alpha_i = 1, 2.$ is some arbitrary constant and

$$\phi_2 = \phi_2(x, y, z).$$

4.2 Semi-analytical solution to 2D Poisson's model

If the potential in the device has variation in the vertical direction z and a single transverse direction x , then equation (4.15) may be reduced to the two-dimensional differential equation (model) namely

$$\begin{aligned} \epsilon(z) \left(\frac{\partial^2 \phi(x, z)}{\partial x^2} + \frac{\partial^2 \phi(x, z)}{\partial z^2} \right) + \frac{\partial \epsilon(z)}{\partial z} \frac{\partial \phi(x, z)}{\partial z} \\ = q[-n + p(\phi) + N_D^+(\phi) - N_A^-(\phi)], \end{aligned} \quad (4.25)$$

which by equations (4.17), (4.18), (C.11), (C.12) and (C.13) can be written approximately and conveniently as

$$\frac{\partial^2 \phi(x, z)}{\partial x^2} + 2\text{sech}^2(x - \sqrt{2}z)\phi(x, z) + \frac{1}{\epsilon(z)} \frac{\partial \epsilon(z)}{\partial z} \frac{\partial \phi(x, z)}{\partial z} = \varphi(\phi(x, z))$$

where

$$\varphi(\phi(x, z)) = \frac{q}{\epsilon(z)} [-n + p(\phi(x, z)) + N_D^+(\phi(x, z)) - N_A^-(\phi(x, z))].$$

Using the same techniques as in the three dimensional case, one finds that two solutions of this equation when $\varphi(\phi(x, z)) = 0$ are

$$\phi_1(x, z) = \tanh(x - \sqrt{2}z) \quad (4.26)$$

and

$$\phi_2(x, z) = \tanh(x - \sqrt{2}z)(x - \coth(x - \sqrt{2}z)) \quad (4.27)$$

with

$$\lim_{x, z \rightarrow 0} [\phi_1(a, c)\phi_2(x, z) - \phi_1(x, z)\phi_2(a, c)] = \frac{1}{\sqrt{2}} \tanh(a - \sqrt{2}c).$$

Therefore, the approximate semi-analytical solution to equation (4.25) is given as

$$\phi(x, z) = \alpha_1 \phi_1(x, z) + \alpha_2 \phi_2(x, z) + \int_{x_0}^x \int_{z_0}^z K(x, z, a, c) \varphi(a, c) da dc,$$

where

$$K(x, z, a, c) = \phi_1(a, c)\phi_2(x, z) - \phi_1(x, z)\phi_2(a, c),$$

$$\varphi(a, c) = \frac{q}{\epsilon(c)} (-n + p(\phi(a, c)) + N_D^+(\phi(a, c)) - N_A^-(\phi(a, c))) - V_1(a, c),$$

and

$$V_1(a, c) = \frac{1}{\epsilon(c)} \frac{\partial \epsilon(c)}{\partial c} \frac{\partial \phi(a, c)}{\partial c}.$$

4.3 Semi-analytical solution to 1D Poisson's model

Finally, for the one-dimensional (1D) case one may write equation (4.25) as

$$\frac{\partial^2 \phi(z)}{\partial z^2} + 4 \operatorname{sech}^2(\sqrt{2}z) \phi(z) + \frac{1}{\epsilon(z)} \frac{\partial \epsilon(z)}{\partial z} \frac{\partial \phi(z)}{\partial z} = \varphi(\phi(z)) \quad (4.28)$$

where

$$\varphi(\phi(z)) = \frac{q}{\epsilon(z)} [-n + p(\phi(z)) + N_D^+(\phi(z)) - N_A^-(\phi(z))].$$

As in the 2D and 3D cases above, one finds that two solutions of this equation are

$$\phi_1(z) = -\tanh(\sqrt{2}z) \quad (4.29)$$

and

$$\phi_2(z) = -\tanh(\sqrt{2}z)\left(z - \frac{\coth(\sqrt{2}z)}{\sqrt{2}}\right) \quad (4.30)$$

with

$$\lim_{z \rightarrow 0} [\phi_1(s)\phi_2(z) - \phi_1(z)\phi_2(s)] = -\frac{1}{\sqrt{2}} \tanh(\sqrt{2}s).$$

Therefore, the approximate semi-analytical solution to (4.28) is given as

$$\phi(z) = \alpha_1\phi_1(z) + \alpha_2\phi_2(z) + \int_{z_0}^z K(s, z)\varphi(s, z) ds,$$

where

$$K(z, s) = \phi_1(s)\phi_2(z) - \phi_1(z)\phi_2(s)$$

and

$$\varphi(s) = \frac{q}{\epsilon(s)} \left(-n + p(\phi(s)) + N_D^+(\phi(s)) - N_A^-(\phi(s))\right) - \frac{1}{\epsilon(s)} \frac{\partial \epsilon(s)}{\partial s} \frac{\partial \phi(s)}{\partial s}.$$

In order to see how these various models may be used to find solutions to Poisson's equations, consider the two-dimensional example below.

4.4 Application to 2D Poisson equation

In order to test the proposed semi-analytical method, consider the two dimensional Poisson's equation [83]. Here the general solution is computed using the semi-analytical method and it is verified with the solution reported

in [83]. This is a general Poisson's equation and it is not based on any specific device geometry. It is given as

$$\frac{\partial^2 \phi(x, y)}{\partial x^2} + \frac{\partial^2 \phi(x, y)}{\partial y^2} = 10e^{2x+y}. \quad (4.31)$$

The homogeneous equation is given as

$$\frac{\partial^2 \phi(x, y)}{\partial x^2} + \frac{\partial^2 \phi(x, y)}{\partial y^2} = 0 \quad (4.32)$$

which has a solution

$$\phi(x, y) = \alpha \tanh(x + iy), \quad (4.33)$$

for arbitrary constant α . Using equation (4.33) gives

$$\frac{\partial^2 \phi(x, y)}{\partial x^2} = -2\alpha \operatorname{sech}^2(x + iy) \tanh(x + iy) \quad (4.34)$$

and

$$\frac{\partial^2 \phi(x, y)}{\partial y^2} = 2\alpha \operatorname{sech}^2(x + iy) \tanh(x + iy). \quad (4.35)$$

From (4.33), (4.34) and (4.35), equation (4.31) may be recast in the form

$$\frac{\partial^2 \phi(x, y)}{\partial x^2} + 2\operatorname{sech}^2(x + iy)\phi(x, y) = 10e^{2x+y}. \quad (4.36)$$

As before consider the homogeneous equation

$$\frac{\partial^2 \phi(x, y)}{\partial x^2} + 2\operatorname{sech}^2(x + iy)\phi(x, y) = 0. \quad (4.37)$$

It can be easily verified that equation (4.37) has two linearly independent solutions which are given as

$$\phi_1(x, y) = \alpha \tanh(x + iy) \quad (4.38)$$

and

$$\phi_2(x, y) = \alpha \tanh(x + iy) \left(y - \frac{1}{i \tanh(x + iy)} \right). \quad (4.39)$$

From equations (4.34 - 4.39), equation (4.31) has general solution

$$\phi(x, y) = \alpha \phi_1(x, y) + \alpha \phi_2(x, y) + \int_{y_0}^y \int_{x_0}^x k(s, x, y) b(a, s) ds da,$$

where

$$k(s, x, y) = \alpha \phi_1(x, s) \phi_2(x, y) - \alpha \phi_1(x, y) \phi_2(x, s).$$

Now $\lim_{x \rightarrow \pm\infty} k(s, x, y) = \alpha(y - s)$. Therefore, taking $\alpha = 2$ (α arbitrary), a particular solution to equation (4.37) is given as

$$\phi(x, y) = 2 \tanh(x + iy) + 2 \times 10 \int_{-\infty}^x \int_{-\infty}^y (y - s) e^{2\alpha+s} ds da \quad (4.40)$$

$$= 2 \tanh(x + iy) + 2e^{2x+y}, \quad (4.41)$$

which can easily be verified to satisfy equation (4.31). Consequently, this solution shows that the proposed semi-analytical method works and produces solutions which compare well with those found in literature [24, 83].

4.5 Application to 3D Schroedinger-Poisson equations for device modelling

Furthermore, the semi-analytical method can be extended to 3D Poisson's equation which is used for device modelling. As will be shown in Chapter 7, this method helps to speed up simulation times in device analysis. In [12],

the coupled system of Schroedinger-Poisson's equations is given as

$$\nabla \cdot (\kappa(z) \cdot \nabla \phi(\vec{x})) = q\rho(\vec{x}) \quad (4.42)$$

$$-\frac{\hbar^2}{2} \nabla \cdot (\beta(z) \nabla \psi(\vec{x})) + [\phi(\vec{x}) + \Delta E_c(z)] \psi(\vec{x}) = E \psi(\vec{x}) \quad (4.43)$$

In equation (4.42), $\kappa(z)$ is the vector of dielectric constant, $\rho(\vec{x})$ is the electron density and

$$\phi(\vec{x}) = \phi(x, y, z)$$

is the electrostatic potential. In equation (4.43),

$$\beta(\vec{x}) = \frac{1}{m_z^*(z)}$$

is the effective mass, $\Delta E_c(z)$ the pseudopotential energy, E the energy and

$$\psi(\vec{x}) = \psi(x, y, z)$$

is the wave function. In this application layered devices are considered, therefore, the dielectric constant, the effective mass and the pseudopotential energy are all piecewise constant functions in the vertical direction. The electron density is

$$\rho(\vec{x}) = N_D(x, y, z) + \sigma_b(x, y, z) - n(x, y, z)$$

and the density of bound state electron is

$$n(x, y, z) = 2 \sum_{E_k < E_F} \psi^*(x, y, z) \psi(x, y, z),$$

where $\psi^*(x, y, z)$ is the complex conjugate of $\psi(x, y, z)$, $N_D(x, y, z)$ is the ionised doping density and $\sigma_b(x, y, z)$ is a background hole concentration.

In rectangular coordinates, Poisson's equation (4.42) is given as

$$\begin{aligned} \kappa(z) \left(\frac{\partial^2 \phi(x, y, z)}{\partial x^2} + \frac{\partial^2 \phi(x, y, z)}{\partial y^2} + \frac{\partial^2 \phi(x, y, z)}{\partial z^2} \right) + \frac{\partial \kappa(z)}{\partial z} \frac{\partial \phi(x, y, z)}{\partial z} & (4.44) \\ & = q[-N_D(x, y, z) + \sigma(x, y, z) - n(x, y, z)]. \end{aligned}$$

Using the original methods which are developed in this thesis, rewrite Poisson's equation (4.42) as

$$\begin{aligned} \phi_{zz} + 4\text{sech}^2(x + i\sqrt{3}y - \sqrt{2}z)\phi(x, y, z) & = (4.45) \\ \frac{-1}{\kappa(z)} \frac{\partial}{\partial z} \kappa(z) \phi_z + \frac{q}{\kappa(z)} [-N_D(x, y, z) + \sigma_b(x, y, z) - n(x, y, z)]. & \end{aligned}$$

Explicit expressions for the ionised doping density $N_D(x, y, z)$, the background doping density $\sigma_b(x, y, z)$ and the electron density $n(x, y, z)$ are given as [12]:

$$\begin{aligned} N_D(x, y, z) & = \begin{cases} 3.5 \times 10^{11} \text{cm}^{-2} & \text{located at 40.5 nm} \\ 0.5 \times 10^{11} \text{cm}^{-2} & \text{located at 167.5 nm} \\ 0 & \text{otherwise,} \end{cases} \\ \sigma_b(x, y, z) & = \begin{cases} 3 \times 10^{15} \text{cm}^{-3} & \text{located in the InP layer} \\ 0 & \text{otherwise.} \end{cases} \end{aligned}$$

Returning to equation (4.45) with the right hand side set to zero, one notes from Chapter 3 that there exist two linearly independent solutions to equation (4.42) which are given as

$$\begin{aligned} \phi_1(x, y, z) & = \tanh(x + i\sqrt{3}y - \sqrt{2}z) \text{ and} & (4.46) \\ \phi_2(x, y, z) & = (x - \coth(x + i\sqrt{3}y - \sqrt{2}z)) \tanh(x + i\sqrt{3}y - \sqrt{2}z). \end{aligned}$$

These solutions can be easily verified to satisfy equation (4.45) when the right hand side is zero. Using these two homogeneous solutions, as previously shown, one can write down a particular solution to (4.45) as

$$\begin{aligned}\phi(x, y, z) &= \tanh(x + \iota\sqrt{3}y - \sqrt{2}z) + \int_{z_0}^z \int_{y_0}^y \int_{x_0}^x K(a, b, c, x, y, z) \\ &\times \left(\frac{-1}{k(c)} \frac{\partial}{\partial c} k(c) \frac{\partial \phi}{\partial c} \right) \\ &+ \frac{q}{k(c)} (\sigma(a, b, c) - n(a, b, c) - N_D(a, b, c)) da db dc, \quad (4.47)\end{aligned}$$

where

$$K(a, b, c, x, y, z) = \phi_1(a, b, c)\phi_2(x, y, z) - \phi_1(x, y, z)\phi_2(a, b, c).$$

Now,

$$\lim_{x, y, z \rightarrow 0} K(a, b, c, x, y, z) \longrightarrow -\tanh(a + \iota\sqrt{3}b - \sqrt{2}c).$$

Hence, equation (4.47) reduces to

$$\begin{aligned}\phi(0, 0, 0) &= - \int_{z_0}^0 \int_{y_0}^0 \int_{x_0}^0 \tanh(a + \iota\sqrt{3}b - \sqrt{2}c) \\ &\times \left[\frac{-1}{k(c)} \frac{\partial}{\partial c} k(c) \frac{\partial \phi}{\partial c} \right. \\ &\left. + \frac{q}{k(c)} (\sigma(a, b, c) - n(a, b, c) - N_D(a, b, c)) \right], \quad (4.48)\end{aligned}$$

Now one evaluates $\phi(0, 0, 0)$. From equation (4.48)

$$\begin{aligned}
\phi(0, 0, 0) &= \frac{3 \times 10^{15} q}{12.61} \int_0^{510} \int_0^{250} \int_0^{250} \tanh(a + \iota\sqrt{3}b - \sqrt{2}c) da db dc \\
&+ \frac{3 \times 10^{15} q}{12.61} \int_{549.2}^{606.8} \int_0^{250} \int_0^{250} \tanh(a + \iota\sqrt{3}b - \sqrt{2}c) da db dc \\
&- \frac{0.5 \times 10^{11} q}{12.61} \int_{166.5}^{168.5} \int_0^{250} \int_0^{250} \tanh(a + \iota\sqrt{3}b - \sqrt{2}c) da db dc \\
&- \frac{0.5 \times 10^{11} q}{12.61} \int_{588.7}^{590.7} \int_0^{250} \int_0^{250} \tanh(a + \iota\sqrt{3}b - \sqrt{2}c) da db dc \\
&- \frac{2q}{12.61} \int_0^{510} \int_0^{250} \int_0^{250} [|\psi_1|^2 + |\psi_2|^2] \tanh(a + \iota\sqrt{3}b - \sqrt{2}c) da db dc \\
&- \frac{2q}{14.11} \int_{510}^{526} \int_0^{250} \int_0^{250} [|\psi_1|^2 + |\psi_2|^2] \tanh(a + \iota\sqrt{3}b - \sqrt{2}c) da db dc \\
&- \frac{2q}{12.61} \int_0^{526} \int_0^{536} \int_0^{250} [|\psi_1|^2 + |\psi_2|^2] \tanh(a + \iota\sqrt{3}b - \sqrt{2}c) da db dc \\
&- \frac{2q}{14.11} \int_{536}^{510} \int_0^{549.2} \int_0^{250} [|\psi_1|^2 + |\psi_2|^2] \tanh(a + \iota\sqrt{3}b - \sqrt{2}c) da db dc \\
&- \frac{2q}{12.61} \int_{549.2}^{510} \int_0^{606.8} \int_0^{250} [|\psi_1|^2 + |\psi_2|^2] \tanh(a + \iota\sqrt{3}b - \sqrt{2}c) da db dc \\
&- \frac{2q}{12.71} \int_0^{606.8} \int_0^{626.8} \int_0^{250} [|\psi_1|^2 + |\psi_2|^2] \phi_1(a, b, c), \tag{4.49}
\end{aligned}$$

where $\phi_1(a, b, c) = \tanh(a + \iota\sqrt{3}b - \sqrt{2}c)$.

In conclusion, it is seen that reducing the Poisson's model to a proposed model certainly provides means to solve this equation efficiently. Particularly, this chapter has shown how to solve the general Poisson's equation in one, two and three dimensions.

Chapter 5

Semi-Analytical Solutions of Schroedinger's Equation

Using the semi-analytical solution of Poisson's equation which is developed in the previous chapter, this chapter addresses the task of finding semi-analytical solution of Schroedinger's equation. Particularly, the bound states of the Schroedinger's operator are found using the Evans function techniques. With these bound states, wave functions are calculated which are the desired semi-analytical solutions.

Furthermore, this chapter contains exact solutions to well known eigenvalue problems. In addition, it develops and extends the Evans function techniques [25, 71, 77] in an original manner to two and three dimensions. More details on the solution of Schroedinger's equation can be found in [10, 11, 50, 55, 68, 73, 79]. The Evans function technique is actually a novel approach, in that there is nothing published in literature to suggest previous application to the analysis of electron transport in semiconductor devices. As

such, it is in order to commence here with a definition of the Evans function which will be used throughout this work.

Definition 2 *The Evans function of an operator is defined as an analytic function whose zeros correspond to the discrete spectrum of the linearised version of the operator.*

In addition, it is necessary to introduce and define the Wronskian [40] in n-dimensions. Until recently, theoretical analysis of the Wronskian was only done for the one-dimensional case. For the purposes of this thesis, the Wronskian in two and three dimensions, sometimes called Partial Wronskian is defined and is essentially an indispensable original tool which this work uses in device analysis.

Suppose ψ_1 and ψ_2 are any two functions of the variables x , y and z defined in the region R ; then the partial Wronskian of ψ_1 and ψ_2 is defined as

Definition 3

$$\Delta(\psi_1, \psi_2) = \det \begin{pmatrix} \psi_1 & \psi_2 \\ D(\psi_1) & D(\psi_2) \end{pmatrix}, \quad (5.1)$$

where

$$D(\psi_i) = \left(\frac{\partial}{\partial x} + \frac{\partial}{\partial y} \right) \psi_i \quad (5.2)$$

for $i = 1, 2$.

Using the definition of the Evans function and the Wronskian, it is necessary to show how the Evans function can be used to assist in finding the

discrete spectrum and the wave functions of the linearised operator. Consequently, consider as an example the following linearised non-linear Klein-Gordon equation which is reported in [24]. Understanding this example is important in the later work developed in this thesis.

5.1 Example: Calculating the eigenvalues and eigenfunctions of Klein-Gordon equation in one dimension

This equation is given as

$$\psi_{xx}(x) - (1 - 2\operatorname{sech}^2 x)\psi(x) + \lambda\psi(x) = 0, \quad (5.3)$$

where λ is an eigenvalue.

In order to compute the bound states (eigenvalues) and the wave functions of equation (5.3), one notes that

$$(1 - 2\operatorname{sech}^2(x)) \rightarrow 1 \text{ as } x \rightarrow \pm\infty.$$

Therefore, as $x \rightarrow \pm\infty$ equation (5.3) reduces to

$$\psi_{xx}(x) - (1 - \lambda)\psi(x) = 0. \quad (5.4)$$

Write a solution of (5.4) in the form $\psi(x) = e^{\mu x}h(x)$ where $\mu = \pm\sqrt{1 - \lambda}$ and assume $\operatorname{Real}(1 - \lambda) > 0$. That is $\operatorname{Real}(\lambda) < 1$. Then the function $h(x)$ satisfies the equation

$$h_{xx}(x) + 2\mu h_x(x) + 2\operatorname{sech}^2 x h(x) = 0. \quad (5.5)$$

Now introduce the new independent variable $z = \tanh(x)$, then using equation (5.5) one gets

$$\frac{dz}{dx} \frac{d}{dx} \left(\frac{dh}{dz} \frac{dz}{dx} \right) + 2\mu \frac{dh}{dz} \frac{dz}{dx} + 2\operatorname{sech}^2 h(x) = 0, \quad (5.6)$$

which simplifies to the transformed equation

$$(1 - z^2) \frac{d^2 h}{dz^2} + 2(\mu - z) \frac{dh}{dz} + 2h = 0, \quad (5.7)$$

upon using

$$\frac{dh}{dx} = \frac{dz}{dx} \cdot \frac{dh}{dz} = \operatorname{sech}^2 x \cdot \frac{dh}{dz} = (1 - z^2) \frac{dh}{dz}.$$

Now equation (5.7) is one with polynomial coefficients, therefore one assumes a solution of the form

$$h(z) = \sum_{n=0}^{\infty} a_n z^n. \quad (5.8)$$

Substituting (5.8) into (5.7) and equating coefficients of each polynomial in z to zero, upon simplification, results in

$$a_0 = -C\mu, a_1 = C \text{ and } a_n = 0, n \geq 2,$$

where C is an arbitrary non-zero complex number. Therefore the general solution to equation (5.3) takes the form $\psi(x) = e^{\mu x} h(z)$ where $h(z) = C(z - \mu)$ and $z = \tanh(x)$. From above, μ can be either $+\sqrt{(1 - \lambda)}$ and $-\sqrt{(1 - \lambda)}$, this gives two solutions, one which decays to 0 as $x \rightarrow +\infty$ and the other decays to 0 as $x \rightarrow -\infty$. Let

$$m_+(x) = e^{-\sqrt{1-\lambda}x} h_+(z), \quad (5.9)$$

$$m_-(x) = e^{\sqrt{1-\lambda}x} h_-(z), \quad (5.10)$$

with

$$h_+(z) = C_+(z - (-\sqrt{1-\lambda})), \quad (5.11)$$

$$= C_+(z + \sqrt{1-\lambda}), \quad (5.12)$$

$$h_-(z) = C_-(z - \sqrt{(1-\lambda)}). \quad (5.13)$$

Thus the Evans function is

$$D(\lambda) = C_+C_-2\sqrt{1-\lambda}(z^2 - (1-\lambda) + (1-z^2)) \quad (5.14)$$

$$= 2C_+C_-\lambda\sqrt{1-\lambda}. \quad (5.15)$$

Analysing equation (5.15) suggests that equation (5.3) has solutions which decay exponentially only if $\text{Real}(1-\lambda) > 0$. This implies that $\lambda < 1$. Thus returning to equation (5.15) one observes that

$$C_+C_- \neq 0, \text{ and } \lambda < 1, \text{ so } \Delta(\lambda) = 0 \text{ only when } \lambda = 0.$$

Furthermore, one should note that when $\lambda = 1$ equation (5.3) has an exact solution $\psi(x) = \tanh(x)$. This can be easily verified by substitution.

5.2 Two-dimensional Schroedinger's equation

Given the one-dimensional analysis above, one can extend this approach to more general two and three dimensional Schroedinger-Poisson model. The source term (right-hand side) of Schroedinger equation admits many different forms depending on the required application. To illustrate how the Evans function may be extended to the two dimensional case, consider Schroedinger's equation in the effective mass approximation given in [6] as

$$(H - qV(x, z))\psi_E(x, y, z) = E\psi_E(x, y, z), \quad (5.16)$$

with $(x, y, z) \in [a, b]$ and H is Hamiltonian, defined by

$$H = -\frac{\hbar^2}{2} \left(\frac{1}{m_x(z)} \Delta_x + \frac{1}{m_y(z)} \Delta_y \right) - \frac{\hbar^2}{2} \frac{\partial}{\partial z} \left(\frac{1}{m_z(z)} \frac{\partial}{\partial z} \right). \quad (5.17)$$

ψ_E is the complex valued wave function which depends on the energy E , \hbar is the Plank's constant, q is the elementary electron charge. In addition, one denotes m_x, m_y, m_z as the z -dependent effective masses in the x, y and z -direction. The electrostatic potential V is x, z dependent and is split into exterior potential v_e and self-consistent potential V_s . In order to obtain V_s one solves the Poisson's equation

$$\Delta V_s(x, z) = -qn(x, z), \quad (5.18)$$

$$\partial_n V_s(a, \cdot) = 0 \quad (5.19)$$

$$\partial_n V_s(\cdot, b) = 0, \quad (5.20)$$

$$V_s(\cdot, 0) = V_g^0, \quad (5.21)$$

$$V_s(\cdot, 1) = V_g^1, \quad (5.22)$$

∂_n denotes the normal derivative to the boundary. Furthermore, V_g^0 and V_g^1 are the applied gate voltages. Finally, the electron density is

$$n = \int |\psi_E(x, y, z)|^2 f_{FD}(E) dE. \quad (5.23)$$

Here f_{FD} is called the Fermi-Dirac distribution function.

In this model one accounts for the anisotropic crystal structure of Si, which is illustrated by six equivalent conduction band ellipsoid. As such,

Schrodinger-Poisson has to be solved three times in order to obtain three different sets of eigenvalue ladder. The three different configurations of the effective mass m^* are given by (m_ℓ, m_t, m_t) , (m_t, m_ℓ, m_t) and (m_t, m_t, m_ℓ) , where m_t and m_ℓ are the transverse and longitudinal masses of the material.

Firstly, consider the effective mass configuration $m^* = (m_\ell, m_t, m_t)$. Let

$$\psi = \psi(x, y, z)$$

and $E = \lambda$. Equation (5.16) in rectangular coordinates is then given as

$$a\psi_{xx} + b\psi_{yy} + c\psi_{zz} = M_1(x, z). \quad (5.24)$$

where

$$M_1(x, z) = \frac{\partial}{\partial z} m_z(z) \psi_z - \frac{2q[m_z(z)]^2}{\hbar^2} V(x, z) \psi - \frac{2E[m_z(z)]^2}{\hbar^2} \psi, \quad (5.25)$$

with

$$a = \frac{[m_z(z)]^2}{m_x(z)}, \quad (5.26)$$

$$b = \frac{[m_z(z)]^2}{m_y(z)}, \quad (5.27)$$

$$(5.28)$$

and

$$c = m_z(z) \quad (5.29)$$

Applying the original semi-analytical method detailed in Chapter 4, the equation for the 2D quasi-model for the electrostatic potential is

$$V_{xx} + 2\text{sech}^2(x + i\sqrt{3}y - \sqrt{2}z)V + \frac{1}{\epsilon(z)} \frac{\partial}{\partial z} \epsilon(z) V_z = M_2(x, z), \quad (5.30)$$

where

$$M_2(x, z) = \frac{q}{\epsilon(z)}(n(x, z) - N_D(z)). \quad (5.31)$$

Now due to translation invariance in y [7], setting $y = 0$ results in

$$V_{xx}(x, z) + 2\text{sech}^2(x - \sqrt{2}z)V(x, z) = M_2(x, z). \quad (5.32)$$

Equation (5.32) has a particular solution

$$V(x, z) = \tanh(x - \sqrt{2}z) - q \int_{x_0}^0 \int_{z_0}^0 \tanh(a - \sqrt{2}b) \frac{M_2(a, b)}{\epsilon(b)} da db.$$

In order to solve the system self-consistently, one introduces an initial electrostatic potential solution to Poisson's equation of the form

$$V(x, z) = \frac{\hbar^2}{2q[m_z(z)]^2} \frac{\partial}{\partial z} m_z(z) \frac{\psi_z}{\psi} - \frac{\lambda}{q} - \frac{\lambda \ell^2 [m_z(z)]^2}{q},$$

where ℓ is the length of the device. Using this initial electrostatic potential solution, equation (5.24) reduces to

$$\psi_{xx} + 2bc \text{sech}^2(\sqrt{bc}x - \sqrt{2}\sqrt{ab}z)\psi - \frac{2\lambda \ell^2 [m_z(z)]^4}{a\hbar^2} \psi = 0. \quad (5.33)$$

In order to solve equation (5.33), note that in the $\lim_{x, z \rightarrow \pm\infty} 2bc \text{sech}^2(\sqrt{bc}x - \sqrt{2}\sqrt{ab}z) \rightarrow 0$. Hence equation (5.33) reduces to

$$\psi_{xx}(x, z) - \frac{2\lambda \ell^2 [m_z(z)]^4}{a\hbar^2} \psi(x, z) = 0. \quad (5.34)$$

Equation (5.34) has solutions which decay exponentially only if $\text{Real}(\lambda) > 0$. Therefore, when looking for solutions restrict λ to the right-half complex-plane. From equation (5.34), $\mu = \pm \sqrt{\frac{2[m_z(z)]^4 \ell^2 \lambda}{a\hbar^2}}$. Using this, write a solution to equation (5.34) in the form $e^{\mu(x+z)}h(x, z)$ and substitute this into equation (5.34). Then the function $h(x, z)$ satisfies

$$h_{xx} + 2\mu h_x + 2bc \text{sech}^2(\sqrt{bc}x - \sqrt{2}\sqrt{ab}z)h = 0. \quad (5.35)$$

In order to solve equation (5.35), introduce the new independent variable $m = \tanh(\sqrt{bc}x - \sqrt{2}\sqrt{ab}z)$. Then one has:

$$\frac{dh}{dx} = \frac{dm}{dx} \cdot \frac{dh}{dm} \quad (5.36)$$

$$= \sqrt{bc} \operatorname{sech}^2(\sqrt{bc}x - \sqrt{2}\sqrt{ab}z) \frac{dh}{dm} \quad (5.37)$$

$$= \sqrt{bc}(1 - m^2) \frac{dh}{dm}. \quad (5.38)$$

Similarly for the second derivative:

$$\frac{d^2h}{dx^2} = \frac{dm}{dx} \frac{d}{dx} \left(\frac{dm}{dx} \cdot \frac{dh}{dm} \right), \quad (5.39)$$

$$= \sqrt{bc}(1 - m^2) \frac{d}{dx} \left(\sqrt{bc}(1 - m^2) \cdot \frac{dh}{dm} \right). \quad (5.40)$$

Therefore, equation (5.35) becomes

$$bc(1 - m^2)h_{mmm} + 2(\mu\sqrt{bc} - bcz)h_m + 2bch = 0. \quad (5.41)$$

This is an equation with polynomial coefficients, therefore, a solution may be obtained in the form of a power series in m . Let

$$h(m) = \sum_{n=0}^{\infty} a_n m^n. \quad (5.42)$$

Now compute the first and second derivatives of equation (5.42). To this end one has

$$\frac{d}{dm} \sum_{n=0}^{\infty} a_n m^n = \sum_{n=1}^{\infty} n a_n m^{n-1} \quad (5.43)$$

$$\frac{d^2}{dm^2} \sum_{n=0}^{\infty} a_n m^n = \sum_{n=2}^{\infty} n(n-1) a_n m^{n-2}. \quad (5.44)$$

Then substitute equations (5.43) and (5.44) into equation (5.41), and use the

fact that

$$\sum_{n=1}^{\infty} 2bcna_n m^n = \sum_{n=0}^{\infty} 2bcna_n m^n \quad (5.45)$$

$$\text{and } \sum_{n=2}^{\infty} n(n-1)a_n m^n = \sum_{n=0}^{\infty} n(n-1)a_n m^n. \quad (5.46)$$

Therefore equation (5.41) reduces to

$$\sum_{n=0}^{\infty} \left(bc(n+2)(n+1)a_{n+2} - bc(n-1)na_n + 2\sqrt{bc}\mu(n+1)a_{n+1} - (2bcn - 2bc)a_n \right) m^n = 0.$$

Equating the coefficients of this polynomial to be equal to zero results in the recursion relation

$$a_{n+2} = \frac{(n(n-1)bc + 2nbc - 2bc)a_n - 2\sqrt{bc}\mu(n+1)a_{n+1}}{bc(n+2)(n+1)} \quad (5.47)$$

From the relation one finds that,

$$a_0 = \frac{-C\mu\sqrt{bc}}{bc} \quad (5.48)$$

$$a_1 = C \quad (5.49)$$

$$a_n = 0, \quad \forall n \geq 2, \quad (5.50)$$

where C is an arbitrary non-zero complex number. Using equations (5.42), (5.48), (5.49) and (5.50), results in

$$h(m) = C \left(-\frac{\mu\sqrt{bc}}{bc} + m \right).$$

That is,

$$h(x, z) = C \tanh(\sqrt{bc}x - \sqrt{2}\sqrt{ab}z) - C\frac{\mu\sqrt{bc}}{bc}. \quad (5.51)$$

Since $\mu = \pm\sqrt{\frac{2[m_z(z)]^4 \ell^2 \lambda}{a\hbar^2}}$ one has two solutions to equation (5.35). One of which decays as $x, z \rightarrow +\infty$ and the other decays as $x, z \rightarrow -\infty$. Let

$$U_+(x, z) = e^{-\sqrt{\frac{2[m_z(z)]^4 \ell^2 \lambda}{a\hbar^2}}(x+z)} h_+(x, z) \quad (5.52)$$

$$U_-(x, z) = e^{\sqrt{\frac{2[m_z(z)]^4 \ell^2 \lambda}{a\hbar^2}}(x+z)} h_-(x, z), \quad (5.53)$$

where

$$h_+(x, z) = C_+ \tanh(\sqrt{bc}x - \sqrt{2}\sqrt{ab}z) - C_+ \frac{\mu_+ \sqrt{bc}}{bc} \quad (5.54)$$

and

$$h_-(x, z) = C_- \tanh(\sqrt{bc}x - \sqrt{2}\sqrt{ab}z) - C_- \frac{\mu_- \sqrt{bc}}{bc}. \quad (5.55)$$

As $x, z \rightarrow +\infty$, $U_+(x, z) \rightarrow 0$ and as $x, z \rightarrow -\infty$, $U_-(x, z) \rightarrow 0$. Therefore, for some $\lambda \in C$, with $\text{Real}(\lambda) > 0$, the functions $U_+(x, z)$ and $U_-(x, z)$ are linearly dependent and bounded for all x, z and decay exponentially as $x, z \rightarrow \pm\infty$. Thus eigen energies (eigenvalues) correspond to values of $\lambda \in C$ where the Wronskian of $U_+(x, z)$ and $U_-(x, z)$ vanishes. Using the definition of the Wronskian, the Evans function is given by

$$D(\lambda) = \det \begin{pmatrix} U^+(x, z, \lambda) & U^-(x, z, \lambda) \\ U_x^+(x, z, \lambda) + U_z^+(x, z, \lambda) & U_x^-(x, z, \lambda) + U_z^-(x, z, \lambda) \end{pmatrix}.$$

Simplifying this, the Evans function is given explicitly as

$$D(\lambda) = -\frac{2\sqrt{2}[m_z(z)]C_+C_- \sqrt{\frac{\lambda}{a}}(g_1(\lambda, \hbar, m_z(z), a, b, c, \ell))}{abc\hbar^3}, \quad (5.56)$$

where

$$g_1(m_z(z), \hbar, a, b, c, \ell, \lambda) = \sqrt{2}a\hbar^2\sqrt{ab}\sqrt{bc} - abc\hbar^2 + 4\lambda\ell^2[m_z(z)]^4 \quad (5.57)$$

The zeros (eigen-energies) of equation (5.56) are

$$\lambda_1 = 0, \quad (5.58)$$

$$\lambda_2 = \frac{a\hbar^2(bc - \sqrt{2}\sqrt{ab}\sqrt{bc})}{4\ell^2[m_z(z)]^4}. \quad (5.59)$$

Since $\text{Real}(\lambda) > 0$, reject λ_1 and accept λ_2 . Therefore, inserting λ_2 into the values for μ , μ_- and using equations (5.52) and (5.53) one arrives at two normalised eigenfunctions. These are given as

$$U_+^1(x, z) = e^{-\alpha(x+z)} h_+^1(x, z), \quad (5.60)$$

$$U_+^2(x, z) = e^{\alpha(x+z)} h_+^2(x, z), \quad (5.61)$$

where

$$h_+^1(x, z) = C_+ \left(\tanh(\sqrt{bc}x - \sqrt{2}\sqrt{ab}z) + \alpha \frac{\sqrt{bc}}{bc} \right), \quad (5.62)$$

$$h_+^2(x, z) = C_- \left(\tanh(\sqrt{bc}x - \sqrt{2}\sqrt{ab}z) - \alpha \frac{\sqrt{bc}}{bc} \right), \quad (5.63)$$

and

$$C_+ = 96124, \quad (5.64)$$

$$C_- = -96124, \quad (5.65)$$

$$\alpha = \frac{\sqrt{2}\sqrt{bc} - \sqrt{2}\sqrt{ab}\sqrt{bc}}{2}. \quad (5.66)$$

Next consider the effective mass configuration $m^* = (m_t, m_\ell, m_t)$. If $\psi(x, y, z) = \tanh(\sqrt{ac}x + i\sqrt{3}\sqrt{bc}y - \sqrt{2}\sqrt{ab}z)$, then this satisfies the homogeneous equation

$$b\psi_{xx} + a\psi_{yy} + c\psi_{zz} = 0. \quad (5.67)$$

With translation invariance in y , set $y = 0$, therefore one has the equation

$$\psi_{xx} + 2ac \text{sech}^2(\sqrt{ac}x - \sqrt{2}\sqrt{ab}z)\psi = \frac{1}{b}M_3(x, z), \quad (5.68)$$

where

$$M_3(x, z) = \frac{\partial}{\partial z} m_z(z)\psi_z - \frac{2q[m_z(z)]^2}{\hbar^2} V(x, z)\psi - \frac{2\lambda[m_z(z)]^2}{\hbar^2} \psi. \quad (5.69)$$

As before, consider the substitution for the initial solution of the electrostatic potential to Poisson's equation,

$$V(x, z) = \frac{\hbar^2}{2q[m_z(z)]^2} \frac{\partial}{\partial z} m_z(z) \frac{\psi_z}{\psi} - \frac{\lambda}{q} - \frac{\lambda \ell^2 [m_z(z)]^2}{q}.$$

This substitution reduces equation (5.68) to

$$\psi_{xx} + 2ac \operatorname{sech}^2(\sqrt{ac}x - \sqrt{2}\sqrt{ab}z) \psi - \frac{2\ell^2 \lambda [m_z(z)]^4}{b\hbar^2} \psi = 0. \quad (5.70)$$

In the limit as $x, z \rightarrow \pm\infty$, $2ac \operatorname{sech}^2(\sqrt{ac}x - \sqrt{2}\sqrt{ab}z) \rightarrow 0$, hence equation (5.70) reduces to

$$\psi_{xx}(x, z) - \frac{2\ell^2 \lambda [m_z(z)]^4}{b\hbar^2} \psi(x, z) = 0. \quad (5.71)$$

Now observe that equation (5.71) has solutions which decay exponentially only if $\operatorname{Real}(\lambda) > 0$. From equation (5.71), $\mu = \pm \sqrt{\frac{2[m_z(z)]^4 \ell^2 \lambda}{b\hbar^2}}$. Then write a solution to equation (5.70) in the form $e^{\mu(x+z)} h(x, z)$ and substitute this into equation (5.70). Thus the function $h(x, z)$ satisfies

$$h_{xx} + 2\mu h_x + 2ac \operatorname{sech}^2(\sqrt{ac}x - \sqrt{2}\sqrt{ab}z) h = 0. \quad (5.72)$$

Introduction of the new independent variable $\rho = \tanh(\sqrt{ac}x - \sqrt{2}\sqrt{ab}z)$, equation (5.72) transforms to

$$ac(1 - z^2) h_{\rho\rho} + 2(\mu\sqrt{ac} - acz) h_{\rho} + 2ac h = 0. \quad (5.73)$$

This equation has solution

$$h(\rho) = C \left(-\frac{\mu\sqrt{ac}}{ac} + \rho \right), \quad (5.74)$$

where C is an arbitrary non-zero complex number.

Using the same techniques as before with $\mu = \pm\sqrt{\frac{2[m_z(z)]^4\ell^2\lambda}{b\hbar^2}}$, there are two solutions to equation (5.68). One of which decays as $x, z \rightarrow +\infty$ and the other decays as $x, z \rightarrow -\infty$. Let

$$U_+(x, z) = e^{-\sqrt{\frac{2[m_z(z)]^4\ell^2\lambda}{b\hbar^2}}(x+z)} h_+(x, z) \quad (5.75)$$

$$U_-(x, z) = e^{\sqrt{\frac{2[m_z(z)]^4\ell^2\lambda}{b\hbar^2}}(x+z)} h_-(x, z), \quad (5.76)$$

where

$$h_+(x, z) = C_+ \tanh(\sqrt{ac}x - \sqrt{2}\sqrt{ab}z) - C_+ \frac{\mu_+ \sqrt{ac}}{ac}$$

and

$$h_-(x, z) = C_- \tanh(\sqrt{ac}x - \sqrt{2}\sqrt{ab}z) - C_- \frac{\mu_- \sqrt{ac}}{ac}.$$

As before, following the same technique, the Evans function is computed and is given as

$$D(\lambda) = -\frac{2\sqrt{2}[m_z(z)]C_+C_- \sqrt{\frac{\lambda}{b}}(g_2(\lambda, \hbar, m_z(z), a, b, c, \ell))}{abc\hbar^3}, \quad (5.77)$$

where

$$g_2(m_z(z), \hbar, a, b, c, \ell, \lambda) = \sqrt{2}b\hbar^2\sqrt{ab}\sqrt{ac} - abc\hbar^2 + 4\ell^2\lambda[m_z(z)]^4 \quad (5.78)$$

The zeros (eigen-energies) of equation (5.77) are

$$\lambda_1 = 0, \quad (5.79)$$

$$\lambda_2 = \frac{b\hbar^2(ac - \sqrt{2}\sqrt{ab}\sqrt{ac})}{4\ell^2[m_z(z)]^4}. \quad (5.80)$$

Since $\text{Real}(\lambda) > 0$, again reject λ_1 and accept λ_2 . Therefore, inserting λ_2 into the values for μ, μ_- and using equations (5.75) and (5.76) results in two

normalised eigenfunctions. These are given as

$$U_+^1(x, z) = e^{-\alpha_1(x+z)} h_+^1(x, z), \quad (5.81)$$

$$U_+^2(x, z) = e^{\alpha_1(x+z)} h_-^2(x, z), \quad (5.82)$$

where

$$h_+^1(x, z) = C_+ \left(\tanh(\sqrt{ac}x - \sqrt{2}\sqrt{ab}z) - \alpha_1 \frac{\sqrt{ac}}{ac} \right), \quad (5.83)$$

$$h_+^2(x, z) = C_- \left(\tanh(\sqrt{ac}x - \sqrt{2}\sqrt{ab}z) - \alpha_2 \frac{\sqrt{ac}}{bc} \right) \quad (5.84)$$

and

$$C_+ = 50715.1, \quad (5.85)$$

$$C_- = -50715.1, \quad (5.86)$$

$$\alpha_1 = -\frac{\sqrt{2}\sqrt{ac} - \sqrt{2}\sqrt{ab}\sqrt{ac}}{2}, \quad (5.87)$$

$$\alpha_2 = \frac{\sqrt{2}\sqrt{ac} - \sqrt{2}\sqrt{ab}\sqrt{ac}}{2}. \quad (5.88)$$

And finally, consider the effective mass configuration $m^* = (m_t, m_t, m_\ell)$.

This results in the Schroedinger's equation

$$\psi_{xx}(x, z) + 2ab \operatorname{sech}^2(\sqrt{ab}x - \sqrt{2}\sqrt{bc}z)\psi(x, z) = \frac{1}{c}M_4(x, z), \quad (5.89)$$

where

$$M_4(x, z) = \frac{\partial}{\partial z} m_z(z) \psi_z - \frac{2q[m_z(z)]^2}{\hbar^2} V(x, z) \psi - \frac{2\lambda[m_z(z)]^2}{\hbar^2} \psi.$$

As before, one may consider the substitution,

$$V(x, z) = \frac{\hbar^2}{2q[m_z(z)]^2} \frac{\partial}{\partial z} m_z(z) \cdot \frac{\psi_z}{\psi} - \frac{\lambda}{q} - \frac{\lambda \ell^2 [m_z(z)]^2}{q}.$$

This substitution reduces equation (5.89) to

$$\psi_{xx} + 2ab \operatorname{sech}^2(\sqrt{ab}x - \sqrt{2}\sqrt{bc}z)\psi - \frac{2\ell^2\lambda[m_z(z)]^4}{c\hbar^2}\psi = 0. \quad (5.90)$$

In the limit as $x, z \rightarrow \pm\infty$, $2ab \operatorname{sech}^2(\sqrt{ab}x - \sqrt{2}\sqrt{bc}z) \rightarrow 0$, hence equation (5.90) reduces to

$$\psi_{xx}(x, z) - \frac{2\ell^2\lambda[m_z(z)]^4}{c\hbar^2}\psi(x, z) = 0. \quad (5.91)$$

With $\mu = \pm\sqrt{\frac{2[m_z(z)]^2\ell^4\lambda}{c\hbar^2}}$ and using the independent variable $\xi = \tanh(\sqrt{ab}x - \sqrt{2}\sqrt{bc}z)$ and applying the method previously discussed above, one obtains the transformed equation

$$ab(1 - \xi^2)h_{\xi\xi} + 2(\mu\sqrt{ba} - abz)h_{\xi} + 2abh(\xi) = 0. \quad (5.92)$$

This equation has solution

$$h(\xi) = C \left(\xi - \frac{\mu\sqrt{ab}}{ab} \right), \quad (5.93)$$

where C is an arbitrary non-zero complex number. Using the same ideas as above one arrives at two solutions to equation (5.89) which are given as

$$U_+(x, z) = e^{-\sqrt{\frac{2[m_z(z)]^4\ell^2\lambda}{c\hbar^2}}(x+z)} h_+(x, z), \quad (5.94)$$

$$U_-(x, z) = e^{\sqrt{\frac{2[m_z(z)]^4\ell^2\lambda}{c\hbar^2}}(x+z)} h_-(x, z), \quad (5.95)$$

where

$$h_+(x, z) = C_+ \tanh(\sqrt{ab}x - \sqrt{2}\sqrt{bc}z) - C_+ \frac{\mu_+ \sqrt{ab}}{ab}, \quad (5.96)$$

and

$$h_-(x, z) = C_- \tanh(\sqrt{ab}x - \sqrt{2}\sqrt{bc}z) - C_- \frac{\mu_- \sqrt{ab}}{ab}. \quad (5.97)$$

Therefore, the Evans function is given as

$$D(\lambda) = \det \begin{pmatrix} U^+(x, z, \lambda) & U^-(x, z, \lambda) \\ U_x^+(x, z, \lambda) + U_z^+(x, z, \lambda) & U_x^-(x, z, \lambda) + U_z^-(x, z, \lambda) \end{pmatrix}.$$

Simplifying this, the Evans function is given explicitly as

$$D(\lambda) = -\frac{2\sqrt{2}[m_z(z)]C_+C_- \sqrt{\frac{\lambda}{a}}(g_3(\lambda, \hbar, m, a, b, c, \ell))}{abc\hbar^3}, \quad (5.98)$$

where

$$g_3(m_z(z), \hbar, a, b, c, \ell, \lambda) = \sqrt{2}a\hbar^2\sqrt{ab}\sqrt{bc} - abc\hbar^2 + 4\ell^2\lambda[m_z(z)]^4 \quad (5.99)$$

The zeros (eigen-energies) of equation (5.98) are

$$\lambda_1 = 0, \quad (5.100)$$

$$\lambda_2 = \frac{c\hbar^2(ab - \sqrt{2}\sqrt{ab}\sqrt{bc})}{4\ell^2[m_z(z)]^4}. \quad (5.101)$$

Since $\text{Real}(\lambda) > 0$, reject λ_1 and accept λ_2 . Therefore, inserting λ_2 into the values for μ, μ_- and using equations (5.94) and (5.95) one arrives at two normalised eigenfunctions. These are given as

$$U_+^1(x, z) = e^{-\alpha_3(x+z)}h_+^1(x, z), \quad (5.102)$$

$$U_+^2(x, z) = e^{\alpha_4(x+z)}h_-^2(x, z), \quad (5.103)$$

where

$$h_+^1(x, z) = C_+ \left(\tanh(\sqrt{ab}x - \sqrt{2}\sqrt{bc}z) - \alpha_3 \frac{\sqrt{ab}}{ab} \right), \quad (5.104)$$

$$h_+^2(x, z) = C_- \left(\tanh(\sqrt{ab}x - \sqrt{2}\sqrt{bc}z) - \alpha_4 \frac{\sqrt{ab}}{ab} \right) \quad (5.105)$$

and

$$C_+ = 108620.4, \quad (5.106)$$

$$C_- = -108620.4, \quad (5.107)$$

$$\alpha_3 = -\frac{\sqrt{2}\sqrt{ab} - \sqrt{2}\sqrt{ab}\sqrt{bc}}{2}, \quad (5.108)$$

$$\alpha_4 = \frac{\sqrt{2}\sqrt{ab} - \sqrt{2}\sqrt{ab}\sqrt{bc}}{2}. \quad (5.109)$$

Given the above calculations, the total electron density can now be readily computed, which by [6] is defined as the sum of all the contributions which correspond to three effective mass configurations. Therefore, in order to calculate the potential in Poisson equation, one must firstly calculate this density which is given as

$$n(x, z) = 2(n_{m_l, m_t, m_t} + n_{m_t, m_\ell, m_t} + n_{m_t, m_t, m_\ell}). \quad (5.110)$$

Now, the Fermi-Dirac distribution function [4-6] is

$$f_{FD}(E, E_f) = \frac{1}{1 + e^{\frac{E-E_f}{k_B T}}}. \quad (5.111)$$

To evaluate this expression, however, the exact location of E_f , which is the Fermi level, is not known, therefore, using Boltzmann approximation [86] one computes

$$E_f = E_c - kT \ln \frac{N_c}{N_d} \quad (5.112)$$

$$= 3.15 eV - 0.0259 eV \ln \frac{2.88 \times 10^{19}}{10^{16}} \quad (5.113)$$

$$= 2.94 eV. \quad (5.114)$$

$$= 4.07 \times 10^{-19} \text{ J}. \quad (5.115)$$

Using this value for E_f one can calculate explicitly the electron density and update Poisson's equation. This electron density is therefore given as

$$n(x, z) = \frac{1}{\pi} \left(\frac{2m_x K_B T}{\hbar^2} \right)^{\frac{1}{2}} \sum_l |\psi_l(x, z)|^2 \wp_{-\frac{1}{2}} \left(\frac{E_F - \lambda_l}{K_B T} \right) \quad (5.116)$$

where $\wp_{-\frac{1}{2}}$ is the Fermi integral of order $-\frac{1}{2}$, which is defined as

$$\wp_{-\frac{1}{2}}(x) = \int_0^\infty \frac{t^{-\frac{1}{2}}}{1 + e^{t-x}} dt. \quad (5.117)$$

5.3 Three-dimensional Schroedinger's equation

Finally, the general form of this equation is given as

$$(H - qV(x, y, z)) \psi_E(x, y, z) = E \psi_E(x, y, z), \quad (5.118)$$

with $(x, y, z) \in [a, b]$ and H is Hamiltonian, defined by

$$H = -\frac{\hbar^2}{2} \left(\frac{1}{m_x(z)} \Delta_x + \frac{1}{m_y(z)} \Delta_y + \frac{1}{m_z(z)} \Delta_z \right) - \frac{\hbar^2}{2} \frac{\partial}{\partial z} \left(\frac{1}{m_z(z)} \frac{\partial}{\partial z} \right).$$

ψ_E is the complex valued wave function which depends on the energy E , \hbar is the plank's constant, q is the elementary electron charge. In addition, we denote m_x, m_y, m_z as the z -dependent effective masses in the x, y and z -direction. The electrostatic potential V is x, y, z dependent and is split into exterior potential v_e and self-consistent potential V_s . In order to obtain V_s ,

one solves the Poisson's equation

$$\Delta V_s(x, y, z) = -qn(x, y, z), \quad (5.119)$$

$$\partial_n V_s(a, \cdot) = 0 \quad (5.120)$$

$$\partial_n V_s(\cdot, b) = 0, \quad (5.121)$$

$$V_s(\cdot, 0) = V_g^0, \quad (5.122)$$

$$V_s(\cdot, 1) = V_g^1, \quad (5.123)$$

∂_n denotes the normal derivative to the boundary. Furthermore, V_g^0 and V_g^1 are the applied gate voltages. Finally, the electron density is

$$n = \int |\psi_E(x, y, z)|^2 f_{FD}(E) dE. \quad (5.124)$$

We call f_{FD} the Fermi-Dirac distribution function.

From Appendix E, let $U^+(x, y, z, \lambda) = U^+$ and $U^-(x, y, z, \lambda) = U^-$ be solutions to equation (5.118), where

$$U_+(x, y, z) = e^{-\sqrt{\frac{2[m_z(z)]^4 \ell^2 \lambda}{a \hbar^2}}(x+y+z)} h_+(x, y, z) \quad (5.125)$$

$$U_-(x, y, z) = e^{\sqrt{\frac{2[m_z(z)]^4 \ell^2 \lambda}{a \hbar^2}}(x+y+z)} h_-(x, y, z), \quad (5.126)$$

where

$$h_+(x, y, z) = C_+ \tanh(\sqrt{bc}x + i\sqrt{3}\sqrt{ac}y - \sqrt{2}\sqrt{ab}z) - C_+ \frac{\mu_+ \sqrt{bc}}{bc}$$

and

$$h_-(x, y, z) = C_- \tanh(\sqrt{bc}x + i\sqrt{3}\sqrt{ac}y - \sqrt{2}\sqrt{ab}z) - C_- \frac{\mu_- \sqrt{bc}}{bc}$$

are the explicit 3D eigenfunctions. Then the Evans function is given as

$$D(\lambda) = \det \begin{pmatrix} U^+(x, z, y, \lambda) & U^-(x, z, y, \lambda) \\ U_x^+ + U_z^+ + U_y^+ & U_x^- + U_z^- + U_y^- \end{pmatrix},$$

where U_x, U_z and U_y are the first derivatives with respect to x, z and y respectively of the functions $U^+(x, y, z, \lambda)$ and $U^-(x, y, z, \lambda)$.

In conclusion, this chapter introduces and defines the Evans function which is a useful tool to capture the bound states of the Schroedinger operator. Its effectiveness is demonstrated in its application to one-dimensional Schroedinger equation. For device analysis, this thesis extends the application in a novel way to finding semi-analytical solutions for the first time to two and three dimensional Schroedinger equations taking into account different effective masses for the crystal structure. In Chapter 7, it will be shown how the Evans function assists in finding eigenvalues and eigenfunctions with improved simulation times. Such improvements in simulation times are instrumental to the Semiconductor Research community [1].

Chapter 6

Proposed semi-analytical method for the coupled Schroedinger and Poisson's equations

The last two chapters of this work are devoted to finding semi-analytical solution of the Schroedinger-Poisson's model. An analytical expression for the electrostatic potential was proposed and substituted into Schroedinger's equation which resulted in a semi-analytical solution to Schroedinger's equation. Using this solution to Schroedinger's equation, Poisson's equation is then solved. Consequently, this chapter addresses the challenge of proving that successive solutions of the coupled system of Schroedinger-Poisson's equations converge locally.

The proof will draw on the usefulness of the Evans function technique,

particularly the boundedness of the wave functions. Although several methods have been suggested which solve successfully this system of equations, the issue of convergence is still a topic of discussion. Whilst no general proof exists on convergence of the solutions, local methods [2, 30, 46] have shown that local convergence can be achieved. In [6, 7, 12, 90, 91], a comprehensive overview on convergence is given and should provide useful sources of reference. For example, in [91], it is shown that in order to solve the system of equations, an iterative method has to be employed. But given the strong nonlinearity between the equations, a straightforward iterative approach will not lead to convergence. To ensure convergence, one has to employ some adaptive approach. One which has proven useful is underrelaxation in the electrostatic potential ϕ or the electron density n , [91]. Regrettably, underrelaxation has its shortcomings namely:

- instability of the outer iteration,
- oscillations from one iteration step to another,
- the choice of the relaxation factor.

Here the problem of the convergence is the choice of the relaxation parameter. The relaxation parameter has to be chosen experimentally. This leads to finding different techniques which lead to rapid convergence. Particularly, in [91], this problem of convergence was solved by:

- using perturbation theory to modify the electron density then
- solving a modified Poisson's equation to obtain the electrostatic potential $\phi(x, y, z)$.

In this thesis, the original approach is the development of a semi-analytical method which is used to solve rapidly the above system of equations.

For the purposes of this thesis, this chapter shows that convergence of the coupled solutions occurs for the semi-analytical method proposed in this thesis. It is not the case that this thesis proposes that the method will in general converge. That is, the method is confined to the problems which are solved in this work. In order to summarise the method, Figure 6.1 shows a diagram which depicts various levels in the computational process. Schroedinger-Poisson model, which is presented in Chapters 4 and 5, is the most appropriate system of equations which describes the quantum and ballistic electron transport in semiconductor devices.

In the case of this thesis, the solution of this system of equations is accomplished via two stages: solution to Schroedinger's equation and then solution to Poisson's equation. The total quantum mechanical electron density is described by the solution of Schroedinger's equation and the electrostatic potential is found by solving Poisson's equation.

In order to commence the iterative procedure, as set out in Figure 6.1, for the resolution of the coupled system of Schroedinger-Poisson equations, an initial electrostatic potential $\phi_0(x, y, z)$ is guessed and substituted into Schroedinger's equation resulting in a conventional eigenvalue problem to be analytically resolved for three different effective masses. The resolution of the eigenvalue problem is achieved via the Evans function techniques.

The application of the Evans function techniques allows for the wave functions and eigenvalues to be computed. Then the total electron density is found and hence the potential in Poisson's equation is calculated. The process

is then iterated to convergence. Convergence occurs when $\|\phi_{n+1} - \phi_n\|_{L^\infty} < \epsilon$, where $L^\infty = L^2(-\infty, +\infty)$ is the complex Hilbert space and ϵ is a specified stopping criterion. It is necessary to mention here that the efficiency of the algorithm is heavily dependent on the semi-analytical component of the procedure. Next this work demonstrates that the semi-analytical method will always lead to local convergence.

6.1 Convergence of the coupled solutions of Schroedinger-Poisson's equations using the semi-analytical method

Here a proof is given which demonstrates that the solutions converge locally using the semi-analytical method. To prove local convergence of the coupled solutions to Schroedinger-Poisson's equations, let

$$\psi_1, \psi_2, \psi_3, \dots, \psi_n$$

be solutions to Schroedinger equation (after an appropriate initial substitution for the electrostatic potential $\psi_0(x, y, z)$). Then by the method demonstrated in Chapter 6 and the Evans function techniques, it is shown that the spectral problem is to find the values of

$$\lambda \in C \text{ such that } \psi_{i=1,2,\dots,n}(x, y, z, \lambda)$$

satisfies the eigenvalue problem

$$\psi_{xx}(x, y, z) + m(x, y, z)\psi(x, y, z) = \lambda\psi(x, y, z), \quad (6.1)$$

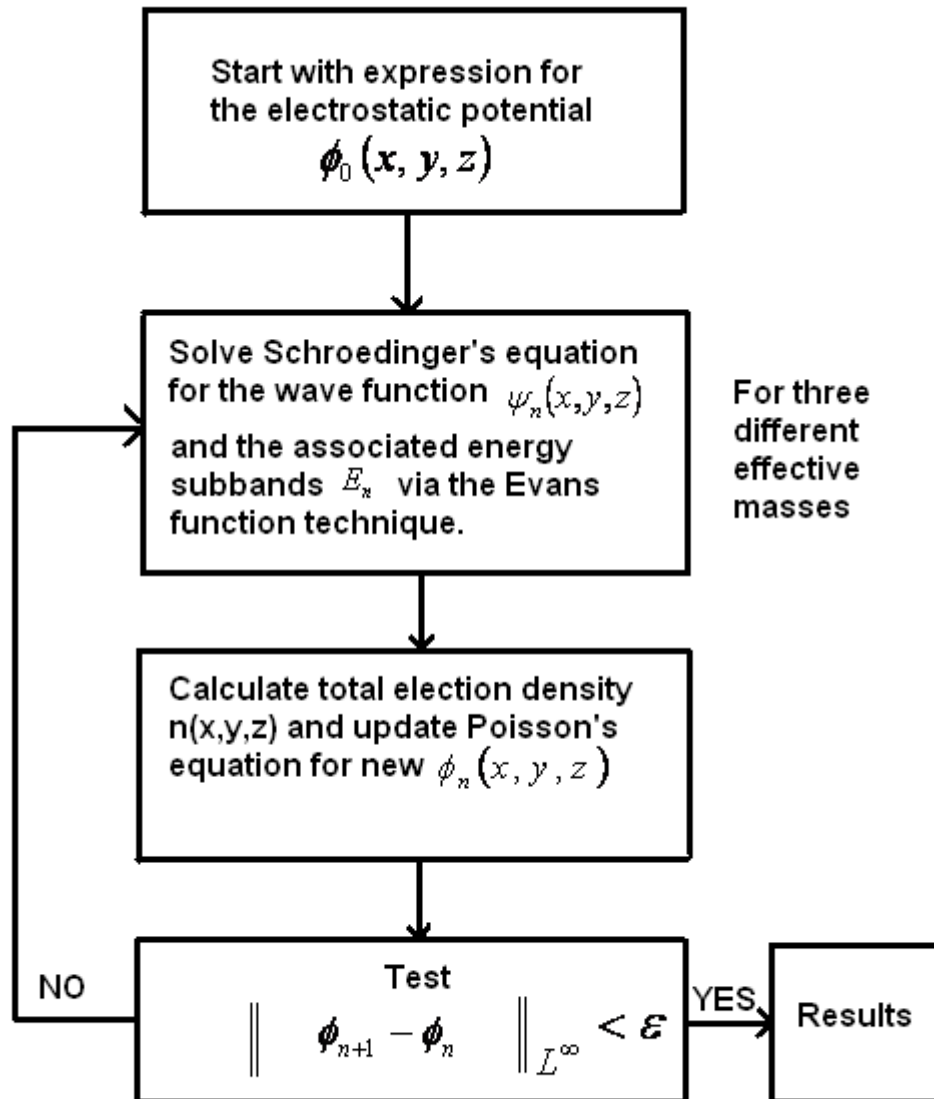


Figure 6.1: Flowchart of the Schroedinger-Poisson iteration process.

$$m(x, y, z) \rightarrow a \text{ as } x, y, z \rightarrow \pm\infty$$

and where C is complex number with

$$\int_{x_0}^x \int_{y_0}^y \int_{z_0}^z |\psi_1(x, y, z)|^2 dx dy dz < \infty,$$

$$\int_{x_0}^x \int_{y_0}^y \int_{z_0}^z |\psi_2(x, y, z)|^2 dx dy dz < \infty$$

⋮

and

$$\int_{x_0}^x \int_{y_0}^y \int_{z_0}^z |\psi_n(x, y, z)|^2 dx dy dz < \infty$$

exist.

Now, denote the sum of these integrals by σ and substitute this sum into Poisson's equation. By the method in Chapters 3 and 4 and using the fact that the Evans function is independent of the variables x, y and z , the solution to Poisson's equation reduces to a constant.

Let this constant be denoted by a . Then it is shown in Chapter 5 that Schroedinger's equation reduces to the conventional eigenvalue problem

$$\psi_{xx}(x, y, z) + (a - \lambda)\psi(x, y, z) = 0. \quad (6.2)$$

Now write a solution to Schroedinger's equation of the form

$$\psi(x, y, z) = e^{\mu(x+y+z)}h(x, y, z). \quad (6.3)$$

Then the function $h = h(x, y, z)$ satisfies

$$h_{xx} + 2\mu h_x + 2\text{sech}^2(x + i\sqrt{3}y - \sqrt{2}z)h = 0. \quad (6.4)$$

Equation (6.4) admits a power series solution [98] of the form

$$h(x, y, z) = \sum_{n=0}^{\infty} a_n \rho^n, \quad (6.5)$$

where $\rho = \tanh(x + \iota\sqrt{3}y - \sqrt{2}z)$. Having found $h(x, y, z)$, the full solutions (eigenfunctions) to Schroedinger's equation may be denoted by $U_+(x, y, z, \lambda)$ and $U_-(x, y, z, \lambda)$. Therefore, if for some $\lambda \in C$ with $\Re(a + \lambda) > 0$, the functions $U_+(x, y, z, \lambda)$ and $U_-(x, y, z, \lambda)$ are linearly dependent, then the functions are bounded for all x, y, z and decay exponentially as $x \rightarrow \pm\infty$, $y \rightarrow \pm\infty$ and $z \rightarrow \pm\infty$.

Using these solutions one constructs the Evans function which may be denoted by $D(\lambda)$. Let

$$\lambda_1, \lambda_2, \lambda_3, \dots, \lambda_n$$

be the zeros of $D(\lambda)$. With these different values of λ one has an iterative procedure between Schroedinger and Poisson. Each iterative process produces different constants. Therefore, convergence occurs when one multiplies the sum σ by a chosen constant α [12]. The need for this constant is that the eigenfunctions are not necessarily normalised. Hence rapid convergence is achieved by this constant. That is

$$\alpha\sigma = n(x, y, z) \quad (6.6)$$

$$= 2\alpha \sum_{i=1}^n |\psi_i(x, y, z)|^2 \quad (6.7)$$

as required.

Therefore, whilst general convergence is not shown here, it is shown that convergence occurs locally by application of the semi-analytical method. It is demonstrated that in practice this method converges. In the next chapter of

this thesis, this new method will be used to simulate different structures and results and run times will be validated against those reported in literature and experimental results where available [51, 74].

Chapter 7

Simulation results and validation of the method

Generally in device analysis, the electronic states and transport are determined through approximate methods. These methods include the finite element, nonequilibrium Green function, predictor-corrector method, the SDM/WKB, finite difference, reduced basis method or a combination of the above methods [6, 7, 12, 57, 91].

Any method has to be validated. Ideally, validation should be carried out against experimental data. However, in the absence of experimental data, simulation results are usually evaluated by comparisons with 1D, 2D and 3D finite element method incorporated in most device simulators. The full 3D finite element method is not computationally fast, but in terms of accuracy, it is a benchmark by which faster methods such as the SDM/WKB and predictor-corrector are evaluated [7, 12, 91]. In the following, the semi-analytical method will be validated by comparison with other alternative

simulation methods reported in the literature [6, 12, 74, 91] and by showing agreement with the experimental results reported in [51].

In this chapter, it is demonstrated through the application of the proposed semi-analytical method in Chapters 4 and 5 that it is possible to capture accurately the eigenvalues of the various electronic devices and subsequently simulate electron transport, thus validating the method developed in Chapters 4 - 6. Knowledge of the energies (eigenvalues) of various devices is essential in understanding electron transport in semiconductor systems. This chapter contains the analysis of five devices already reported in literature, using the semi-analytical method in order to test and validate it. These devices are:

- Device 1 - a model Ga-As-GaAlAs device, [91];
- Device 2 - a Si-SiO₂ based quantum device, [91];
- Device 3 - a double quantum well device, [12];
- Device 4 - a double gate NMOSFET, [6];
- Device 5 - a single-walled carbon nanotube field effect transistor SWNT-FET, [51].

In the analysis, 1D, 2D and 3D simulations of transport are considered and the results of the semi-analytical method are compared with those reported in [6, 12, 51, 74, 91]. It will also be shown that the proposed method improves the simulation times for these devices compared with those reported in [6, 12, 74, 91]. The method was implemented in Matlab (version

7.11, R2010b) (see code in Appendix F) and the simulations were performed on a Toshiba laptop equipped with an Intel R Processor with clock speed 3 GHz, memory 2.10 GB and 1.87 GB of RAM.

7.1 Device 1: A GaAs - GaAlAs device

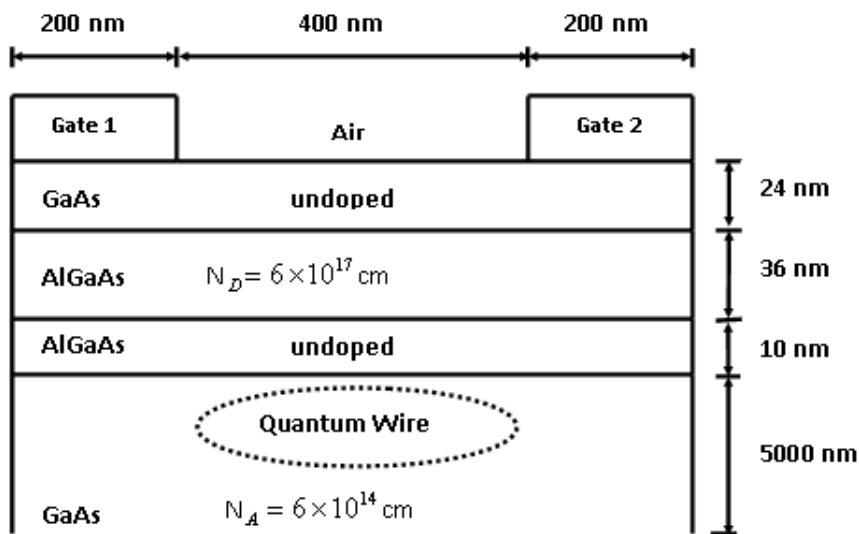


Figure 7.1: [91]. Architecture of Device 1: A model GaAs-GaAlAs device structure.

Figure 7.1 shows a cross-section of this device (Device 1) with double gates. It has two undoped GaAs and AlGaAs layers. This device has lateral dimension 800 nm and height 5070 nm. The height is composed of four layers, GaAs (24 nm), AlGaAs (36 nm), AlGaAs (10 nm) and GaAs (5000 nm). The device contains two doping strengths of $N_D = 6 \times 10^{17} \text{ cm}^{-3}$ and $N_A = 10^{14} \text{ cm}^{-3}$ which are located between 0 nm - 5000 nm and 5010 nm - 5046 nm, respectively.

The dielectric constant ϵ changes with each layer. For GaAs it is 12.9 and for AlGaAs it is 13.1. The transverse effective mass is $m_t = 0.19 \times m_0$ and the longitudinal effective mass is $m_\ell = 0.98 \times m_0$, where m_0 represents the electron rest mass. In the analysis a temperature of 4.2K is used.

For the GaAs based structure, Schroedinger equation [91] is analysed by considering an initial electrostatic potential

$$\phi(x, z) = \frac{\hbar^2 q}{2m_z(z)} \frac{1}{m_z(z)} \frac{\partial}{\partial z} m_z(z) \frac{\psi_z}{\psi} - \frac{2m_z(z)}{\hbar^2} V_{xc}(n) \psi, \quad (7.1)$$

where V_h and $V_{xc}(n)$ are given in chapter 4. Using this initial potential, Schroedinger's equation in 2D becomes

$$\psi_{xx} + 2\text{sech}^2(x - \sqrt{2}z)\psi - \frac{2m_z(z)}{\hbar^2}(V_h - \lambda)\psi = 0. \quad (7.2)$$

The main interest here is to calculate the bound states (eigenvalues) of Schroedinger's equation using the Evans function and each calculated electrostatic potential obtained from Poisson's equation. The Evans function for equation (7.2) is

$$D(\lambda) = \frac{-2\sqrt{2}C_-C_+(\hbar^2(\sqrt{2}-1) + 4m_z(z)(V_h - \lambda))\sqrt{(m_z(z)(V_h - \lambda))}}{\hbar^3}.$$

The zeros of this functions are

$$\lambda_1 = V_h \quad (7.3)$$

$$\lambda_2 = \frac{\hbar^2(\sqrt{2}-1) + 4m_z(z)V_h}{4m_z(z)}. \quad (7.4)$$

By hypothesis (see chapter 5), one rejects $\lambda_1 = V_h$. Using these eigenvalues the eigenfunctions are calculated and one iterates between Schroedinger and Poisson's equation until convergence.

| Ladder | State | Semi-analytical energy (meV) | Trellakis [91] energy (meV) | Relative error (%) |
|--------|-------|---------------------------------|-----------------------------------|--------------------|
| 1 | 1 | 39 | 38 | 2.63 |
| 1 | 2 | 42 | 41 | 2.44 |
| 1 | 3 | 44 | 43 | 2.33 |
| 1 | 4 | 47 | - | - |
| 1 | 5 | 49 | - | - |

Table 7.1: Eigenvalues (meV) for Device 1, obtained via the semi-analytical method.

The simulation results obtained via the semi-analytical method are displayed in Table 7.1. In Figure 7.2 the graph of the eigenvalues is plotted for various gate voltages. In addition, applying a temperature of 4.2 K and a voltage of 1.3V on the gate, the distribution of eigenvalues is displayed in Figure 7.3. These results are in good agreement with those reported in [91]. Furthermore, it is reported in [91] that simulation run time of 10 minutes were obtained on Hewlett-Packard C-110 workstations. Using the semi-analytical method, the improved run time 7.38 seconds is achieved, suggesting a significant improvement in simulation run time using the semi-analytical method.

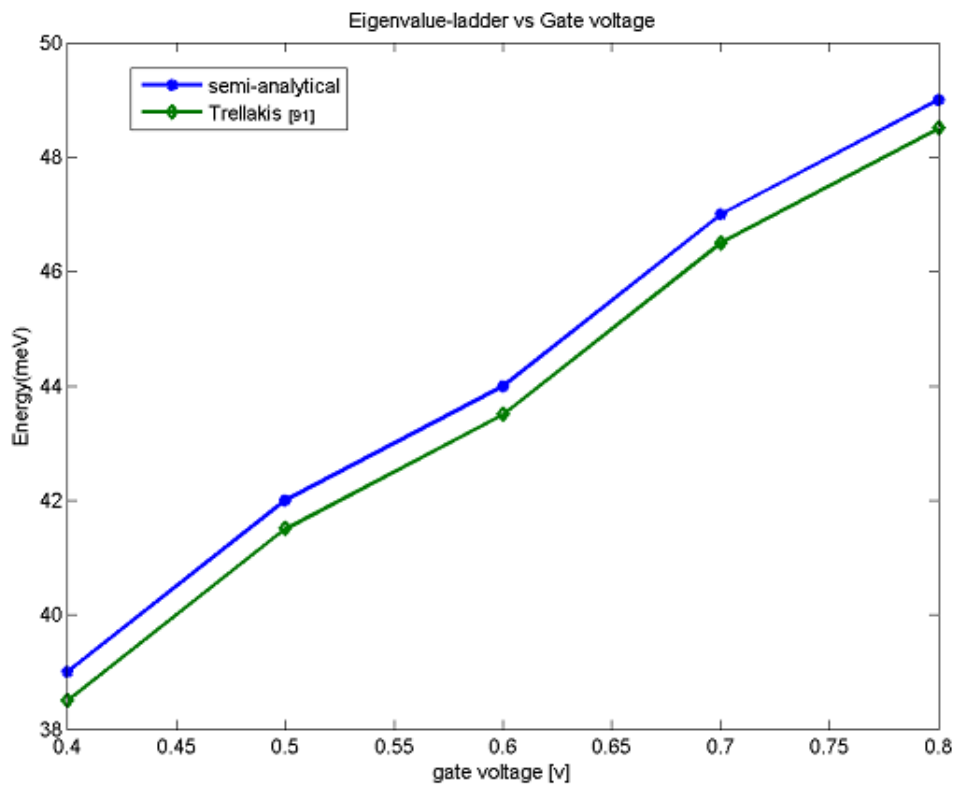


Figure 7.2: Gate voltage vs. Energy-subband (meV) for Device 1.

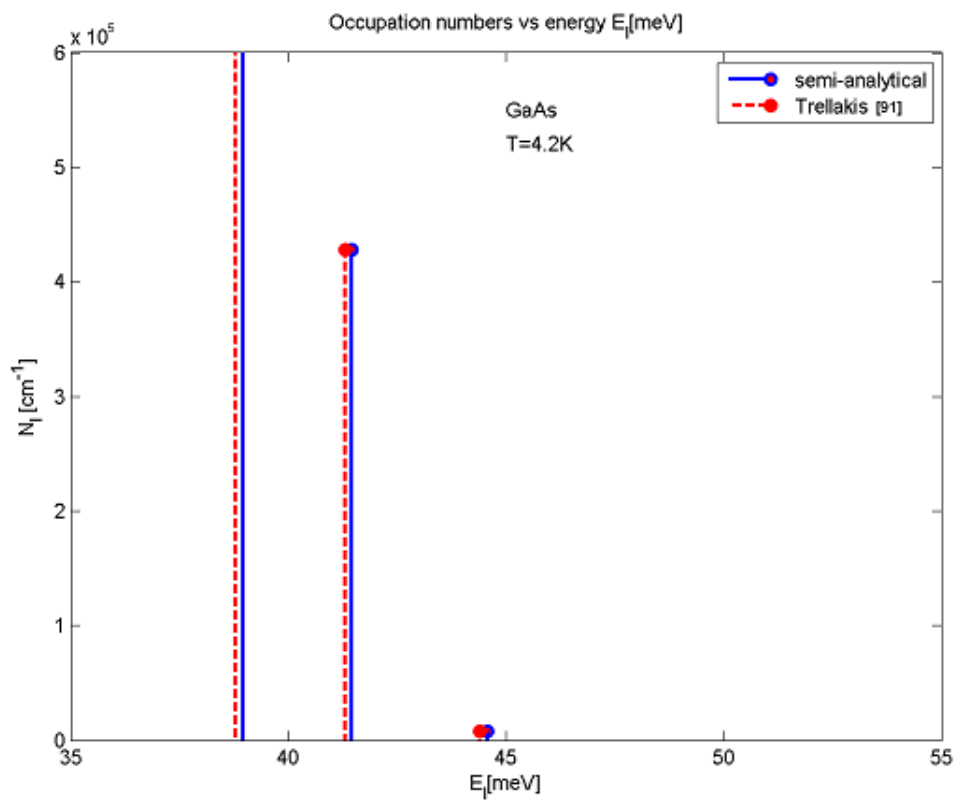


Figure 7.3: Occupation numbers N_ℓ of states E_ℓ for Device 1 shown in Figure 7.1.

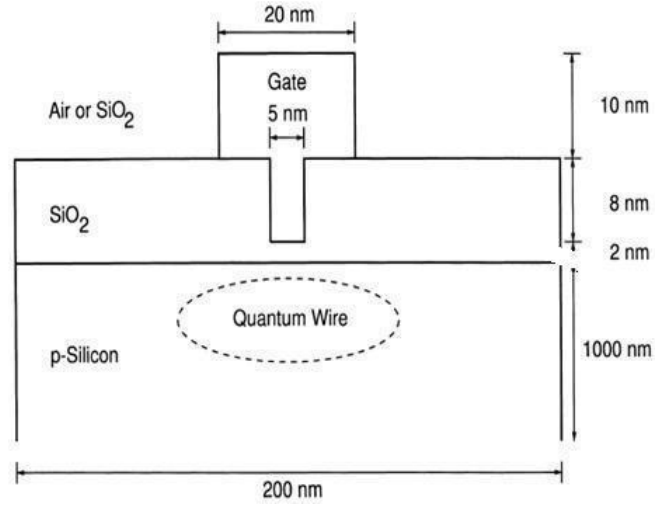


Figure 7.4: [91]. Device 2: A $Si - SiO_2$ based quantum device with a T-shaped gate.

7.2 Device 2: A $Si-SiO_2$ based quantum device with a T-shaped gate

A second device considered is the SiO_2 based quantum device with a T-shaped gate given in Figure 7.4. which is previously considered in [91]. For this device a 2D simulation of transport is considered. The cross-section of the device is shown in Figure 7.4. It has lateral dimension 200 nm and vertical height 1020 nm. Two values of the acceptor concentration in the substrate, $N_A = 10^{10} cm^{-3}$, and $N_A = 10^{18} cm^{-3}$ are considered. The parameter for dielectric constant is 11.8 in the silicon substrate. The transverse effective mass is $m_t = 0.19 \times m_0$ and the longitudinal effective mass is $m_\ell = 0.98 \times m_0$. In the calculation, room temperature of $300K$ is applied in the simulation process. These parameters are summarised in Table 7.2.

| Parameter | Value |
|---------------------------------|--------------------------|
| L_x | $0 \times 200nm$ |
| L_y | $0 \times 1020nm$ |
| Temperature T | 300K |
| N_A^{Si} | $10^{18}cm^{-3}$ |
| $N_A^{SiO_2}$ | $10^{10}cm^{-3}$ |
| Electron mass (m_0) | $9.11 \times 10^{-31}kg$ |
| m_l | $0.98 \times m_0$ |
| m_t | $0.19 \times m_0$ |
| Dielectric constant (Si) | 11.7 |
| Dielectric constant (SiO_2) | 3.9 |

Table 7.2: Parameters for modelled Device 2 which is displayed in Figure 7.4.

As the conduction band in silicon has six valleys which are aligned in pairs along the principal axes, the valleys are described by three different tensors for the effective mass. Consequently, Schroedinger's equation has to be solved three times in order to obtain three different sets of eigenvalues ladders for the quantum state, [91].

7.2.1 Eigenvalues for simulated structure

The three different sets of eigenvalues ladders for the device in Figure 7.4 obtained, via the Semi-analytical method, are presented below. In particular, Tables 7.3, 7.5 and 7.7 give those eigenvalues obtained in [91] and those obtained through the application of the Semi-analytical method which are in good agreement. Furthermore, the simulation times achieved in [91] and the Semi-analytical method are compared. The comparison shows improved simulation times using the Semi-analytical method.

Table 7.3 displays the simulated eigenvalues (in meV) obtained via the Evans function. It also shows those obtained in [91] and it gives error estimates for the first ladder. The errors are quite small suggesting that the Evans function is quite robust in capturing the eigenvalues of the considered device.

In addition, shown in Table 7.4 below are the relative errors with respect to the reference solutions reported in [91] for ladder 1.

Figure 7.5 shows graph of ladder 1 of the eigenvalues obtained via the Evans function plotted against gate voltages. It can be seen that as the gate voltages increase the energy levels also increase suggesting a linear relation-

| Ladder | State | Energy (meV) | Trellakis(meV) [91] | Error |
|--------|-------|--------------|---------------------|----------|
| 1 | 1 | 207.993076 | 208 | 0.006924 |
| 1 | 2 | 267.010722 | 267 | 0.010722 |
| 1 | 3 | 328.008028 | 328 | 0.008028 |
| 1 | 4 | 348.971027 | 349 | 0.028973 |
| 1 | 5 | 383.011987 | 383 | 0.011987 |

Table 7.3: Device 2 - Eigenvalues (meV) for Ladder 1 obtained via Semi-analytical method and Trellakis [91].

| Ladder | State | Relative Error (%) |
|--------|-------|--------------------------|
| 1 | 1 | 3.32885×10^{-3} |
| 1 | 2 | 4.01573×10^{-3} |
| 1 | 3 | 2.44756×10^{-3} |
| 1 | 4 | 8.30172×10^{-3} |
| 1 | 5 | 3.12977×10^{-3} |

Table 7.4: Device 2: Relative errors (meV) of the Semi-analytical method- Ladder 1.

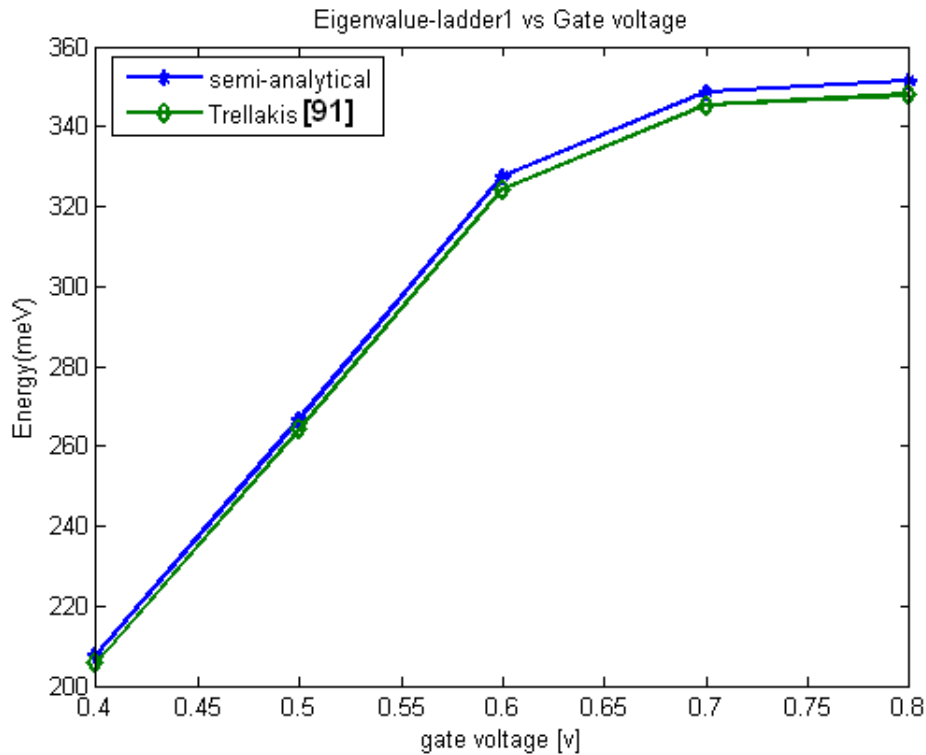


Figure 7.5: Device 2: Gate voltage vs. energy (meV) for quantum wire.

ship between both variables.

In addition, Table 7.6 presents the relative errors obtained through the semi-analytical method for ladder 2.

Furthermore, Table 7.5 shows the second eigenvalue ladder as well as the error estimates. From the calculations, it is clear that the two sets of results are in good agreement and the Semi-analytical method has the advantage of improved simulation time.

Figure 7.6 shows that as the gate voltage increases for the second eigenvalue ladder, the energy levels increase. Again, this suggests a linear relationship between both variables. Table 7.7 shows the details for the third

| Ladder | State | Energy (meV) | Trellakis(meV) [91] | Error |
|--------|-------|--------------|---------------------|----------|
| 2 | 1 | 298.999998 | 299 | 0.000002 |
| 2 | 2 | 322.014321 | 322 | 0.014321 |
| 2 | 3 | 347.214807 | 347 | 0.214807 |
| 2 | 4 | 371.999998 | 372 | 0.000002 |
| 2 | 5 | 396.472145 | 396 | 0.472145 |

Table 7.5: Device 2: Eigenvalues (meV) for ladder 2.

| Ladder | State | Relative Error (%) |
|--------|-------|---------------------------|
| 2 | 1 | 6.68896×10^{-7} |
| 2 | 2 | 4.44752×10^{-3} |
| 2 | 3 | 6.1904×10^{-2} |
| 2 | 4 | 5.37634×10^{-7} |
| 2 | 5 | 1.192285×10^{-1} |

Table 7.6: Device 2: Relative errors (meV) of the semi-analytical method for Ladder 2.

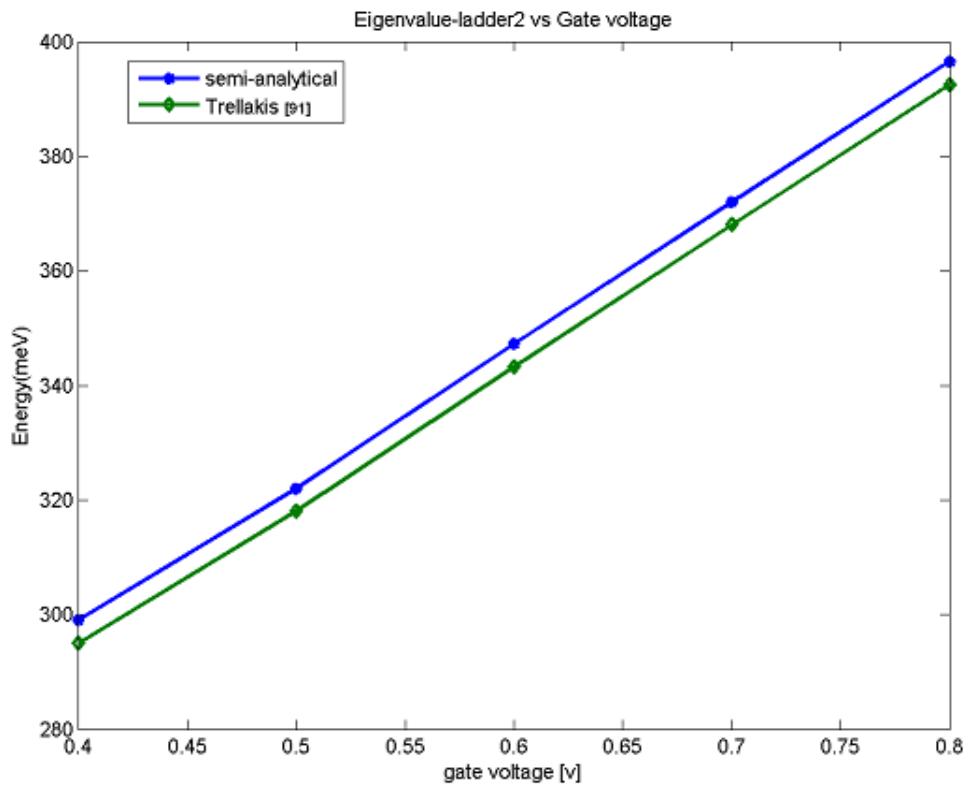


Figure 7.6: Device 2: Gate voltage vs. energy (meV) for quantum wire for ladder 2.

| Ladder | State | Energy (meV) | Trellakis(meV) [91] | Error |
|--------|-------|--------------|---------------------|----------|
| 3 | 1 | 314.241562 | 314 | 0.241562 |
| 3 | 2 | 368.472178 | 368 | 0.472178 |
| 3 | 3 | 424.814264 | 424 | 0.814264 |
| 3 | 4 | 476.067852 | 476 | 0.067852 |
| 3 | 5 | 523.492615 | 523 | 0.492615 |

Table 7.7: Device 2: Ladder 3 eigenvalues (meV).

| Ladder | State | Relative Error (%) |
|--------|-------|---------------------------|
| 3 | 1 | 7.69306×10^{-2} |
| 3 | 2 | 1.283092×10^{-1} |
| 3 | 3 | 1.920434×10^{-1} |
| 3 | 4 | 1.42546×10^{-2} |
| 3 | 5 | 9.41902×10^{-2} |

Table 7.8: Device 2: Relative errors (meV) of the semi-analytical method for ladder 3.

eigenvalue ladder with the error estimates. Figure 7.7 plots gate voltages against different energy levels for ladder 3.

Below in Table 7.8 are the relative errors for Ladder 3 obtained through the semi-analytical method.

Table 7.9 gives improved simulation times obtained through the semi-analytical method compared to the total run-time of 30 minutes reported in [91] for the highly doped silicon device. It is clear that the semi-analytical

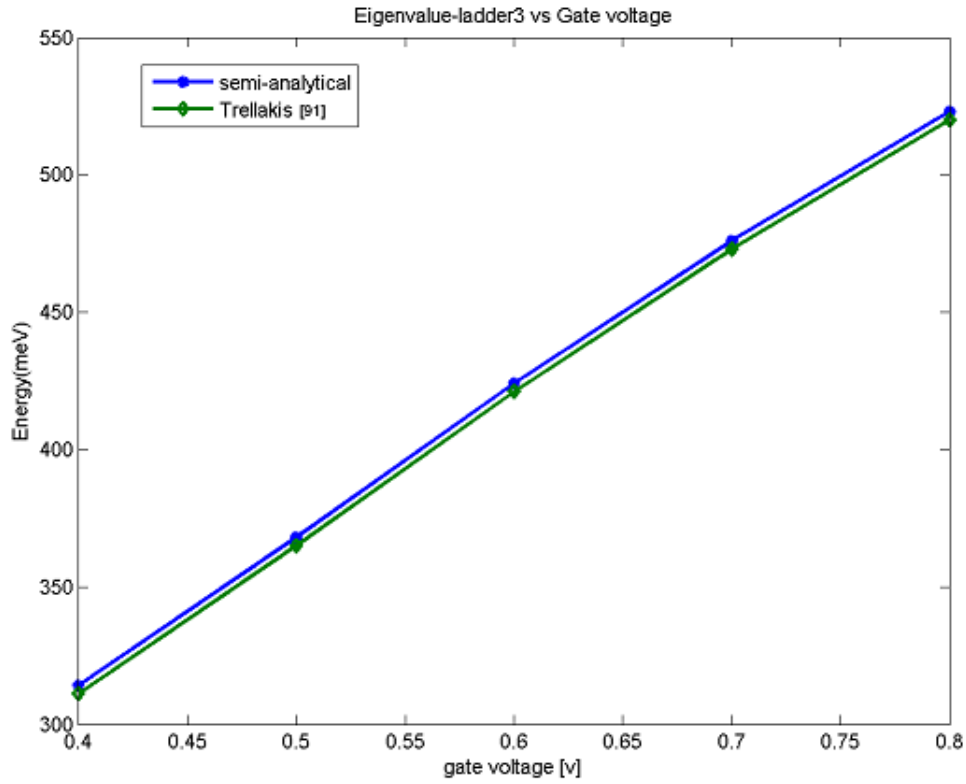


Figure 7.7: Device 2: Ladder 3 gate voltage vs. energy(meV) for quantum wire.

method shows considerable improvement in simulation time. Finally, Figure 7.8 shows a direct comparison of the energy plotted against various gate voltages for the three different eigenvalues (energies) ladders obtained via the Semi-analytical method.

Figure 7.8 shows a combination of all three eigenvalue ladders which are plotted for gate voltages. It can be seen that there is more variation in the electron transport of the device corresponding to ladder1.

The results for the distribution of eigenvalues are depicted in Figure 7.9. The occupation numbers N_ℓ of states E_ℓ for the first ladder are dis-

| Ladder | Times (secs.) | Device |
|--------|---------------|-----------------------------|
| 1 | 3.063924 | <i>Si – SiO₂</i> |
| 2 | 4.046392 | <i>Si – SiO₂</i> |
| 3 | 4.040628 | <i>Si – SiO₂</i> |

Table 7.9: Device 2: Computational times (seconds) for *Si – SiO₂* Device 2 by the semi-analytical method.

played. There is a clear exponential decay of occupation numbers. It can be seen that at a temperature of $300K$, almost all energies are located above the Fermi level E_F . This suggests that the distribution function which describes the occupation numbers decays exponentially with a decaying constant $K_B T = 0.025\text{eV}$, [91]. Whilst only a few states are occupied for the highly doped structure, where $N_A = 10^{18}\text{cm}^{-3}$, it can be seen in Figure 7.10 that the spectrum is dense in the case of the undoped structure, where $N_A = 10^{10}\text{cm}^{-3}$.

By analysis of the cross-sections of the electron density n parallel to the *Si–SiO₂* interface, one can explain this difference in that the quantum wire is very compact for highly doped devices with a width of approximately 20 nm, Figure 7.11 and a core shell of $6 \times 10^{19}\text{cm}^{-3}$. This tight confinement results in size quantisation and large separation of energy levels. For the undoped case, the quantum wire is much wider as indicated in Figure 7.12, and the spread of electron density is much wider extending to a larger distance of 60nm with a core shell of 4×10^{18} , [91].

Lastly, in this section the dependence of electron density on gate voltage is

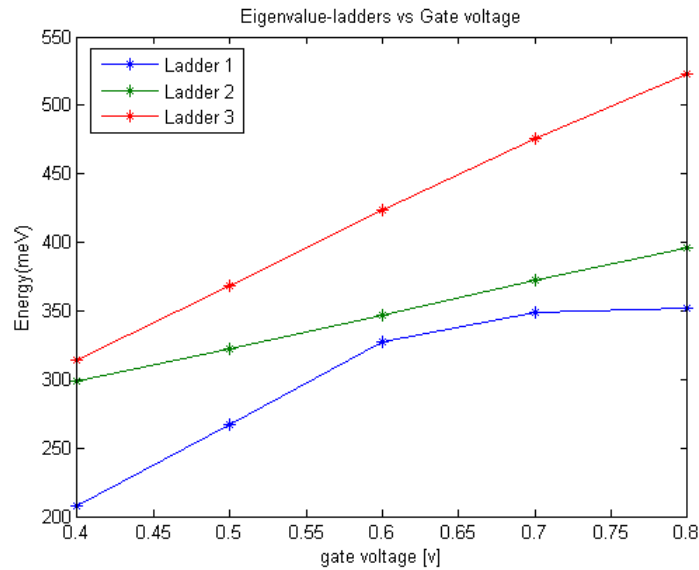


Figure 7.8: Device 2: Energy for different effective masses vs. gate voltage.

analysed for both doping cases. The in Figure 7.13 shows a threshold voltage of approximately 2.1 V for the highly doped structure and approximate 0.5V for the undoped structure displayed in Figure 7.14.

7.3 Device 3: A double well quantum device

In order to compare simulation results with those in [12], Device 3 is analysed in three dimensions and one dimension for the simulation of transport. Figure 7.15 shows a double gate quantum well device which was previously analysed in [12]. The lightly (yellow) shaded regions show the locations of the applied potential (gates). The lightly shaded (yellow) internal regions are the layers of InGaAs.

It has lateral dimensions 250 nm by 250 nm. The height is 626.8 nm. It

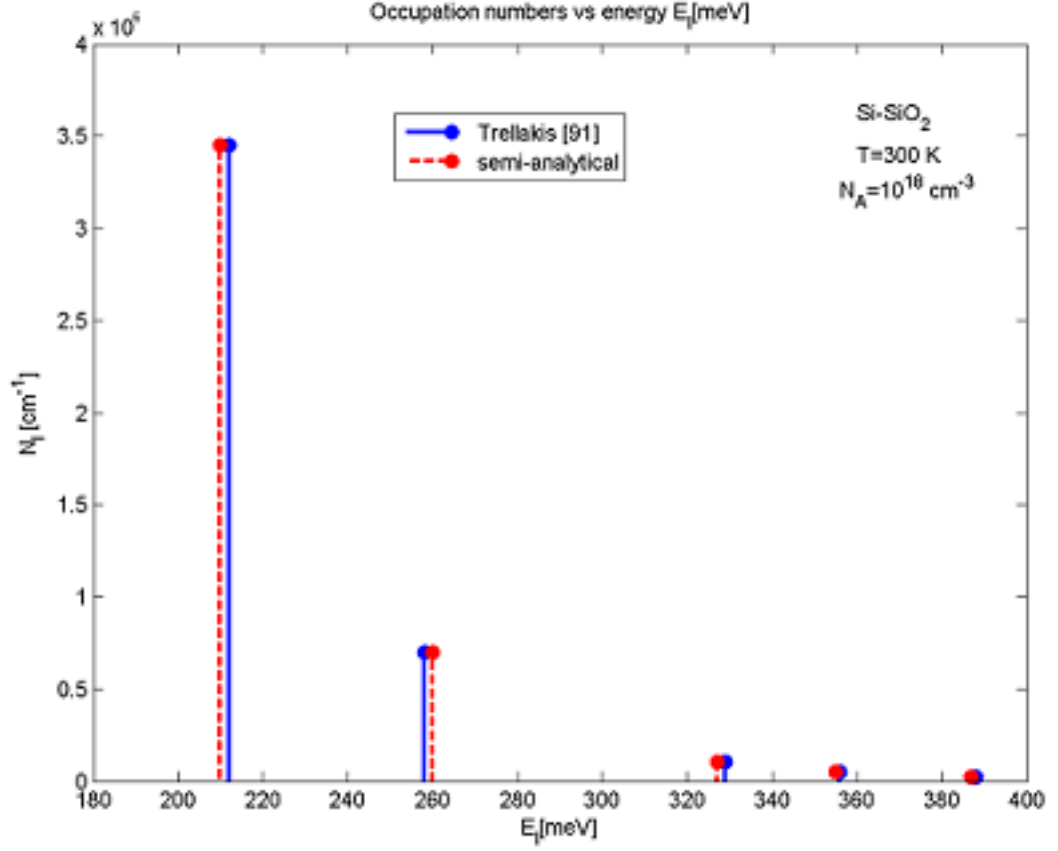


Figure 7.9: Device 2: Occupation numbers N_ℓ of states E_ℓ for first eigenvalue ladder with $N_A = 10^{18} \text{cm}^{-3}$.

has six layers in its vertical structure. These are AlInAs (20 nm), InP (57.6 nm), InGaAs (12.6 nm), another InP layer (10.6 nm) followed by InGaAs (16 nm) and InP (510 nm). Furthermore, this device has two doping strengths $N_D = 3.5 \times 10^{11} \text{cm}^{-2}$ and $N_D = 0.5 \times 10^{11} \text{cm}^{-2}$ which are located at 40.5 nm and 167.5 nm respectively. In each layer, the dielectric constant and the effective masses were constant. For AlInAs, the dielectric constant is 12.71 and the effective mass is $0.073 m_0$, in InGaAs, dielectric constant is 14.11 and

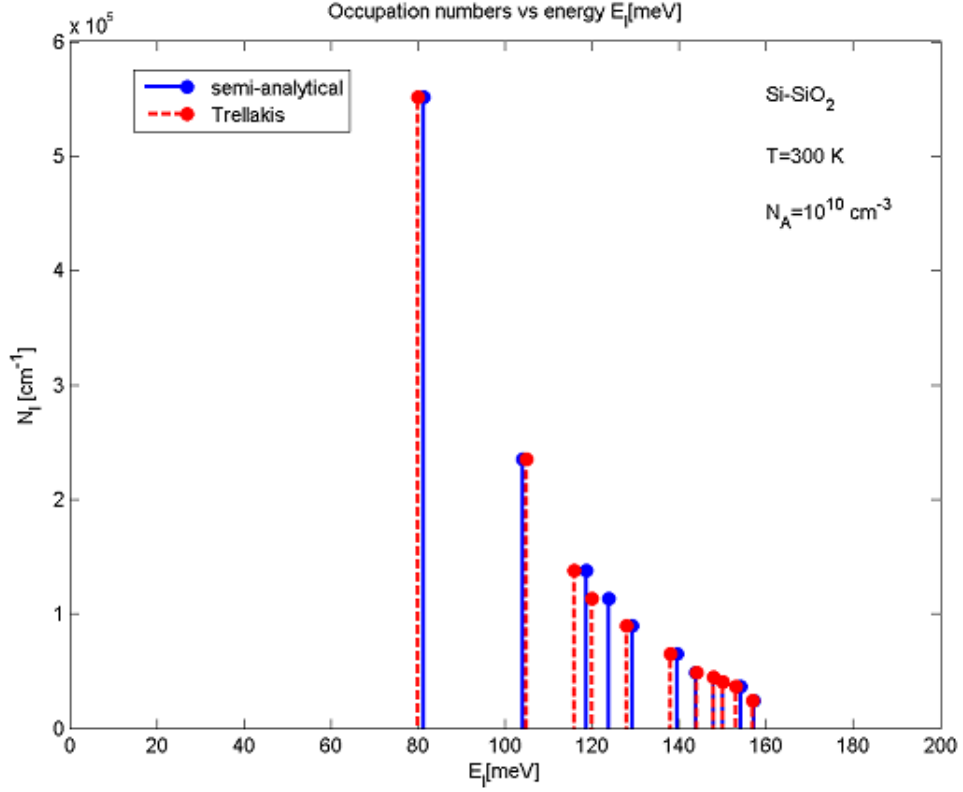


Figure 7.10: Device 2: Occupation numbers N_ℓ of states E_ℓ for first eigenvalue ladder $N_A = 10^{10} \text{cm}^{-3}$.

effective mass is $0.043 m_0$ and for InP the dielectric constant and effective masses are 12.61 and $0.0795 m_0$ respectively. For the band offset, 0.252 eV is used for AlInAs and -0.216 eV for InGaAs. In the InP layer the doping density is $3 \times 10^{15} \text{cm}^{-3}$. Finally, all computations are done at a temperature of 4.2K.

The material properties of the layers of InGaAs induce potential wells in the vertical direction while voltages applied to the gate on top of the device induce a potential confining electrons in the transverse directions. In

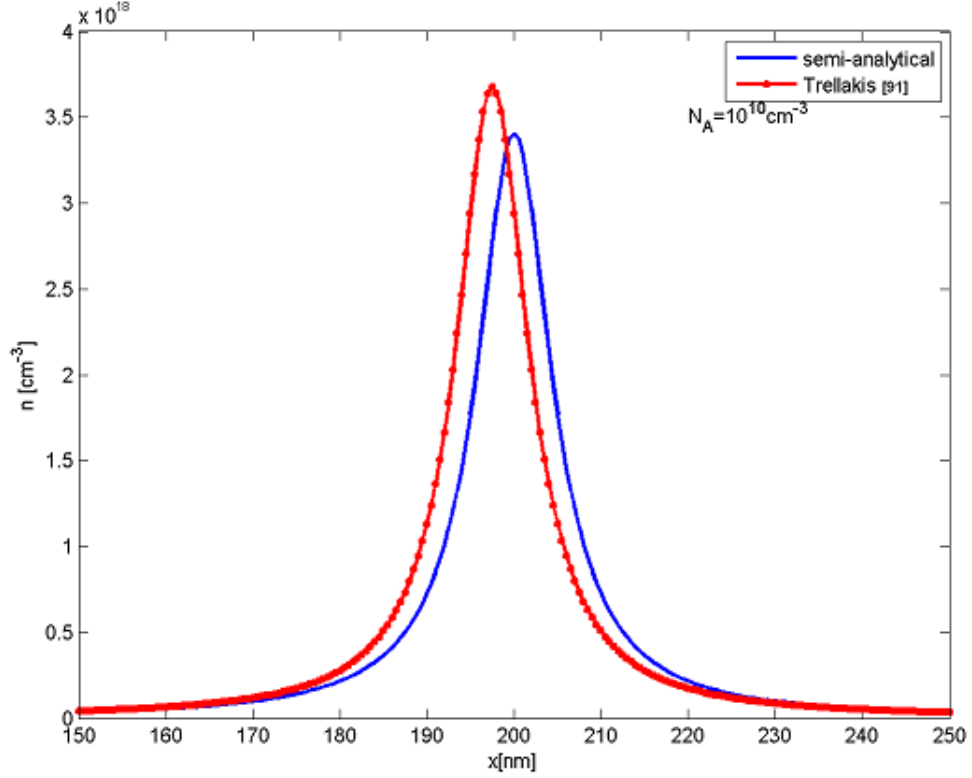


Figure 7.11: Device 2: Cross-section of quantum electron density parallel to $Si - SiO_2$ with $N_A = 10^{18} cm^{-3}$.

Figure 7.16, the potential at $x = 0, y = 0, z \in [0, 400nm]$ for Device 3 is shown. Further, Figure 7.17 shows the transverse slice of the potential in the upper well (at $z=84 nm$ for $(x, y) \in [-250nm, -250nm] \times [250nm, 250nm]$) is shown. A significant feature of the potential in the transverse direction is the dip in the centre. The dip in the potential confines states laterally in the upper well.

Figure 7.18 presents the energy of the lowest energy state in the upper well given as a function of the gate voltage. One curve shows the results

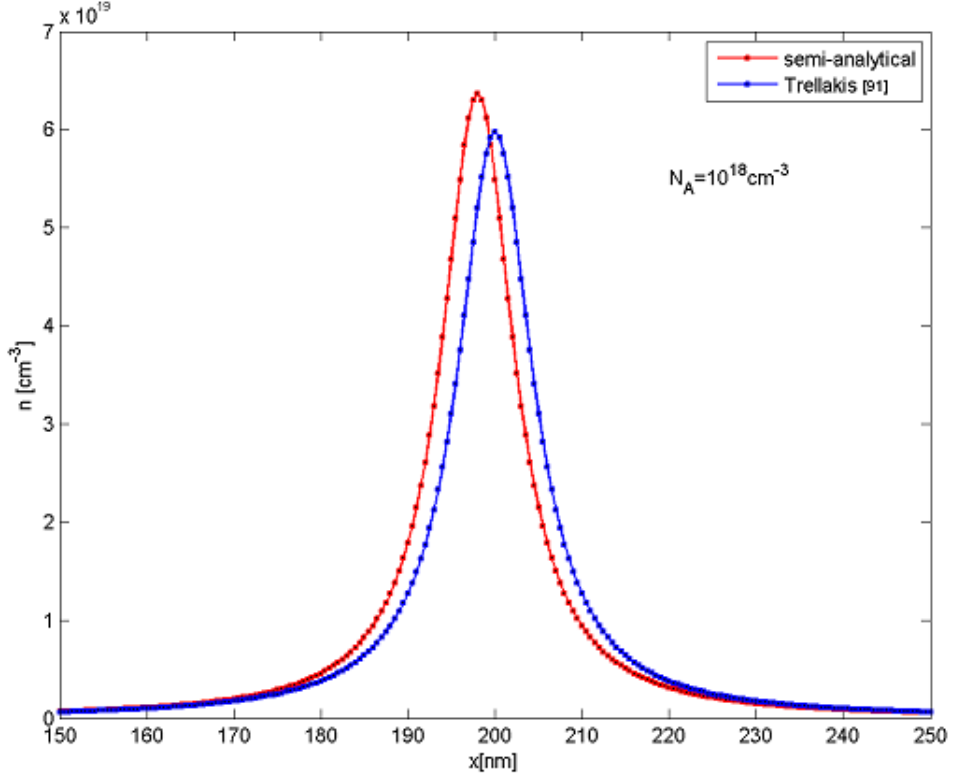


Figure 7.12: Device 2: Cross-section of quantum electron density parallel to $Si - SiO_2$ with $N_A = 10^{18} cm^{-3}$.

obtained via the semi-analytical method and the other shows those results given in [12]. Furthermore, the computational times are presented in Figure 7.19. The results show improved simulation time is achieved using the Semi-analytical method.

Turning to the one -dimensional case, the eigenvalues obtained via the Evans function are set out in Table 7.10. Clearly, the results are in good agreement with those found in [12]. Moreover, there is the achievement of improved simulation times compared with those reported in [12]. The total

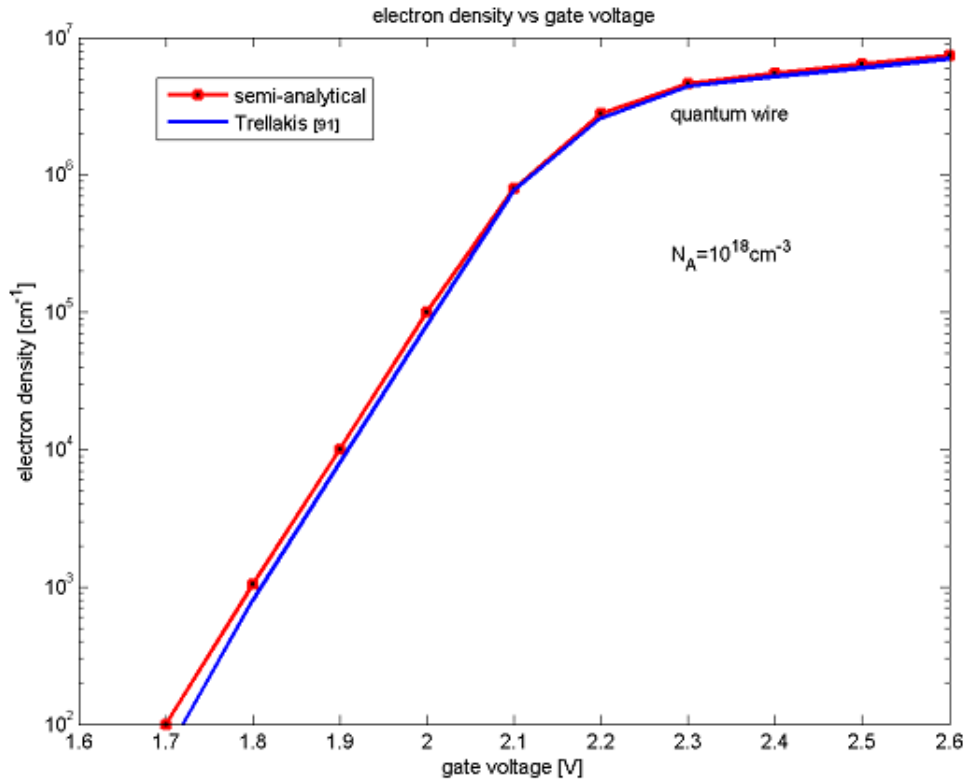


Figure 7.13: Device 2: Electron density in quantum wire as well as undoped substrate as a function of gate potential with $N_A = 10^{18} \text{cm}^{-3}$.

simulation time achieved is 10 mins. and 42 secs. compared with a total of 15 mins. and 30 secs. reported in [12]. The results obtained by the semi-analytical method were achieved using Intel(R) Core (TM)2 Duo CPU T6570 with speed 2.10 GHz. In [12] the computer used for the simulation was not reported.

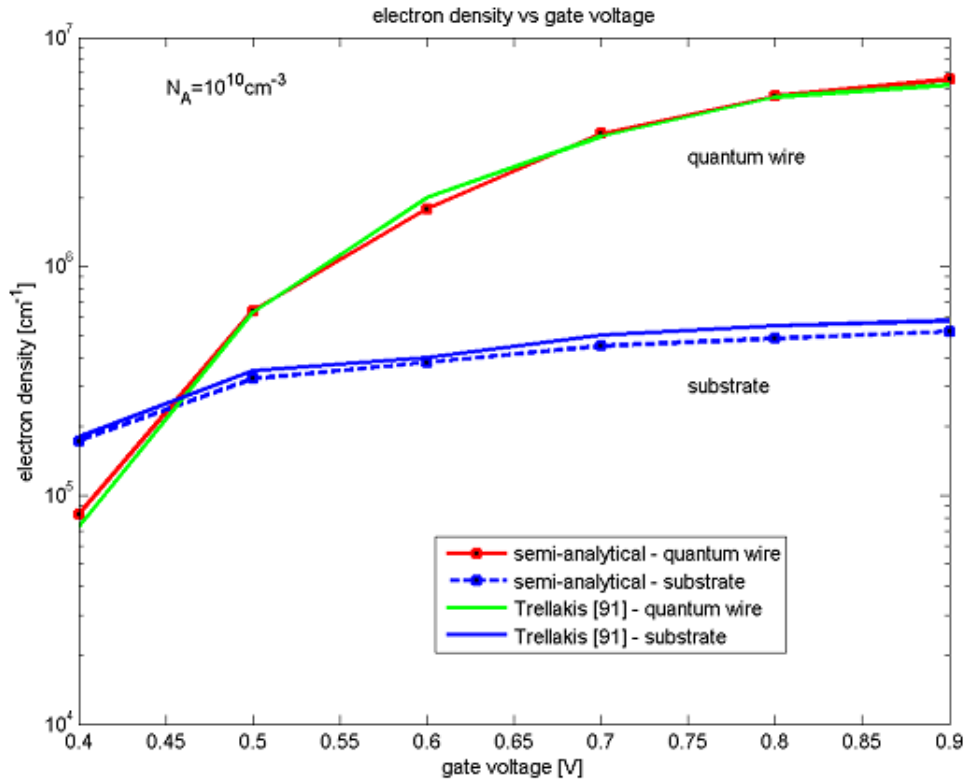


Figure 7.14: Device 2: Electron density in quantum wire as well as undoped substrate as a function of gate potential with $N_A = 10^{10} \text{cm}^{-3}$.

7.4 Device 4: Analysis of the double gate 10 nm by 10 nm MOSFET

This section of the thesis analyses a double gate 10 nm by 10 nm MOSFET which has been previously analysed in [6]. The various parameters are given in Table 7.12. Figure 7.20 shows the double gate NMOSFET. The simulation results obtained by the semi-analytical results are given and compared with those given in [6]. The analysis here relates to a 2-D simulation of transport.

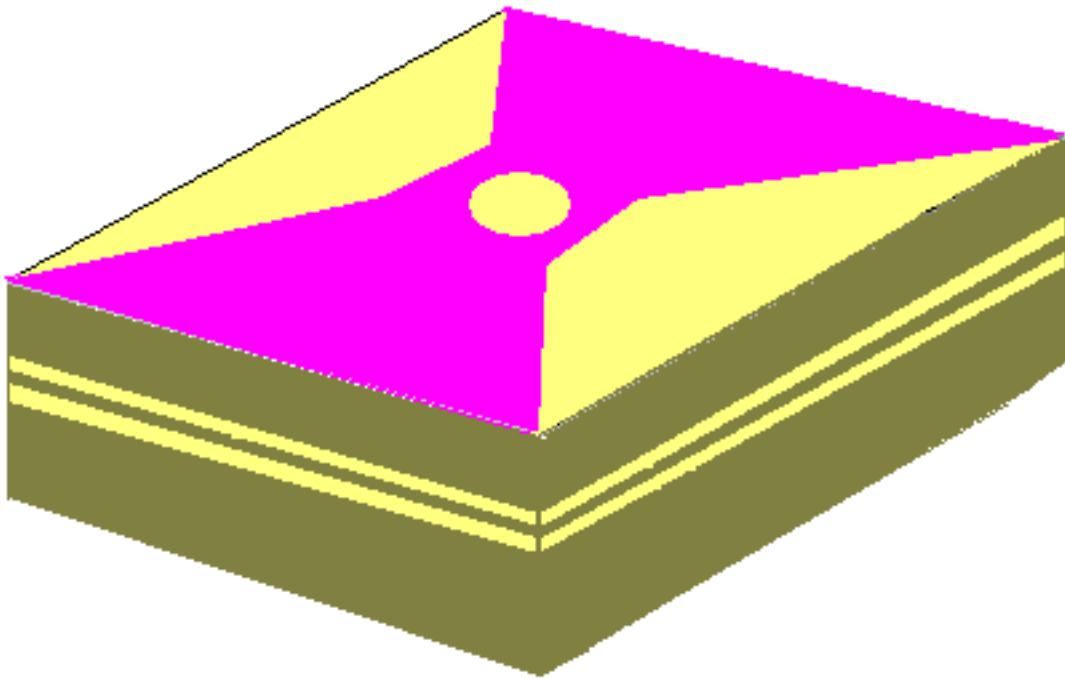


Figure 7.15: Architecture of Device 3: Lightly shaded regions on top are the locations of the applied gates. The internal lightly shaded regions are InGaAs layers [12].

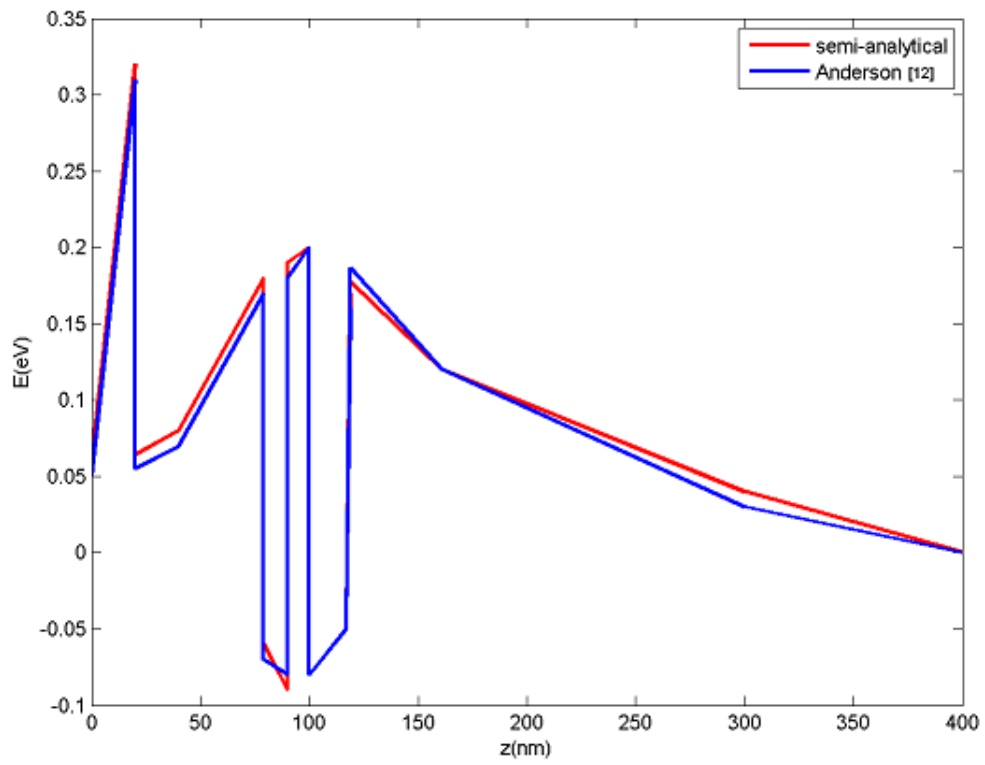


Figure 7.16: Potential in Device 3 obtained by the semi-analytical method compared to that reported in Anderson [12].

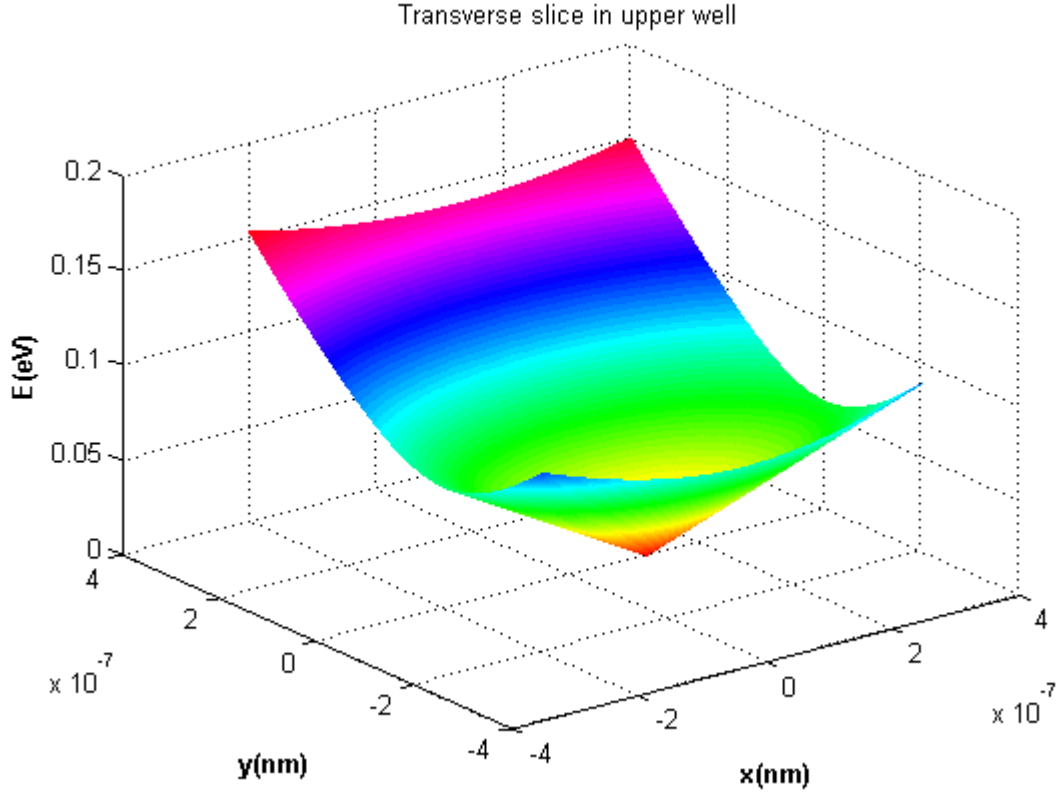


Figure 7.17: Device 3: Potential in the transverse directions in the centre of the upper quantum well as shown in [12]. This plot is obtained by the semi-analytical method.

This section studies the following system of coupled Schrodinger-Poisson's equation which is used to analyse the above NMOSFET. In [6] this equation is given as:

$$(H - qV(x, z)) \psi_E(x, y, z) = E\psi_E(x, y, z), \quad (7.5)$$

with $(x, y, z) \in [a, b]$ and H is Hamiltonian, defined by

$$H = -\frac{\hbar^2}{2} \left(\frac{1}{m_x(z)} \Delta_x + \frac{1}{m_y(z)} \Delta_y \right) - \frac{\hbar^2}{2} \frac{\partial}{\partial z} \left(\frac{1}{m_z(z)} \frac{\partial}{\partial z} \right). \quad (7.6)$$

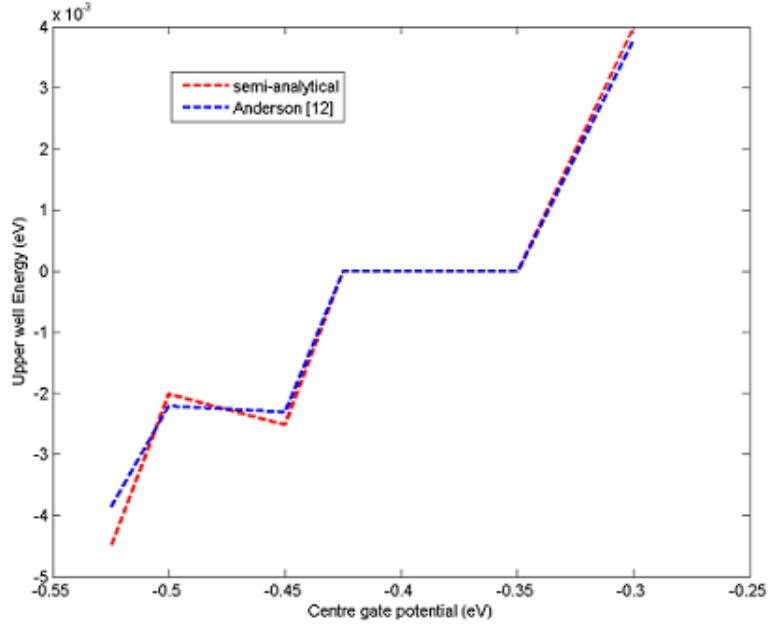


Figure 7.18: Device 3: Upper well energy (lowest state) as a function of gate voltage obtained by the semi-analytical method. Comparison with the simulation results reported in Anderson [12].

ψ_E is the complex valued wave function which depends on the energy E , \hbar is the plank's constant, q is the elementary electron charge. In addition, we denote m_x, m_y, m_z as the z -dependent effective masses in the x, y and z -direction. The electrostatic potential V is x, z dependent and is split into exterior potential v_e and self-consistent potential V_s . In order to obtain V_s

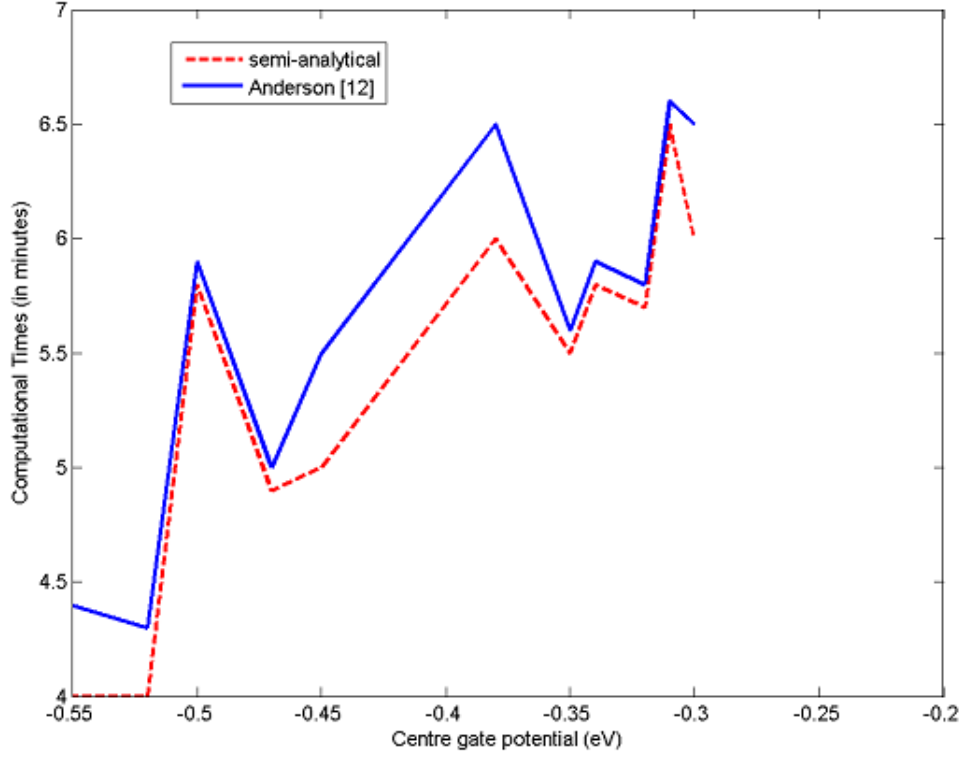


Figure 7.19: Device 3: Computation times for the results shown in Figure 7.18.

we solve the Poisson's equation

$$\Delta V_s(x, z) = -qn(x, z), \quad (7.7)$$

$$\partial_n V_s(a, \cdot) = 0 \quad (7.8)$$

$$\partial_n V_s(\cdot, b) = 0, \quad (7.9)$$

$$V_s(\cdot, 0) = V_g^0, \quad (7.10)$$

$$V_s(\cdot, 1) = V_g^1, \quad (7.11)$$

∂_n denotes the normal derivative to the boundary. Furthermore, V_g^0 and V_g^1

| Eigenvalues via Evans function | Eigenvalues in [12] | Error | Relative Error |
|--------------------------------|---------------------|-------------------------|----------------|
| -0.01214986 | -0.01217886 | 2.9×10^{-5} | 0.2381 |
| -0.01217912 | -0.01217918 | 6×10^{-8} | 0.2407 |
| -0.01216957 | -0.01217957 | 1×10^{-5} | 0.0821 |
| -0.01214525 | -0.01217969 | 3.444×10^{-5} | 0.2828 |
| -0.01214576 | -0.01217972 | 3.3396×10^{-5} | 0.2788 |
| -0.01218723 | -0.01217974 | 7.49×10^{-6} | 0.0615 |

Table 7.10: Device 3: Eigenvalues for modelled device with relative error given in percentage.

are the applied gate voltages. Finally, the electron density is

$$n = \int |\psi_E(x, y, z)|^2 f_{FD}(E) dE. \quad (7.12)$$

We call f_{FD} the Fermi-Dirac distribution function.

In this model one accounts for the anisotropic crystal structure Si, which is illustrated by six equivalent conduction band ellipsoid. As such we have to solve Schroedinger-Poisson three times and obtain three different sets of eigenvalue ladder. The three different configurations of the effective mass m^* are given by (m_ℓ, m_t, m_t) , (m_t, m_ℓ, m_t) and (m_t, m_t, m_ℓ) , where m_t and m_ℓ are the transverse and longitudinal masses of the material.

Figure 7.21 displays three conduction energy subbands for voltage $V_{DS} = 0.2V$ and $V_{GS} = 0V$. These results are obtained by the semi-analytical method. Similar results are obtained by the SDM/WKB method and are reported in [6]. In order to validate the results obtained by the semi-analytical method, the dotted line (extracted from [6]) suggests good agreement of the

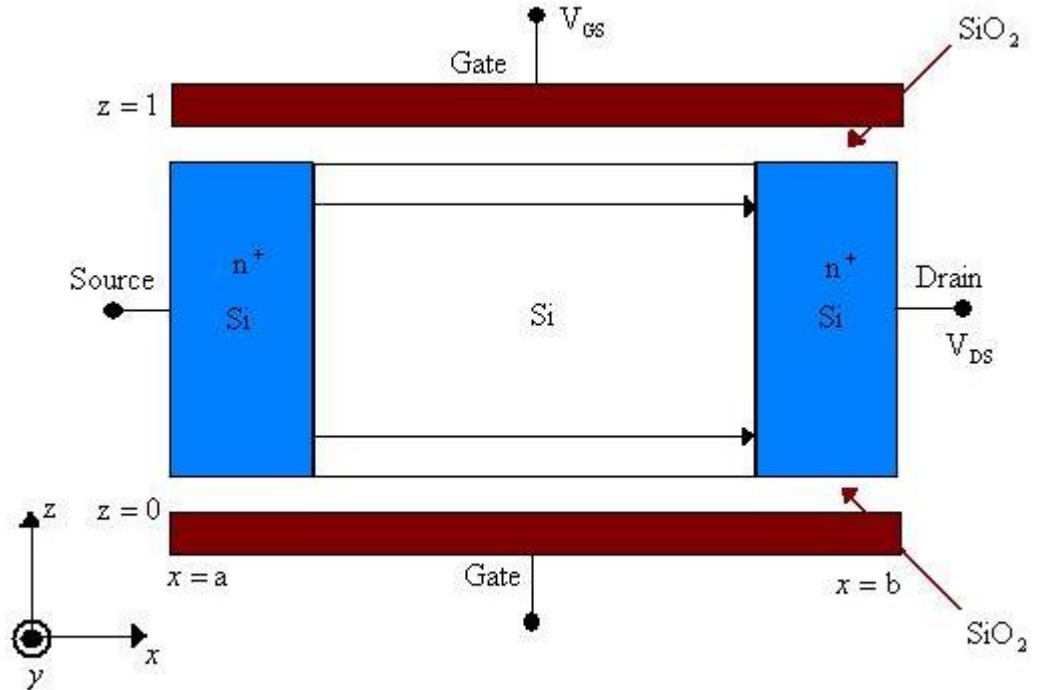


Figure 7.20: Architecture of Device 4: Double-gate NMOSFET.

semi-analytical method with SDM/WKB for conduction energy subband m_t .

Furthermore, Figure 7.22 represents the profile of the first m_t energy subband for various drain-source voltages. These results are obtained by application of the semi-analytical method. In [6], similar results which are obtained by the SDM/WKB method are reported and compared to a reference solution. The results obtained by the semi-analytical method were achieved using Intel(R) Core(TM)2 Duo CPU T6570 with speed 2.10 GHz. In [6] the computer used for the simulation was not reported.

And finally, Figure 7.23 displays the current voltage characteristics of the

| Ladder1 | Ladder2 | ladder3 |
|--------------|--------------|---------------|
| -0.023005358 | -0.266777769 | -0.0298676008 |
| -0.017901324 | -0.182224116 | -0.0150325876 |
| -0.013099594 | -0.085786000 | -0.0047394417 |
| -0.022388273 | -0.261897300 | -0.0309407186 |
| -0.019499282 | -0.173129433 | -0.0151024436 |

Table 7.11: Device 4: eigenvalues (eV). These results are obtained by the semi-analytical method.

modelled double-gate NMOSFET.

7.5 Device 5: A single walled carbon nanotube device

Single walled carbon nanotubes (SWCNTs) having structures and properties of very small dimensions with short channel scaled down to 50 nm exhibit nearly ballistic carrier transport making them good candidates for electronic devices [51]. Therefore, it is necessary to study the physics with which these structures are associated. This section of the thesis analyses the simulation results obtained by the semi-analytical method for a cylindrical structure [56] which is an approximation of the real device structure given in Figure 7.24.

The device shown in Figure 7.24 is comprised of five layers. A channel length $L \sim 50\text{nm}$ long SWNT is situated between the drain and source. In

| Parameter | Value |
|-------------|----------------------|
| L_x | $18nm$ |
| L_z | $12nm, 7nm, 5nm$ |
| L_{OX} | $1nm$ |
| L_{Si} | $10nm, 5nm, 3nm$ |
| L_R | $4nm$ |
| L_{CH} | $10nm$ |
| m_{SiO_2} | $0.5 \times m_0$ |
| m_l | $0.98 \times m_0$ |
| m_t | $0.19 \times m_0$ |
| T | $300K$ |
| n^+ | $10^{20}cm^{-3}$ |
| V_{GS} | $-0.3, \dots, 0.5eV$ |
| V_{DS} | $-0, \dots, 0.5eV$ |
| E_C | $3.15eV$ |

Table 7.12: Device 4: Parameters for the modelled device [6].

addition, it consists of 8 nm thick HfO_2 high- κ ($\kappa \sim 15$) gate insulator which is formed on top of the SWNT by a process called atomic layer deposition (ALD) at temperature $90^\circ C$ and a top Al gate electrode. Sandwiched between the source and the drain and the p++ Si substrate exists a 10 nm SiO_2 layer. The S (source), D (drain) and G (gate) structures are designed in such a way that edges are positioned precisely so that no overlapping or significant gaps exist between them [51]. The various parameters used in

the simulation process are given in Table 7.13.

Figure 7.25 is a sketch of the cylindrical device [56] which is comprised of the same geometrical and material properties as reported in [51]. It has a height of approximately 17 nm. Figure 7.26 displays the drain voltage plotted against drain current for a p-type ohmic device [74] showing the current-voltage characteristics.

Modelling the static response of carbon nanotube field effect transistors (CNTFETs) is achieved by solving the coupled system of Schroedinger-Poisson equations [74]:

$$\frac{\partial^2 V}{\partial \rho^2} + \frac{1}{\rho} \frac{\partial V}{\partial \rho} + \frac{\partial^2 V}{\partial z^2} = -\frac{Q}{\epsilon}, \quad (7.13)$$

$$-\frac{\hbar^2}{2m^*} \frac{\partial^2 \Psi_{n,d}^{n,p}}{\partial z^2} + (U^{n,p} - E) \Psi_{n,d}^{n,p} = 0. \quad (7.14)$$

The various terms in equations (7.13) and (7.14) are explained in Chapter 3.

Using the original techniques which are reported in Chapters 3 and 4 of this thesis, equations (7.13) and (7.14) are reduced to

$$V_{zz}(\rho, z) + 2\text{sech}^2(z - \sqrt{2}\rho)V(\rho, z) = -P(\rho, z), \quad (7.15)$$

$$\frac{\partial^2 \Psi_{s,d}^{n,p}}{\partial z^2} + 2\text{sech}^2(-\sqrt{2}z)\Psi_{s,d}^{n,p} - \frac{2m^*}{\hbar^2}(U^{n,p} - E)\Psi_{s,d}^{n,p} = 0, \quad (7.16)$$

where $P(\rho, z) = \left(\frac{1}{\rho}V_\rho + \frac{Q}{\epsilon}\right)$. Next the total electron density is calculated and once the Schroedinger-Poisson iteration is accomplished, the electron current is calculated.

The solution for the potential $V(\rho, z)$ in equation (7.15) is given by

$$V(\rho, z) = \tanh(z - \sqrt{2}\rho) + \int_{\rho_0}^0 \int_{z_0}^0 \tanh(a - \sqrt{2}b) + \left(\frac{1}{\rho}V_\rho + \frac{Q}{\epsilon}\right) da db,$$

and the equation for the current is given by

$$j(z) = 2 \sum_{s,d} \int_0^\infty \frac{\sqrt{2m^*}}{\pi \hbar \sqrt{E_{s,d}}} |\Psi_{s,d}^{n,p}|^2 \left(\int_{-\infty}^{+\infty} f_{s,d}(E) \frac{dk_d}{2\pi} \right) \frac{dk_s}{2\pi}. \quad (7.17)$$

To obtain these results, the semi-analytical method reported in Chapters 3 and 4 is applied to the coupled system of Schroedinger-Poisson equations (7.13) and (7.14). This results in a solution to Poisson's equation (7.15) for the electrostatic potential which then enables the equation (7.17) of the current in the device to be computed. As a result of the application of the solution $V(\rho, z)$ to equation (7.15) and using equation (7.17), Figures 7.26 and 7.27 show the comparisons of the simulation results for the semi-analytical method with experimental results [51] and the adaptive integration method [74]. Good agreement of the semi-analytical method with the adaptive integration method of [74] and the experimental results of [51] is thus proven. The simulation platform employed in [74] is an IBM-RS6000.

7.6 Validation of the semi-analytical method and comparison with experimental data

In sections 7.1 - 7.5, the semi-analytical method has been proven to provide results that agree with other simulation results reported in the literature ([6, 12, 74, 91]) and with the experimental results reported in [51]. As already emphasised in Chapter 3, experimental results in this area of semiconductor device research are scarce. Typically, proposed electron state and transport simulation methods are tested against benchmark finite element method solutions of the Schroedinger-Poisson model.

For the devices reported in [6], there are currently no experimental results available with which the simulation results may be validated. However, comparable results are generated by the standard variation method, the subband decomposition method and the Green's function method. In [91], comparisons are done with an adaptive nonlinear version of the standard Gauss-Seidel algorithm whereas in [12], the comparisons based on those obtained from the simplified models are compared with results of the full quantum solution by the finite element method.

To validate the effectiveness of the semi-analytical method, Figures 7.26 and 7.27 show the comparisons of simulation and experimental results. The comparisons show good agreement between simulation results obtained by the semi-analytical method, the adaptive integration method [74] and experimental results in [51]. The simulations were done for a cylindrical structure which is an approximation of the real device reported in [51]. Gate voltages of 1.0 V and 1.3 V are considered and the simulation results are displayed along with the experimental results which are extracted from [51, 74]. In this analysis, the parameters for the simulated structure are found in [51] and are displayed in Table 7.13 and Poisson's equation is solved in two dimensions, whilst Schroedinger's equation is solved in one dimension [74]. The successful comparison shows that the semi-analytical method is validated against experimental results, as well.

| | |
|----------------------|------------------------|
| Band gap E_G | 0.5 eV |
| effective mass m^* | $0.05 m_0$ |
| ϵ | 12.1 |
| Temperature T | 300 K |
| L_s | 5 nm |
| L_D | 5 nm |
| Channel length L | 50 nm |
| V_G | 0.1 0.4 0.7 1.0 1.3 eV |
| E_C | 22 eV |

Table 7.13: Device 5: Parameters for the modelled device [51, 74].

7.7 Discussion of simulation time performance

This section analyses the simulation times for devices 1 - 5. In particular, the simulation times reported in [6, 12, 74, 91] are compared with the semi-analytical method. The simulation times are displayed in Table 7.14. Clearly the semi-analytical method converges faster when compared to the other methods reported in this thesis and shows significant reduction in simulation times. The improvement in simulation times may be due in part to using a more advanced simulation platform than in [91]. In general, it is difficult to make a definitive judgement on the simulation time comparison in the absence of the code used by the other authors and, in some cases, when the computing platform used for simulation was not reported [6, 12]. However, we reckon that the proposed method is comparable if not better than alternative methods in terms of computation time and that it can be

| Simulation Time | | |
|-----------------|------------------------|---|
| Device | semi-analytical method | alternative method |
| 1 | 7.38 secs. | 10 mins. (predictor-corrector method) |
| 2 | 11.15 secs. | 30 mins. (predictor-corrector method) |
| 3 | 10 mins. 42 secs. | 15 mins. 42 secs. (reduced basis method) |
| 4 | 40 mins. 18 secs. | 46mins. 28 secs. (SDM/WKB method) |
| 5 | 1 min. 27 secs. | approx. 100 secs. (adaptive integration method) |

Table 7.14: Comparison of simulation times of the semi-analytical, SDM/WKB [6], predictor-corrector [91] reduced basis [12] and the adaptive integration [74] methods.

made even faster with an implementation using C++ rather than Matlab.

7.8 Summary

This section of the thesis summarises the simulation results of various semiconductor devices and comparison with other reported methods and with experimental results. Various authors [6, 12, 74, 91] have applied robust numerical procedures in order to analyse the electron transport in semiconductor devices. Furthermore, as shown in section 7.5, the semi-analytical method also produces accurate results when compared to experimental results reported in literature [51]. In this thesis it is demonstrated that the applications of the semi-analytical method and the Evans function techniques are effective in analysing electronic devices. Particularly, the Evans function is a useful tool in finding the eigenvalues (energies) of many semiconductor

devices and explains accurately the phenomena regarding electron transport in semiconductor systems. In addition, it is shown that this method shows improved simulation times. This procedure can be generalised as a standalone method or can be coupled with other methods which are used in device simulation.

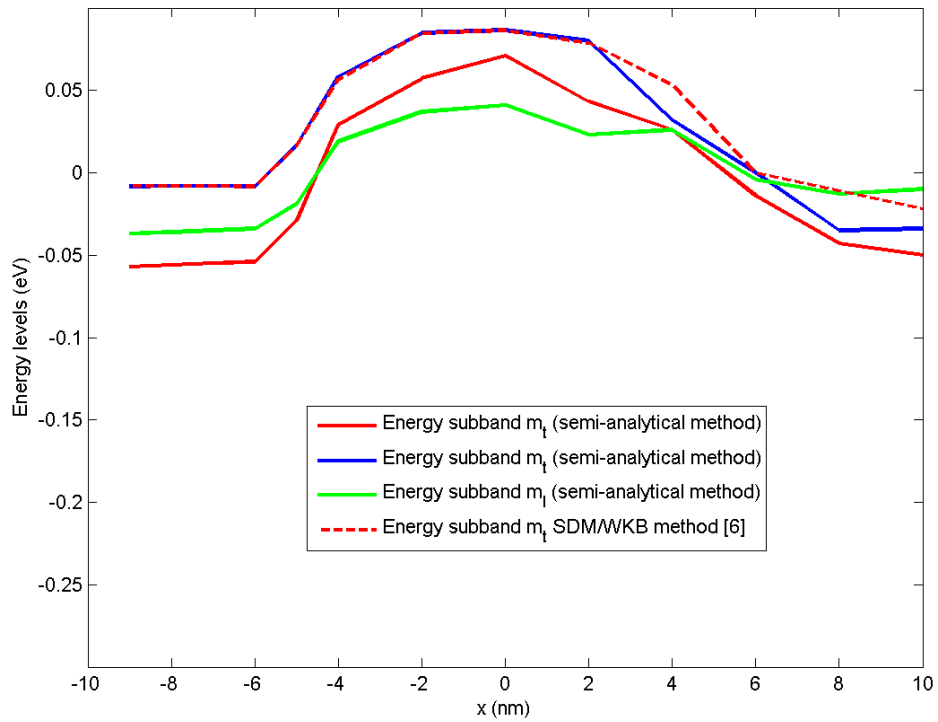


Figure 7.21: Device 4: Double-gate NMOSFET-conduction energy subbands for three different effective masses with $V_{DS} = 0 \cdot 2V$ and $V_{GS} = 0V$. The red and blue continuous lines are the energy subband for m_t , the green line is the energy subband for m_l and the broken red line is the energy subband for m_t which is extracted from [6].

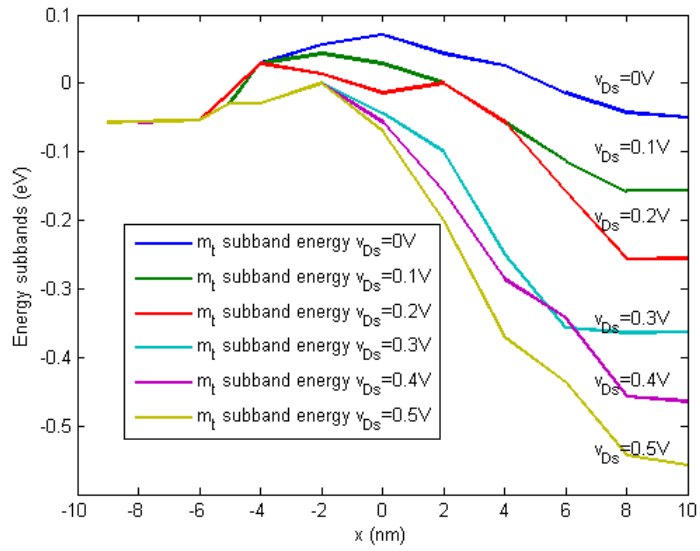


Figure 7.22: Device 4: Double-gate NMOSFET-energy subbands for different drain-source voltages.

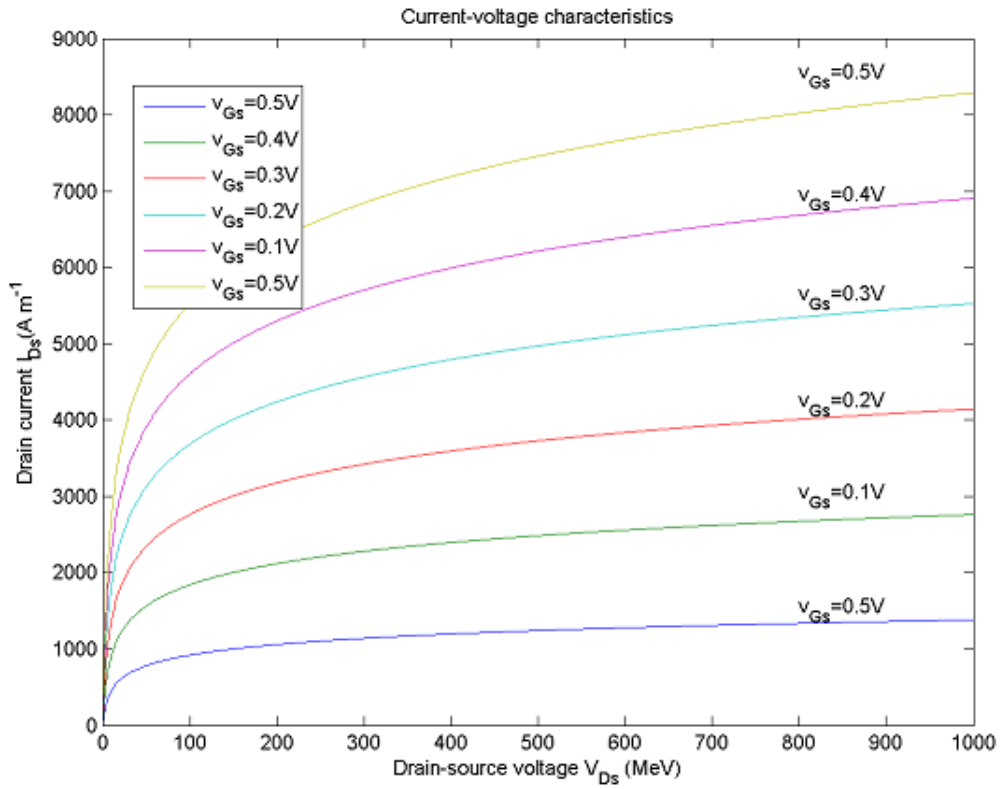


Figure 7.23: Device 4: Double-gate NMOSFET- I-V characteristics, current vs. drain-source potential V_{DS} .

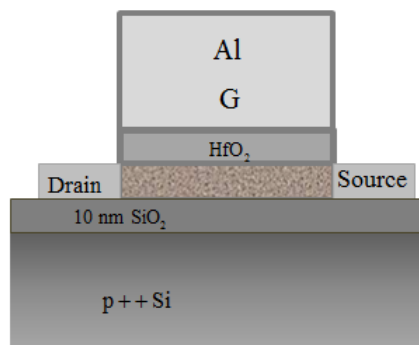


Figure 7.24: Architecture of Device 5: a single walled carbon nanotube field effect transistor (SWNT-FET) device structure.

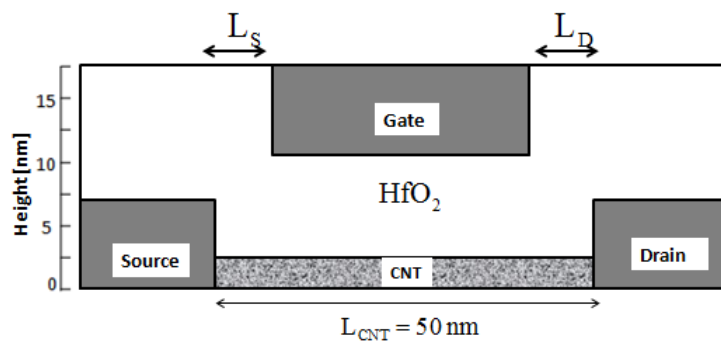


Figure 7.25: [56] Sketch of CNTFET. This cylindrical structure is an approximation to the real Device 5. Simulations for this structure are carried out using the semi-analytical method. The same parameters for the SWNT are used in the simulation of the CNTFET.

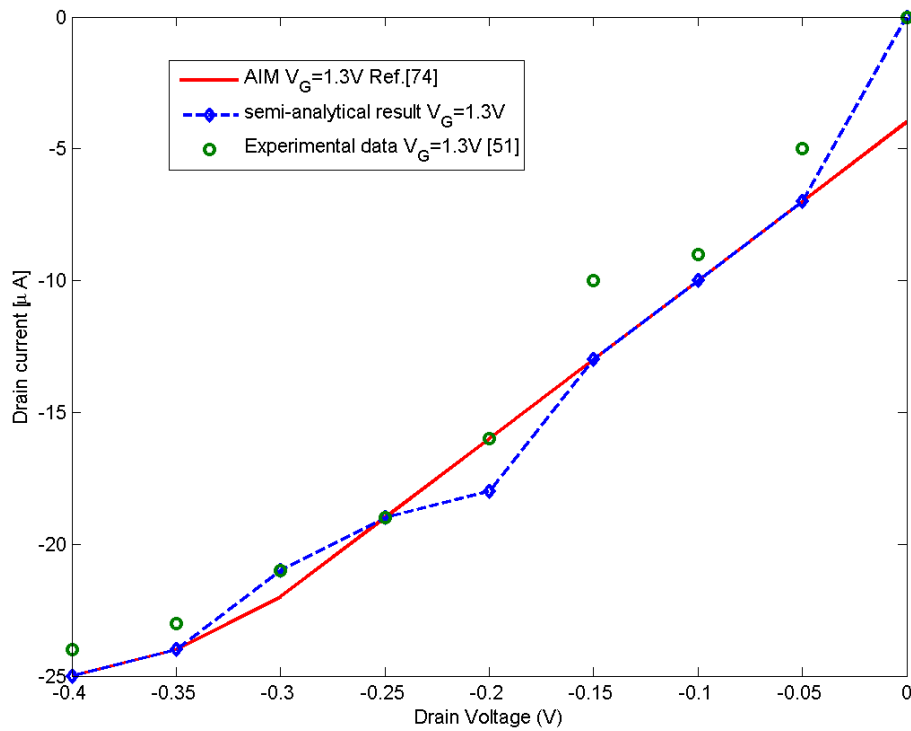


Figure 7.26: Device 5: current-voltage characteristics. Comparisons of simulation for adaptive integration method (AIM) (red curve) [74], semi-analytical method (blue curve) [74] and experimental results (extracted from [74]) (green circle) with $V_G = 1.3V$, where drain current [μ, A] is plotted against drain voltage (v) for CNTFET reported in [74].

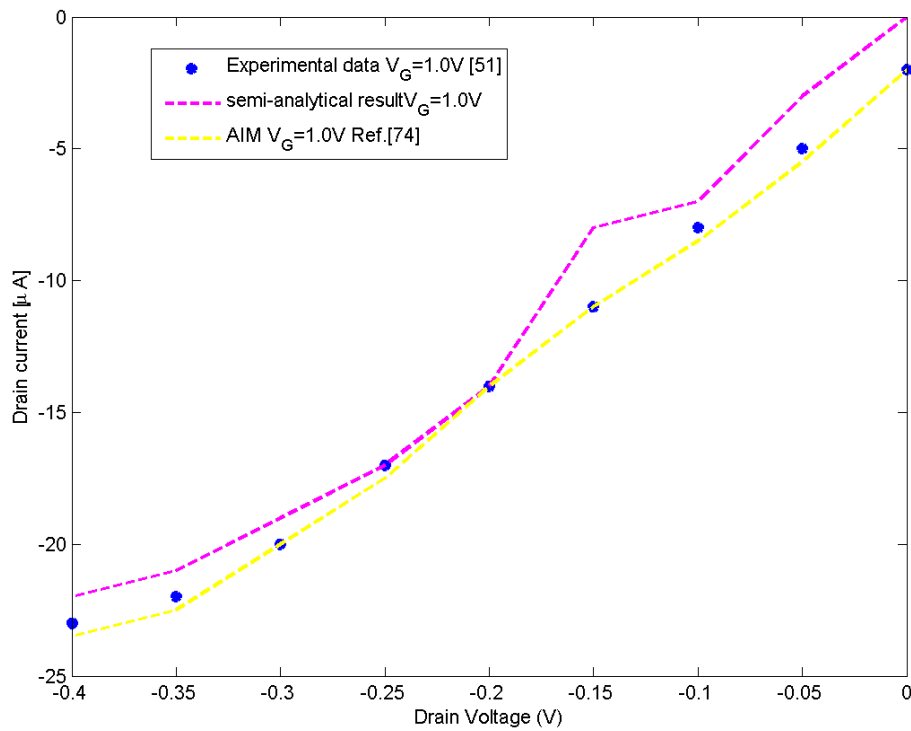


Figure 7.27: Device 5: current-voltage characteristics. Comparisons of simulation for adaptive integration method (AIM) (yellow curve) [74], semi-analytical method (magenta curve) and experimental results (extracted from [74]) (blue dots) with $V_G = 1.0V$, where drain current [μA] is plotted against drain voltage (v) for CNTFET reported in [74].

Chapter 8

Conclusions and Further Work

8.1 Conclusions

Efficient solutions of the electron transport problem constitute a long term goal of the Semiconductor Research Consortium (SRC) [1]. A fundamental part of this goal is concerned with the efficient solution of the coupled system of Schroedinger-Poisson equations. The objectives of this thesis indicate investigating efficient solutions of the above system of equations. Much work has been done in this area and is heavily numerical and computational. The work in this thesis is concerned with a combination of analytical and computational approaches.

The literature review was carried out in order to investigate new ways to solve the problem of electron transport in semiconductor systems quicker and more efficiently. A close study of the approaches which are used to solve this problem is heavily computational and in three dimensions, the problem is computationally intensive. Naturally, it is good practice to seek new ways to

solve this problem. A closer examination of the coupled system of equations suggests that the employment of hyperbolic functions helps to reduce the problem to a simpler one for which approximate solutions are determined. Given the application of the hyperbolic functions, the coupled system of equations is then recast into new approximate system of coupled equations with variable coefficients.

For this new system, an initial electrostatic potential is introduced which results in the reduction of this system of equations to a conventional eigenvalue problem whose eigenfunctions and eigenvalues are calculated by applying the methods of variation of parameters and Powers series. In order to analytically determine the eigenfunctions, the Evans function, which is analytical function, is extended in a novel way in two and three dimensions such that the discrete spectrum is calculated. With the successful calculation of the eigenfunctions, the complete electron density is determined and the inhomogeneous Poisson's differential equation is updated and solved analytically.

Solving the inhomogeneous Poisson's differential equation analytically requires establishing two solutions of the resulting homogeneous equation. Using these two solutions, an approximate semi-analytical solution to the inhomogeneous Poisson's equation is calculated using the methods of variation of parameters and power series. These solutions are then fed back into Schroedinger's equation and new eigenvalues and eigenfunctions are determined. The electrostatic potential is updated and the process is repeated until convergence. The significance of this novel approach is that the transformed equation resulting from the initial guess of the electrostatic potential creates opportunity for analysing the system of equations using analytical

and numerical methods. The analytical component of the method improves greatly simulation times. The method has been validated by comparison with alternative methods and experimental results reported in literature.

The original technique of computing the eigenvalues of the differential operator of Schroedinger's equation is quite significant, in that, it had not been previously applied to analyse the electron transport in semiconductor systems or device analysis. From the results obtained, this function clearly plays an instrumental role in improving the simulation times in the electron transport in semiconductor systems. And as indicated above, in 3D, simulation is computationally intensive and time consuming, suggesting the advantage of the semi-analytical approach.

The method was implemented numerically using Matlab (Appendix F) and tested on a number of device architectures. The test was done initially on different elements of the problem. For example, initially, eigenfunctions and eigenvalues of Schroedinger's equation are calculated for each electrostatic potential then extended to the full model where a complete solution to the problem is determined. Comparing with results reported in literature, faster and improved simulation times are achieved using the novel semi-analytical method. In some cases, the improvement in simulation time is quite significant. It is the ability of this method to transform the coupled system of partial differential equations into a conventional eigenvalue problem and the subsequent introduction and extension of the Evans function techniques in two and three dimensions which accounts for such marked improvements in simulation times.

Whilst the implementation of the computational procedure is done in

Matlab and produces improved simulation times, it is believed that even faster and improved simulation times may be achieved if the implementation is done using C++ language or a combination of both C++ and Matlab languages. Furthermore, it is believed that this approach can be extended to incorporate other models such as the Non-equilibrium Green function approach and the Monte Carlo methods which are used to simulate electron transport in semiconductor systems.

One may argue that the semi-analytical method, and in particular the Evans function techniques may be limited in their ability to handle a wider class of coupled partial differential equations, however, for the purposes of this thesis, the method has proved to be effective and is believed to be able to be included in other robust methods as a valuable tool in simulating microelectronic devices.

8.2 Further Work

Clearly, as shown, the Evans function is a useful tool to capture the bound states in various electronic devices. It has been shown that the zeros of the Evans function coincide with the bound states of the device under simulation. There are various questions which arise when one employs the Evans function technique, namely, to what class of devices can it be applied, how does it compare with capturing the bound states of semiconductor devices and as our case suggests, how accurately does it compare with numerical methods? The 1D, 2D and 3D eigenvalue problem of the Schroedinger-Poisson model have been fully investigated using the Evans function technique and the results

are in good agreement with those reported in literature.

Therefore, as the Evans function is a complex analytical function, its study implies complex analytical functions theory. Hence, one must understand the properties of complex analytical functions in order to proceed. In other words, one can commence with this function and apply complex analysis theory to it. Consequently, properties such as convergence, analytical continuation and Branch cuts and Branch points can then be analysed. This is very important as device dimensions get smaller. This function captures accurately the eigenvalues of the system whereby conventional methods may require improvement in order to accurately predict the performance of semiconductor devices.

With reference to complex variable theory, this is a new and unexplored area in which efficient device analysis can be done. The work in this thesis on the Evans function techniques and the semi-analytical method supports this view. Further analysis is indicated with the employment of complex analytical function in device analysis. Therefore, it is suggested that a better understanding of the properties of the Evans function may be an advantageous place to start when analysing future micro-electronic devices for energy state and eigenfunctions.

One of the uses of the Evans function method is to determine the stability of the bound states in a large class of differential equations. Therefore, as these bound states (energy states) are crucial to device analysis, knowledge of their stability may be deemed a useful tool to determine when devices may breakdown or the extent to which one can scale these devices which are currently sub 100 nm range.

Thus, in this thesis it is demonstrated that the original semi-analytical method has been successful in assisting in solving the coupled system of Schroedinger-Poisson's equations. Its subsequent implementation into Matlab shows improved simulation times compared to the cases reported in literature with which this work is concerned. Particularly, the semi-analytical method coupled with the Evans function technique has shown that it is possible to capture accurately the eigenfunctions and the energies (eigenvalues) of the coupled system of equations. Additionally, the method is easily implemented into Matlab in order to simulate accurate electron transport in semiconductor systems. It is shown that the semi-analytical method is general and it is believed to be able to be applied to a wider class of coupled system of partial differential equations. When this method is combined with the Evans function technique it provides a robust approach to analysing electron transport in semiconductor systems, at least those to which this thesis is devoted.

References

- [1] *www.src.org*, [Accessed: April, 2014].
- [2] K. Abbaoui and Y. Cherruault. Convergence of Adomian's method applied to differential equations. *Comput. Math. Applic.*, 28(5):103–109, 1994.
- [3] S. Abbasbandy. The application of homotopy analysis method to solve a generalized Hirota-Satsuma coupled KdV equation. *Phys. Lett. A*, 361:478–483, 2007.
- [4] N. Abdallah and O. Pinaud. Multiscale simulation of transport in an open quantum system: resonances and WKB interpolation. *Comput. Phys.*, 213(1):288–310, 2006.
- [5] N. Abdallah and E. Pollizi. Self-consistent three dimensional models for quantum ballistic transport in open systems. *Phys. Rev. B*, 66(24):245–301, 2002.
- [6] N. B. Abdallah, M. Mouis, and C. Negulescu. An accelerated algorithm for 2D simulations of the quantum ballistic transport in nanoscale MOS-FETs. *J. Comput. Phys.*, 225(1):74–99, 2007.

- [7] N. B. Abdallah and E. Polizzi. Subband decomposition approach for the simulation of quantum electron transport in nanostructures. *J. Comput. Phys.*, 202(1):150–180, 2005.
- [8] M. A. Abdou. New exact travelling wave solutions for the generalized nonlinear Schroedinger equation with a source. *Chaos, Solitons Fractals*, 38:949–955, 2008.
- [9] W. Abdul-Majid. The variation iteration method for exact solutions of Laplace equation. *Phys. Lett. A*, 363:260–262, 2007.
- [10] K. Amaratunga and J. R. Williams. Wavelet-Galerkin solutions of one-dimensional partial-differential equations. *Int. J. Numer. Methods. Eng.*, 37:2705–2716, 1994.
- [11] P. Amore. An accurate calculation of the complex eigenvalues of the Schroedinger equation with an exponential potential. *Phys. Lett. A*, 372:3149–3152, 2008.
- [12] C. R. Anderson. Efficient solution of the Schroedinger-Poisson equations in layered semiconductor devices. *J. Comput. Phys.*, 228(15):4745–4756, 2009.
- [13] C. R. Anderson and T. Cecil. A Fourier-Wachspress method for solving Helmholtz’s equation in three-dimensional layered domains. *J. Comput. Phys.*, 205(2):706–718, 2005.
- [14] T. Ando, B. Fowler, and F. Stern. Electronic properties of two-dimensional systems. *Rev. Mod. Phys.*, 54:437–672, 1982.

- [15] H. Anitia. Rational function approximations for Fermi-Dirac integrals. *The Astrophy. J. Suppl. Series*, 84:101–108, 1993.
- [16] G. Avdelas, A. Konguetsof, and T. E. Simos. A generalization of Nemerov’s method for the numerical solution of the Schroedinger equation in two dimensions. *Comput. Chem.*, 24(5):577–584, 2000.
- [17] A. Averbuch, M. Israeli, and L. Vozovoi. A fast Poisson solver for arbitrary order accuracy in rectangular regions. *SIAM J. Sci. Comput.*, 19(3):933–952, 1998.
- [18] N. Baker, M. Holst, and F. Wang. Adaptive multilevel finite element solution of the Poisson-Boltzmann equation; i: algorithms and examples. *J. Comput. Chem.*, 21:1319–1342, 2000.
- [19] J. Biazar and H. Ghazvini. Exact solution for non-linear Schroedinger equations by He’s homotopy perturbation method. *Phys. Lett. A*, 366:79–84, 2007.
- [20] A. Blokhin and D. Tkachev. Representation of the solution in semiconductor physics. *J. Math. Anal. Appl.*, 341:1468–1475, 2008.
- [21] W. R. Bowen and P. M. Williams. Finite difference solution of the 2-dimensional Poisson-Boltzmann Equation for spheres in confined geometries. *Colloids Surf., A: Physicochemical and Engineering Aspects*, 204:103–115, 2002.
- [22] E. Braverman, M. Israeli, and A. Averbuch. A fast Poisson solver for 3D Helmholtz equations. *SIAM J. Sci. Comput.*, 20(6):2237–2260, 1999.

- [23] E. Braverman, M. Israeli, A. Averbuch, and L. Vozovoi. A fast 3D Poisson solver for arbitrary order accuracy. *J. Comput. Phys.*, 144(1):109–136, 1998.
- [24] H. Brezis. Partial differential equations in the 20th century. *Adv. Math.*, 135(AI971713):76–144, 1998.
- [25] T. Bridges and G. Derks. Hodge duality and the Evans function. *Phys. Lett. A*, 251:363–372, 1999.
- [26] C. Candong and H. Z. Massoud. The spectral grid method: A novel fast Schroedinger-equation solver for semiconductor nanodevice simulation. *IEEE Trans. Comput. Aided Des. Integr. Circuits Syst.*, 23:1200–1208, 2004.
- [27] F. Carlo, G. Emilio, L. Andrea, and S. Ricardo. Quantum-corrected drift-diffusion models for transport in semiconductor devices. *J. Comput. Phys.*, 2(204):533–561, 2005.
- [28] Z. Chai and B. Shi. A novel lattice Boltzmann model for the Poisson equation. *Appl. Math. Modell.*, 32:2050–2058, 2008.
- [29] A. M. Chaudhry and A. Qadir. Operator representation of Fermi-Dirac and Bose-Einstein integral functions with applications. *Int. J. Math. and Math. Sci.*, 2007.
- [30] Y. Cherruault. Convergence of Adomian’s method. *Kybernetes*, 18:31–38, 1989.

- [31] T. Chiang. A new two-dimensional threshold voltage model for cylindrical fully depleted surrounding-gate (SG) MOSFETs. *Microelectron. Reliab.*, 47:379–383, 2007.
- [32] M. Chohong, G. Frederic, and D. Hector. A supra-convergent finite difference scheme for the variable coefficient Poisson equation on non-graded grids. *J. Comput. Phys.*, 218:123–140, 2006.
- [33] M. Chohong, G. Frederic, and D. Hector. On the existence of solutions for the Schroedinger-Poisson equations. *J. Math. Anal. Appl.*, 346:155–159, 2008.
- [34] F. Chorlton. *Ordinary differential and difference equations: theory and applications*. London: D Van Nostrand Company Ltd., 1965.
- [35] S. Datta. Exclusion principle and the Landauer-Büttiker formalism. *Phys. Rev. B*, 45:1347–1362, 1992.
- [36] M. Dehghan and S. Ali. A numerical method for two-dimensional Schroedinger equation using collocation and radial basis functions. *Comput. Math. Appl.*, 202(1):150–180, 2005.
- [37] P. Dyshlovenko. Adaptive numerical method for Poisson-Boltzmann equation and its application. *Comput. Phys. Commun.*, 147:335–338, 2002.
- [38] M. V. Fischetti. Theory of electron transport in small semiconductor devices using the Pauli master equation. *J. Appl. Phys.*, 83:270–291, 1998.

- [39] T. Galick, A. and Kerkhoven, U. Ravaioli, and Y. Saad. Efficient numerical simulation of electron states in quantum wires. *J. Appl. Phys.*, 68(7):3461–3469, 1990.
- [40] G. Ganapathy, S. Murthy, and M. Arunkumar. Properties of Wronskian and partial wronskian. *Int. J. Pure Appl. Math.*, 63(1):21–30, 2010.
- [41] A. George. How to simulate a semiconductor quantum laser: general description. *Revista Brasileira de Ensino de Fisica*, 31(2):2302–2308, 2009.
- [42] L. Gerrer, S. Markov, S. Amoroso, F. Adamu-Lema, and A. Asenov. Impact of random dopant fluctuations on trap-assisted tunnelling in nanoscale MOSFETs. *J. Microelectron. Reliab.*, 52(9-10):1918 – 1923.
- [43] F. Gesztesy, Y. Latushkin, and K. Zumbrun. Derivatives of (modified) Fredholm determinants and stability of standing and travelling waves. *J. Math. Pures Appl.*, 90:160–200, 2008.
- [44] C. Giuseppe, F. Carlo, G. Claudio, and S. Ricardo. Numerical simulation of tunnelling effects in nanoscale semiconductor devices using quantum corrected drift-diffusion models. *Comput. Methods Appl. Mech. Engrg.*, 195:2193–2208, 2006.
- [45] F. Hernandez, J. Castillo, and G. Larrazabal. Large sparse linear systems arising from mimetic discretization. *Comput. Math. Appl.*, 53:1–11, 2007.

- [46] N. Himoun, K. Abbaoui, and Y. Cherruault. New results of convergence of Adomian's method. *Kybernetes*, 28(4-5):423–429, 1999.
- [47] R. W. Hockney. A fast direct solution of Poisson's equation using Fourier analysis. *J. Assoc. Comput. Mach.*, 12:95–113, 1965.
- [48] J. Hoist, S. Chang, C. Chien, and B. Jeng. An efficient algorithm for the Schroedinger-Poisson eigenvalue problem. *J. Comput. Appl. Math.*, 205:509–532, 2007.
- [49] L. Ixaru. Efficient computation of the Airy propagators. *J. Comput. Phys. Commun.*, 176:637–641, 2007.
- [50] T. Janik and B. Majkusiak. Analysis of the MOS transistor based on the self-consistent solution to the Schroedinger and Poisson equations and on the local mobility model. *IEEE Trans. Electron Devices*, 45:1263–1271, 1998.
- [51] A. Javey, J. Guo, D. Farmer, Q. Wang, E. Yenilmez, R. Gordon, M. Lundstrom, and H. Dai. Self-aligned ballistic molecular transistors and electrically parallel nanotube arrays. *Nano Lett.*, 4(7):1319–1322, 2004.
- [52] L. Joon-Ho and H. L. Qing. An efficient 3-D spectral-element method for Schroedinger-equation in nanodevice simulation. *IEEE Trans. Comput. Aided Des. Integr. Circuits Syst.*, 24:1848–1858, 2005.

- [53] T. Kerkhoven. A spectral analysis of the decoupling algorithm for semiconductor simulation. *SIAM J. of Numer. Anal.*, 25(6):1299–1312, 1998.
- [54] G. Klimeck, F. Oyafuso, T. Boykin, R. Bowen, and P. von Allmen. Development of a nanoelectronic 3-D (NEMO 3-D) simulator for multimillion atom simulations and its application to alloyed quantum dots. *Comput. Modell. Eng. Sci.*, 3:601–642, 2002.
- [55] R. KOC and D. Haydargil. Solution of the Schroedinger equation with one and two dimensional double-well potentials. *Turk J. Phys.*, 28:161–167, 2004.
- [56] H. Kosina, M. Pourfath, and S. Selberherr. A fast and stable Poisson-Schroedinger solver for the analysis of carbon nanotube transistors. *J. Comput. Electron.*, 5:155–159, 2006.
- [57] P. B. Kurniawan and E. Li. Ballistic calculations of nonequilibrium Green’s functions in nanoscale devices using finite element method. *J. Phys. D: Appl. Phys*, 42:1–11, 2009.
- [58] S. Lai. Explicit solutions of two nonlinear dispersive equations with variable coefficients. *Phys. Lett. A*, 372:7001–7006, 2008.
- [59] S. Lapaul, A. de Lustrac, and F. Bouillault. Solving the Poisson’s and Schroedinger’s equations to calculate the electron states in quantum nanostructures using the finite element method. *IEEE Trans. Magn.*, 32(3):1018–1021, 1996.

- [60] L. Lehtovaara, J. Toivanen, and J. Eloranta. Solution of time-independent Schroedinger equation by the imaginary time propagation method. *J. Comput. Phys.*, 221:148–157, 2007.
- [61] W. Lingquan, W. Deli, and P. M. Asbeck. A numerical Schroedinger-Poisson solver for radially symmetric nanowire core-shell structures. *Solid-State Electron.*, 50(11):1732–1739, 2006.
- [62] E. Machowska-Podsiadlo, M. Maczka, and M. Bugajski. 3D self-consistent solution of Poisson and Schroedinger equations for electrostatically formed quantum dot. *Bull. Pol. Acad. Sci., Tech. Sci.*, 55(2):245–249, 2007.
- [63] L.-F. Mao. Effects of quantum coupling on the performance of metal-oxide-semiconductor field transistors. *Pramana*, 72(2):407–414, 2009.
- [64] S. Markov, B. Cheng, and A. Asenov. Statistical variability in fully depleted SOI MOSFETs due to random dopant fluctuations in the source and drain extensions. *IEEE Electron Device Lett.*, 3(3):315–317, 2012.
- [65] G. Miller. An iterative boundary potential method for the infinite domain Poisson problem with interior Dirichlet boundaries. *J. Comput. Phys.*, 227:7917–7928, 2008.
- [66] S. Mischler. On the initial boundary value problem for the Vlosov-Poisson-Boltzmann system. *Comm. Math. Phys.*, 210(2):447–466, 2000.
- [67] N. Mohankumar. Two new series for the Fermi-Dirac integral. *Comput. Phys. Commun.*, 202:665–669, 2007.

- [68] T. Monovasilis, Z. Kalogiratou, and T. Simos. Computation of the eigenvalues of the Schroedinger equation by symplectic and trigonometrically fitted symplectic partitioned Runge-Kutta methods. *Phys. Lett. A*, 372:569–573, 2008.
- [69] D. A. Murray. *Differential And Integral Calculus*. Longmans, Green, And Co., 1918.
- [70] I. Mustafa. On exact solution of Laplace equation with Dirichlet and Neumann boundary conditions by the homotopy analysis method. *Phys. Lett. A*, 365:412–415, 2007.
- [71] O. Myunghyun and B. Sandstede. Evans functions for periodic waves on infinite cylindrical domains. *J. Differ. Equ.*, 248:544–555, 2010.
- [72] C. Negulescu, N. Abdallah, E. Pollizi, and M. Mouis. Simulation schemes in 2D nanoscale MOSFETs: a WKB based method. *J. Comp. Elect.*, 3:397–400, 2004.
- [73] F. Nier. A stationary Schroedinger-Poisson system arising from the modelling of electronic devices. *Forum Math.*, 5(2):489–510, 1990.
- [74] M. Pourfath and H. Kosina. Fast convergent Schroedinger-Poisson solver for the static and dynamic analysis of carbon nanotube field effect transistors. *Large-Scale Sci. Comput.*, 3743:578–585, 2006.
- [75] K. Rektorys. *Survey of Applicable Mathematics*. ILIFFE, Inc, 1968.
- [76] Y. Ruo-xia and L. Zhi-bin. New exact solutions for three nonlinear evolution equations. *Phys. Lett. A*, 297:196–204, 2002.

- [77] K. Saad and A. El-shrae. Numerical methods for computing the Evans function. *Anziam J.*, 52:76–99, 2011.
- [78] A. Sadighi and D. D. Ganji. Exact solutions of Laplace equations by homotopy-perturbation and Adomian decomposition methods. *Phys. Lett. A*, 367:83–87, 2007.
- [79] E. Samuel and D. Patil. Analysis of wavefunction distribution in quantum well biased laser diode using transfer matrix method. *Pro. Electromagn. Res. Lett.*, 1:119–128, 2008.
- [80] S. R. Santanu. Solution of the coupled Klein-Gordon-Schroedinger equation using the modified decomposition method. *Int. J. Nonlinear Sci.*, 4(3):227–234, 2007.
- [81] L. Shih-Ching, L. Yiming, and Y. Shao-Ming. Analytical solution of nonlinear Poisson equation for symmetric double-gate metal-oxide-semiconductor field effect transistors. *Math. Comput. Modell.*, 46:180–188, 2007.
- [82] L. Shikuo, F. Zuntao, and L. Shida. Periodic solutions for a class of coupled nonlinear partial differential equations. *Phys. Lett. A*, 336:175–179, 2005.
- [83] M. R. Spiegel. *Theory and problems of complex variables with an introduction to conformal mapping and its applications*. McGraw-Hill, Inc, 1981.

- [84] S. Steiger. *NEMO5 User Manual*. Network for Computational Nanotechnology, Purdue University West Lafayette IN, USA, 2012.
- [85] F. Stern and S. D. Sarma. Electron energy levels in GaAs-Ga_{1-x}Al_xAs heterojunctions. *Phys. Rev. B*, 30(2):840–848, 1984.
- [86] B. G. Streetman and S. Banerjee. *Solid State Electronic devices*. Prentice Hall, Inc, 2000.
- [87] A. Svizhenko, M. Antram, T. R. Govinda, B. Biegel, and R. Venugopal. Two dimensional quantum mechanical modeling of nanotransistors. *J. Appl. Phys.*, 91:23–43, 2002.
- [88] T. M.-D. Syed, A. N. Muhammad, and W. Asif. Variation of parameters method for initial and boundary value problems. *World Appl. Sci. J.*, 11:622–639, 2010.
- [89] A. Trellakis, A. Galick, A. Pacelli, and U. Ravaioli. Comparisons of iteration schemes for the solution of the multidimensional Schroedinger-Poisson equations. *VLSI Design*, 8(1-4):105–109, 1998.
- [90] A. Trellakis and U. Ravaioli. Three-dimensional spectral solution of Schroedinger equation. *VLSI Design*, 13(1-4):341–347, 1999.
- [91] A. Trellakis and U. Ravaioli. Computational issues in the simulation of semiconductor quantum wires. *Comput. Methods Appl. Mech. Engrg.*, 181(15):437–449, 2000.
- [92] D. Vasileska, R. Akis, I. Knezevic, S. N. Milčić, S. S. Ahmed, and D. K. Ferry. Role of quantization effects in the operation of ultrasmall

- MOSFETs and SOI device structures. *Microelectron. Eng.*, 63:233–240, 2002.
- [93] R. Venugopal, Z. Ren, S. Datta, M. S. Lundstrom, and D. Jovanovic. Simulating quantum transport in nanoscale MOSFETs: real vs. mode space approaches. *J. Appl. Phys.*, 92:3730–3739, 2002.
- [94] C. Vömel, S. Z. Tomov, O. A. Marques, A. Canning, L.-W. Wang, and J. J. Dongarra. State-of-the art eigensolvers for electronic structure calculations of large scale nano-systems. *J. Comput. Phys.*, 227:7113–7124, 2008.
- [95] X. Wang, G. Roy, O. Saxod, A. Bajolet, A. Juge, and A. Asenov. Simulation study of dominant statistical variability sources in 32-nm high-k/metak gate CMOS. *IEEE Electron Device Lett.*, 33(5):643–645, 2012.
- [96] L. Yeping. Asymptotic profile in a multi-dimensional stationary non-isentropic hydrodynamic semiconductor model. *J. Math. Anal. Appl.*, 332:367–380, 2007.
- [97] L. Yiming and Y. Shao-Ming. A numerical iterative method for solving Schroedinger and Poisson equations in nanoscale, double and surrounding gate metal-oxide-semiconductor structures. *Comput. Phys. Commun.*, 169:309–312, 2005.
- [98] J. Yu. Series solution of the Schroedinger equation with position-dependent mass for the Morse potential. *Phys. Lett. A*, 322:290–297, 2004.

Appendix A

Energy band diagram - MOS diode

Appendix A presents details of the energy band diagrams for the MOS diode, as shown in Figure 2.1. When the metal plate, the oxide (insulator) and the semiconductor substrate are separated (not in contact), Figure A.1 illustrates three separate energy band diagrams of the MOS diode components. As such there exist the following notations and definitions. Φ_m is the work function, χ the semiconductor electron affinity and E_g is the semiconductor band gap.

Using these notations, one defines an ideal Metal Oxide Semiconductor diode as follows:

1. $\Phi_m - q \cdot \Phi_s = 0$. Therefore, no charge is flowing when the metal, oxide and semiconductor are put in contact;
2. under any biasing conditions, the only charges that can exist in the structure are those in the semiconductor structure and those with equal

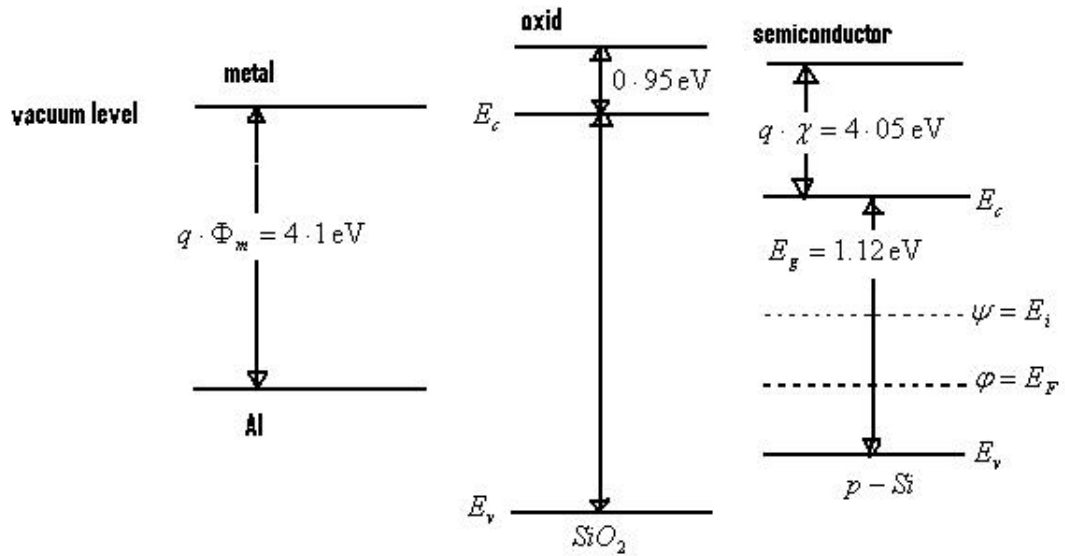


Figure A.1: Metal, oxide and semiconductor energy band diagrams are separately shown.

but with opposite sign on the metal surface adjacent to the insulator;

3. The resistivity of the of of the insulator is such that there is no carrier transport under dc-bias.

where q is the electronic charge, and $q \cdot \Phi_s$ is the work function of the semiconductor [86].

Equally, in Figure A.2 one considers the energy band diagram when the semiconductor, metal and insulator are in contact and under no applied bias, that is $V = 0$. Here a p-type semiconductor is considered.

In the case when an ideal MOS diode is biased with negative or positive voltages, Figures A.3, A.4 and A.5 illustrate three cases may exist at the semiconductor surface. These cases are the *accumulation case*, the *depletion*

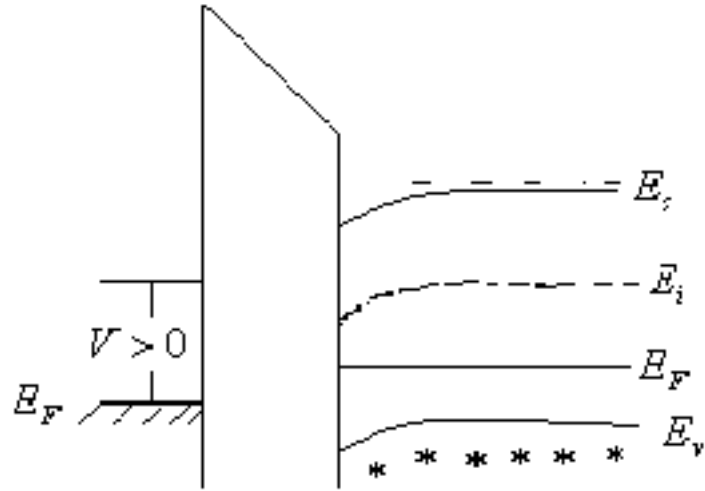


Figure A.4: Energy-band diagram of an ideal MOS at $V \neq 0$ for a p-type semiconductor. The depletion case.

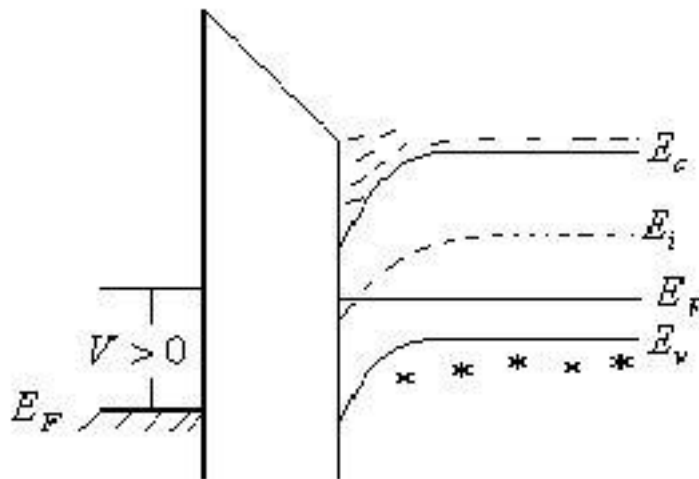


Figure A.5: Energy-band diagram of an ideal MOS at $V \neq 0$ for a p-type semiconductor. The inversion case.

Appendix B

MOSFET characteristics

Under normal operating conditions of a MOSFET, the drain and source voltages should be applied in a way that the source and drain to substrate p-n junctions will be reverse biased, that is, a negative voltage is applied to the p-side with respect to the n-side. There will be no significant current until the voltage reaches the critical value called the junction breakdown voltage, after which the current dramatically increases. In Figure B.1, a cross-section of an n-channel MOSFET is illustrated where the depletion region is shown.

B.1 Operating regions of the n-channel MOSFET

B.1.0.1 Linear region

There is the region where I_{ds} increases linearly with V_{ds} for a given V_{gs} , which is higher than V_{th} . Given the application of a small drain voltage, electrons

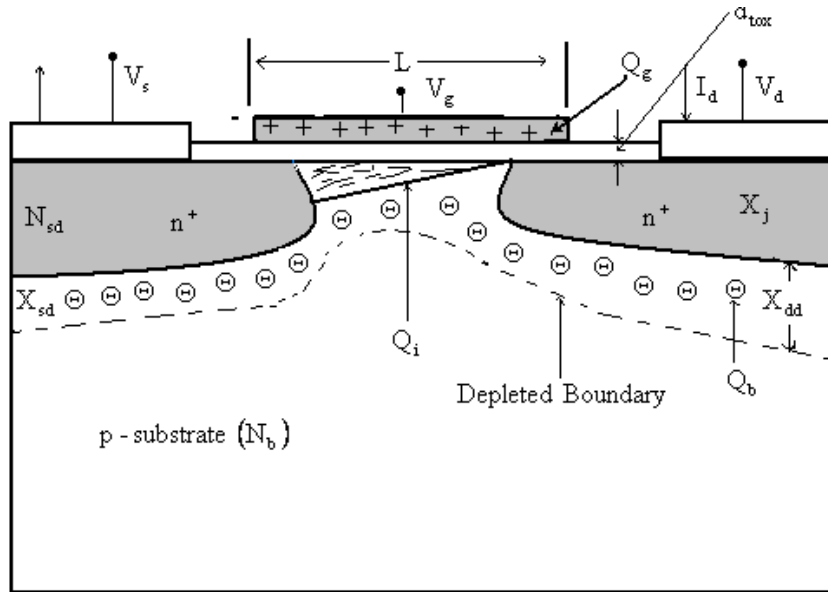


Figure B.1: The cross-section of n-channel MOSFET.

will flow from source to drain. Consequently, current will flow in the reverse direction from drain to source through the conduction channel, (see Figure B.2 (a)) [86].

B.2 Saturation region

In this region I_{ds} no longer increases with V_{ds} , I_{ds} is saturated. When the drain voltage increases, eventually it will reach V_{Dsat} , the thickness of the inversion layer will reduce to zero. This is called the pinch-off region as shown in Figure B.2 (b), [86]. At this point, the drain current remains the same since $V_d > V_{Dsat}$. If the voltage V_{Dsat} increases beyond pinch off, the channel length will decrease as illustrated in Figure. B.2 (c), [86].

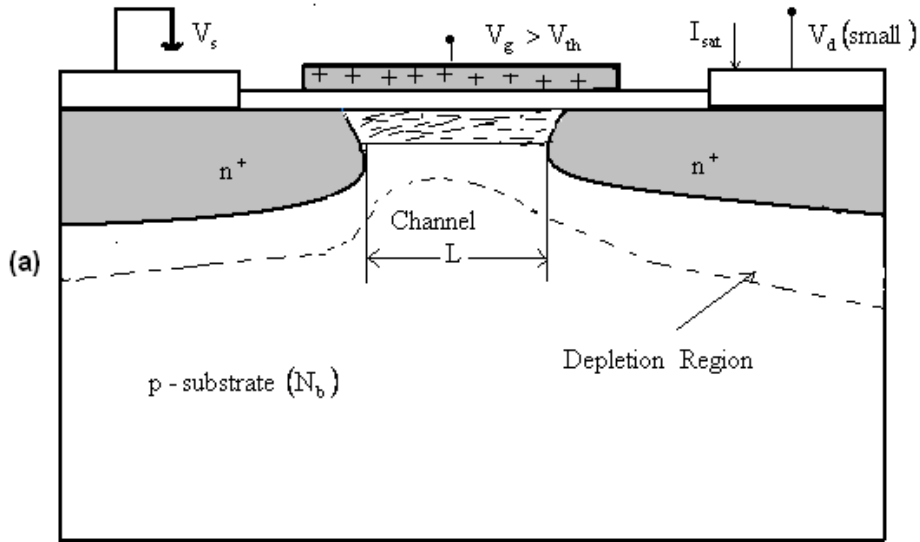


Figure B.2: The linear operating region in the n-channel MOSFET.

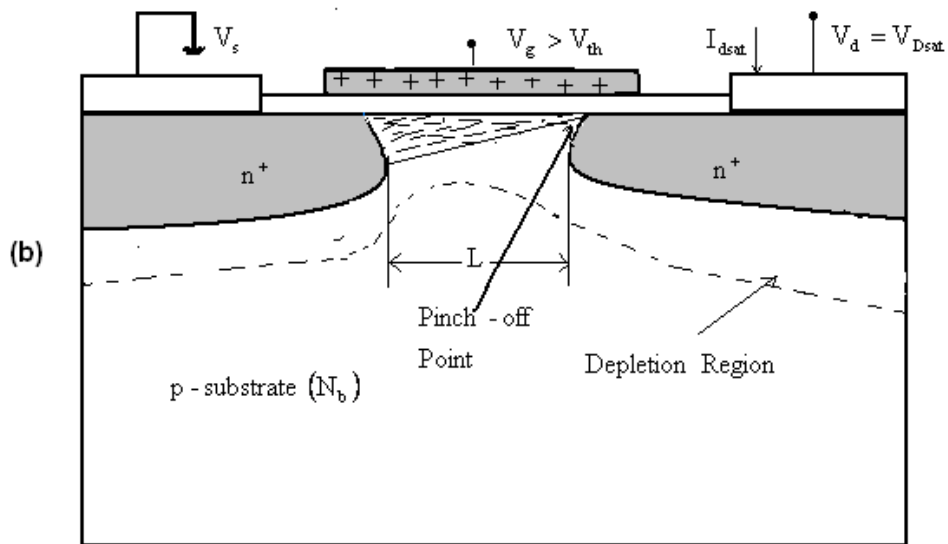


Figure B.3: The pinch-off point operating region in the n-channel MOSFET.

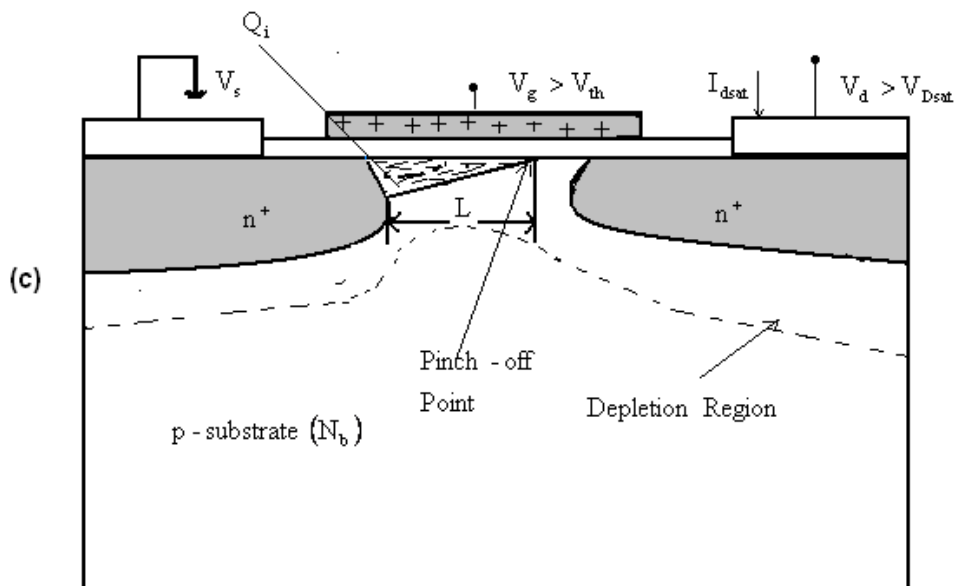


Figure B.4: The saturation operating region in the n-channel MOSFET.

Appendix C

The Wronskian

The Wronskian can be used to find solutions to PDEs. Its definition will be derived in the following. Consider the differential equation

$$\phi_{xx}(x) + 2\operatorname{sech}^2(x)\phi(x) = 0. \quad (\text{C.1})$$

It can be easily shown that two linearly independent solutions to this equation are given as

$$\phi_1(x) = \tanh(x) \quad (\text{C.2})$$

and

$$\phi_2(x) = \tanh(x)(x - \operatorname{coth}(x)). \quad (\text{C.3})$$

These are verified as follows:

$$\frac{d^2}{dx^2}\phi_1(x) = -2\operatorname{sech}^2(x)\tanh(x) \quad (\text{C.4})$$

and

$$2\operatorname{sech}^2(x)\phi_1(x) = 2\operatorname{sech}^2(x)\tanh(x). \quad (\text{C.5})$$

Then the sum of (C.4) and (C.5) verifies (C.1). Similarly,

$$\frac{d^2}{dx^2}\phi_2(x) = -2x\operatorname{sech}^2(x)\tanh(x) + 2\operatorname{sech}^2(x) \quad (\text{C.6})$$

and

$$2\operatorname{sech}^2(x)\phi_2(x) = 2\operatorname{sech}^2(x)(\tanh(x)((x - \coth(x)))) \quad (\text{C.7})$$

$$= 2x\operatorname{sech}^2(x)\tanh(x) - 2\operatorname{sech}^2(x). \quad (\text{C.8})$$

Then the sum of (C.6) and (C.8) verifies (C.1).

Now consider the problem in three dimensions.

$$\frac{\partial^2\phi(x, y, z)}{\partial x^2} + \frac{\partial^2\phi(x, y, z)}{\partial y^2} + \frac{\partial^2\phi(x, y, z)}{\partial z^2} = 0. \quad (\text{C.9})$$

It is easily verified that

$$\phi(x, y, z) = \tanh(x + \iota\sqrt{3}y - \sqrt{2}z). \quad (\text{C.10})$$

Indeed, let $\phi = \phi(x, y, z)$. Then,

$$\phi_{xx} = -2\operatorname{sech}^2(x + \iota\sqrt{3}y - \sqrt{2}z)\tanh(x + \iota\sqrt{3}y - \sqrt{2}z), \quad (\text{C.11})$$

$$\phi_{yy} = 6\operatorname{sech}^2(x + \iota\sqrt{3}y - \sqrt{2}z)\tanh(x + \iota\sqrt{3}y - \sqrt{2}z) \quad (\text{C.12})$$

and

$$\phi_{zz} = -4\operatorname{sech}^2(x + \iota\sqrt{3}y - \sqrt{2}z)\tanh(x + \iota\sqrt{3}y - \sqrt{2}z). \quad (\text{C.13})$$

Summing (C.11), (C.12) and (C.13) verifies (C.9).

C.1 Definition of the Wronskian

Now the Wronskian can be defined. Using (C.2) and (C.3), the Wronskian in one dimension is defined to be the determinant

$$W(\phi_1(x), \phi_2(x)) = \det \begin{pmatrix} \phi_1(x) & \phi_2(x) \\ \frac{d}{dx}\phi_1(x) & \frac{d}{dx}\phi_2(x) \end{pmatrix}. \quad (\text{C.14})$$

Simplifying (C.14) gives $W(\phi_1(x), \phi_2(x)) = 1$. Since $W(\phi_1(x), \phi_2(x)) \neq 0$, $\phi_1(x)$ and $\phi_2(x)$ are linearly independent solutions. Given this background, the Evans function can be defined and discussed (Appendix D).

Appendix D

The Evans Function

The Evans function is a useful tool to calculate the discrete spectrum (eigenvalues) for the Schrodinger's equation. To illustrate how this function works, this thesis looks at an example below in one-dimension and defines this function. Moreover, from the one-dimensional analysis, this function is naturally extended to two and three dimensions in Chapters 4 and 5. In this section, the scalar reaction-diffusion equation [24] is discussed as a basic example. In the discussion, linearisation of this equation is illustrated and the Evans function is defined. The scalar reaction-diffusion equation is

$$u_t = u_{xx}(x) - u(x) + u^3(x), \quad (\text{D.1})$$

where $(x, t) \in \mathbf{R} \times \mathbf{R}^+$. A stationary (time independent) solution to (D.1) is given by $u(x) = U(x) = \text{sech}(x)$. Let $u(x) = U(x) + P(x)$ and substitute this into (D.1), then neglect nonlinear terms in $P(x)$, use the fact that from (D.1), $u_{xx}(x) - u(x) + u^3(x) - u_t = 0$ and introduce the spectral ansatz

$u(x, t) = e^{\lambda t}U(x)$, results in the eigenvalue equation

$$P_{xx}(x) - P(x) + 6U^2(x)P(x) = \lambda P(x), \quad (\text{D.2})$$

where λ is an eigenvalue. The process of obtaining (D.2), which is a linear eigenvalue problem is called linearisation of (D.1) about the stationary solution $u(x) = U(x) = \text{sech}(x)$. That is, equation (D.2) is one which is linear in the function $P(x)$ and therefore a solution using linear techniques can be employed.

Now the linearised equation for the one dimensional Klein-Gordon equation is

$$\psi_{xx}(x) - (1 - 2\text{sech}^2(x))\psi(x) + \lambda\psi(x) = 0. \quad (\text{D.3})$$

Two solutions of (D.3) which decay to 0 as $x \rightarrow +\infty$ and $x \rightarrow -\infty$ are given as

$$m_+(x) = e^{-\sqrt{1-\lambda}x}h_+z \quad (\text{D.4})$$

and

$$m_-(x) = e^{\sqrt{1-\lambda}x}h_-z, \quad (\text{D.5})$$

with

$$h_+(z) = C_+(z - (-\sqrt{1-\lambda})), \quad (\text{D.6})$$

$$= C_+(z + \sqrt{1-\lambda}), \quad (\text{D.7})$$

$$h_-(z) = C_-(z - \sqrt{(1-\lambda)}). \quad (\text{D.8})$$

Now,

$$\lim_{x \rightarrow +\infty} m_+(x) = 0 \text{ and } \lim_{x \rightarrow -\infty} m_-(x) = 0.$$

D.1 Definition of Evans function in one-dimension

The Evans function is given by $D(\lambda)$ which is defined as

$$D(\lambda) = \det \begin{pmatrix} m_+(x) & m_-(x) \\ \frac{d}{dx}m_+(x) & \frac{d}{dx}m_-(x) \end{pmatrix}. \quad (\text{D.9})$$

The roots of $D(\lambda)$ correspond to eigenvalues. Now, $m_+(x) = e^{-\sqrt{1-\lambda}x}h_+(z)$, thus one has

$$\begin{aligned} \frac{d}{dx}m_+(x) &= -\sqrt{1-\lambda}e^{-\sqrt{1-\lambda}x}h_+(z) + e^{-\sqrt{1-\lambda}x}\frac{d}{dx}h_+(z), \\ &= -\sqrt{1-\lambda}e^{-\sqrt{1-\lambda}x}h_+(z) + e^{-\sqrt{1-\lambda}x}\frac{d}{dx}h_+(z), \\ &= -\sqrt{1-\lambda}e^{-\sqrt{1-\lambda}x}h_+(z) + e^{-\sqrt{1-\lambda}x}(1-z^2)\frac{d}{dx}h_+(z). \end{aligned}$$

Similarly,

$$\begin{aligned} \frac{d}{dx}m_-(x) &= \sqrt{1-\lambda}e^{\sqrt{1-\lambda}x}h_-(z) + e^{\sqrt{1-\lambda}x}\frac{d}{dx}h_-(z), \\ &= \sqrt{1-\lambda}e^{\sqrt{1-\lambda}x}h_-(z) + e^{\sqrt{1-\lambda}x}\frac{d}{dx}h_-(z), \\ &= \sqrt{1-\lambda}e^{\sqrt{1-\lambda}x}h_-(z) + e^{\sqrt{1-\lambda}x}(1-z^2)\frac{d}{dx}h_-(z). \end{aligned}$$

Therefore,

$$\begin{aligned} D(\lambda) &= m_+(x)\frac{d}{dx}m_-(x) - m_-(x)\frac{d}{dx}m_+, \\ &= e^{-\sqrt{1-\lambda}x}h_+(z)(e^{\sqrt{1-\lambda}x}(\sqrt{1-\lambda}h_-(z) + (1-z^2)\frac{d}{dz}h_-(z))) \\ &\quad - e^{-\sqrt{1-\lambda}x}h_+(z)(e^{-\sqrt{1-\lambda}x}(-\sqrt{1-\lambda}h_+(z) + (1-z^2)\frac{d}{dz}h_-(z))), \end{aligned}$$

which, after simplification, gives

$$D(\lambda) = 2\sqrt{1-\lambda}h_+(z)h_-(z) + (1-z^2)(h_+(z)\frac{d}{dz}h_-(z) - h_-(z)\frac{d}{dz}h_+(z)).$$

Now $h_+(z) = C_+(z + \sqrt{1-\lambda})$ and $h_-(z) = C_-(z - \sqrt{1-\lambda})$. This implies that $h_+(z) \times h_-(z) = C_+C_-(z^2 - (1-\lambda))$. Thus equation (D.9) reduces to

$$D(\lambda) = C_+C_-2\sqrt{1-\lambda}(z^2 - (1-\lambda) + (1-z^2)) \quad (\text{D.10})$$

$$= 2C_+C_-\lambda\sqrt{1-\lambda}. \quad (\text{D.11})$$

To conclude,

$$C_+C_- \neq 0, \text{ and } \lambda < 1, \text{ so } D(\lambda) = 0 \text{ only when } \lambda = 0,$$

therefore the two eigenfunctions which satisfy (D.3) are

$$m_+(x) = C_+e^{-x}(\tanh(x) + 1) \quad (\text{D.12})$$

and

$$m_-(x) = C_-e^x(\tanh(x) - 1). \quad (\text{D.13})$$

Furthermore, when $\lambda = 1$, there exists an exact solution to equation (D.3). This is given as

$$\psi(x) = \tanh(x). \quad (\text{D.14})$$

Appendix E

Derivation of 3D

Eigenfunctions

Appendix E gives details of the derivation of the 3D eigenfunctions which are presented in Chapter 5, Section 5.3. As in the 2D case (Chapter 5, Section 5.3), Schroedinger's equation has to be solved three times to obtain three sets of eigenvalues. Therefore, consider the effective mass configuration $m^* = (m_\ell, m_t, m_\ell)$. Using the techniques of Chapter 5, with the initial electrostatic potential

$$V(x, y, z) = \frac{\hbar^2}{2q[m_z(z)]^2} \frac{\partial}{\partial z} m_z(z) \frac{\psi_z}{\psi} - \frac{\lambda}{q} - \frac{\lambda \ell^2 [m_z(z)]^2}{q}, \quad (\text{E.1})$$

where ℓ is the length of the device, then equation (5.118) is reduced to

$$\psi_{xx} + 2bc \operatorname{sech}^2(\sqrt{bc}x + \iota\sqrt{3}\sqrt{acy} - \sqrt{2}\sqrt{abz})\psi - \frac{2\lambda\ell^2 [m_z(z)]^4}{a\hbar^2} \psi = 0.$$

In order to solve this equation, note that in the $\lim_{x,z \rightarrow \pm\infty} 2bc \operatorname{sech}^2(\sqrt{bc}x + \iota\sqrt{3}\sqrt{acy} - \sqrt{2}\sqrt{abz}) \rightarrow 0$. Hence, one has the reduced equation

$$\psi_{xx}(x, y, z) - \frac{2\lambda\ell^2 [m_z(z)]^4}{a\hbar^2} \psi(x, z) = 0. \quad (\text{E.2})$$

Equation (E.2) has solutions which decay exponentially only if $\text{Real}(\lambda) > 0$. Therefore, when looking for solutions restrict λ to the right-half complex-plane. From equation (E.2), $\mu = \pm \sqrt{\frac{2[m_z(z)]^4 \ell^2 \lambda}{a \hbar^2}}$. Using this, write a solution to equation (5.118) in the form $e^{\mu(x+y+z)} h(x, y, z)$ and substitute this into equation (5.118). Then the function $h(x, y, z)$ satisfies

$$h_{xx} + 2\mu h_x + 2bc \operatorname{sech}^2(\sqrt{bc}x + i\sqrt{3}\sqrt{ac}y - \sqrt{2}\sqrt{ab}z)h = 0. \quad (\text{E.3})$$

From Chapter 5, equation (E.3) has solution

$$h(x, y, z) = C \tanh(\sqrt{bc}x + i\sqrt{3}\sqrt{ac}y - \sqrt{2}\sqrt{ab}z) - C \frac{\mu \sqrt{bc}}{bc}, \quad (\text{E.4})$$

for some complex constant C .

Since $\mu = \pm \sqrt{\frac{2[m_z(z)]^4 \ell^2 \lambda}{a \hbar^2}}$, one has two solutions to equation (5.118). One of which decays as $x, z \rightarrow +\infty$ and the other decays as $x, z \rightarrow -\infty$. Let

$$U_+(x, y, z) = e^{-\sqrt{\frac{2[m_z(z)]^4 \ell^2 \lambda}{a \hbar^2}}(x+y+z)} h_+(x, y, z), \quad (\text{E.5})$$

$$U_-(x, y, z) = e^{\sqrt{\frac{2[m_z(z)]^4 \ell^2 \lambda}{a \hbar^2}}(x+y+z)} h_-(x, y, z), \quad (\text{E.6})$$

where

$$h_+(x, y, z) = C_+ \tanh(\sqrt{bc}x + i\sqrt{ac}y - \sqrt{2}\sqrt{ab}z) - C_+ \frac{\mu_+ \sqrt{bc}}{bc} \quad (\text{E.7})$$

and

$$h_-(x, y, z) = C_- \tanh(\sqrt{bc}x + i\sqrt{ac}y - \sqrt{2}\sqrt{ab}z) - C_- \frac{\mu_- \sqrt{bc}}{bc}. \quad (\text{E.8})$$

As $x, z \rightarrow +\infty$, $U_+(x, y, z) \rightarrow 0$ and as $x, z \rightarrow -\infty$, $U_-(x, y, z) \rightarrow 0$. Therefore, for some $\lambda \in C$, with $\text{Real}(\lambda) > 0$, the functions $U_+(x, y, z)$ and $U_-(x, y, z)$ are linearly dependent and bounded for all x, z and decay

exponentially as $x, z \rightarrow \pm\infty$. Thus eigen energies (eigenvalues) correspond to values of $\lambda \in C$ where the Wronskian of $U_+(x, y, z)$ and $U_-(x, y, z)$ vanishes.

Let $U^+(x, y, z, \lambda) = U^+$ and $U^-(x, y, z, \lambda) = U^-$ be solutions to equation (5.118). Then the Evans function is given as

$$D(\lambda) = \det \begin{pmatrix} U^+(x, z, y, \lambda) & U^-(x, z, y, \lambda) \\ U_x^+ + U_z^+ + U_y^+ & U_x^- + U_z^- + U_y^- \end{pmatrix},$$

where U_x, U_z and U_y are the first derivatives with respect to x, z and y respectively of the functions $U^+(x, y, z, \lambda)$ and $U^-(x, y, z, \lambda)$.

Simplifying this, the Evans function is given explicitly as

$$D(\lambda) = \frac{2\sqrt{2}\ell C_+ C_- [m_z(z)]^2 \sqrt{\lambda} (\sqrt{2}\sqrt{a} - \sqrt{c})}{\sqrt{a}\sqrt{c}\hbar} - \frac{2\sqrt{6}\ell [m_z(z)]^2 \sqrt{\lambda}}{\sqrt{b}\hbar} \quad (\text{E.9})$$

The zeros (eigen-energies) of equation (E.9) are

$$\lambda_1 = 0, \quad (\text{E.10})$$

$$\lambda_2 = \frac{\ell^2 [m_z(z)]^4 (a(2b+3c) - 2\sqrt{2}\sqrt{ab}\sqrt{c} + bc)}{abc\hbar^2}. \quad (\text{E.11})$$

Since $\text{Real}(\lambda) > 0$, reject λ_1 and accept λ_2 . Therefore, inserting λ_2 into the values for μ, μ_- and using equations (E.10) and (E.11) one arrives at two normalised eigenfunctions. These are given as

$$U_+^1(x, y, z) = e^{-\alpha(x+y+z)} h_+^1(x, y, z), \quad (\text{E.12})$$

$$U_+^2(x, y, z) = e^{\alpha(x+y+z)} h_-^2(x, y, z), \quad (\text{E.13})$$

where

$$h_+^1(x, y, z) = C_+ \left(\tanh(\sqrt{bc}x + \imath\sqrt{3}\sqrt{ac}y - \sqrt{2}\sqrt{ab}z) + \alpha \frac{\sqrt{bc}}{bc} \right) \quad (\text{E.14})$$

$$h_+^2(x, y, z) = C_- \left(\tanh(\sqrt{bc}x + \imath\sqrt{3}\sqrt{ac}y - \sqrt{2}\sqrt{ab}z) - \alpha \frac{\sqrt{bc}}{bc} \right) \quad (\text{E.15})$$

and

$$C_+ = 46424, \quad (\text{E.16})$$

$$C_- = -46424, \quad (\text{E.17})$$

$$\alpha = \frac{\sqrt{2}\ell^2[m_z(z)]^4(a(2b+3c) - 2\sqrt{2}\sqrt{ab}\sqrt{c} + bc)}{a\sqrt{b}\sqrt{c}\hbar^2}. \quad (\text{E.18})$$

Appendix F

Matlab Code

```
function [Eigenvalues,Wavefunctions] = sim1(ElectroP,Evans,DiracFermi)
%Matlab code for solving coupled system of Schroedinger-Poisson equations.
%Schroedinger's equation is solved using an initial guess for the
%electrostatic potential. The implementation procedure requires an initial
%analytical expression for the electrostatic potential phi such that
%Schroedinger equation is reduced to a conventional eigenvalue problem
%which is solved analytically where the wave functions and eigenvalues are
%calculated via Evans function approach. Then electron density is computed
%and calculation of new electrostatic potential via Poisson's equation is
%implemented. The process continues until convergence.

%.....

%Constants for calculations. These can be updated for the required device
%under consideration
```

```

massa =9.1095*10(-31); %mass of an electron (kg)
m_dh = 0.81*massa; %default value;
m_de = 0.36*massa; %density of state mass of conduction band, default value
T=300;%Temperature expressed in K, default is 300K
k_B = 8.62*10(-5);%Boltzmann constant expressed in eV/K
q=1.60217733*10(-19);% electron charge expressed in C
V_h=3.31;%heterjunction step potential, default value used
E_G=1.1;%energy gap default value
E_F=0.0;%equilibrium Fermi level,default value given
E_d=0.044;%donor atom ionization energy of phosphoros, default value given
G_A=4.0;%ground state energy with respect to N_A, default value given
G_d=2.0;%ground state energy with respect to N_D, default value given
E_A=0.048;%acceptor atom energy of boron, default value given
hbar=6.5821189916*10(-16);%Reduced Plank's constant expressed in eV.s
alpha0=1/(k_B*T);
alpha1=(E_F-V_h+E_d)/(k_B*T);
alpha2=-1/(k_B*T);
alpha3=(V_h-E_G+E_A-E_F)/(k_B*T);
alpha4=2*((m_de*k_B*T)/(2*pi*hbar2))(3/2);
alpha5=(E_F-V_h)/(k_B*T);
alpha6=2*((m_dh*k_B*T)/(2*pi*hbar2))(3/2);
alpha7=(V_h-E_G-E_F)/(k_B*T);
m_0=9.1095*10(-31);

%.....

```

```

%.....Coding and simulating Anderson's device.....
%Here it is shown how to determine the loop for simulating layered
%structures which are considered in this work. The Work in Trellakis and
%Abdallah follows the same procedure for simulating the device under
%consideration.

[x,y]= meshgrid(0:10^-9:626.8*10^-9,0:10^-9:626.8*10^-9);

%the loop calculates the dielectric coefficients
eps1 = zeros(length(x), length(y));
for ii = 1:length(x)
    for jj = 1:length(y)
        eps1(ii,jj)=12.61;
        if y(jj)<20*10^-9
            eps1(ii,jj)=12.71;
        elseif y(jj)>=77.6*10^-9 && y(jj)<90.2*10^-9 %
            eps1(ii,jj)=14.11;
        elseif y(jj)>=100.8*10^-9 && y(jj)<116.8*10^-9
            eps1(ii,jj)=14.11;
        end;
    end;
end;

% the loop calculates the N_D doping at different locations
N_D=zeros(length(x),length(y));

```

```

for ii = 1:length(x)
    for jj = 1:length(y)
        N_D(ii,jj)=0;
        if y(jj)>=39.5*10-9 && y(jj)<41.5*10-9
            N_D(ii,jj)=3.5*10(11);
        elseif y(jj)>166.5*10(-9)&& y(jj)<168.5*10-9
            N_D(ii,jj)=0.5*10(11);
        end;
    end;
end;

% the loop calculates the delta background doping in different InP layers
delta_b=zeros(length(x),length(y));
for ii = 1:length(x)
    for jj = 1:length(y)
        delta_b(ii,jj)=0;
        if y(jj)>=20*10-9 && y(jj)<=77.6*10-9;
            delta_b(ii,jj)=3*10(15);
        elseif y(jj)>=90.2*10-9 && y(jj)<=100.8*10-9;
            delta_b(ii,jj)=3*10(15);
        elseif y(jj)>116.8*10-9;
            delta_b(ii,jj)=3*10(15);
        end;
    end;
end;
end;

```

```

% the loop calculates the band offsets used for AlInAs and InGaAs.
delta_c=zeros(length(x),length(y));
for ii = 1:length(x)
    for jj = 1:length(y)
        delta_c(ii,jj)=0;
        if y(jj)>=510*10(-9) && y(jj)<526*10(-9)
            delta_c(ii,jj)=-0.216;%eV
        elseif y(jj)>606.8*10(-9);
            delta_c(ii,jj)=0.252;%eV
        end;
    end;
end;

% the loop calculates the effective mass coefficients
m_star=zeros(length(x),length(y));
for ii=1:length(x)
    for jj=1:length(y)
        m_star(ii,jj)=0.0795*m_0;
        if y(jj)>=510*10(-9) && y(jj)<526*10(-9);
            m_star(ii,jj)=0.043*m_0;
            elseif y(jj)>=536*10(-9) && y(jj)<549.2*10(-9);
                m_star(ii,jj)=0.043*m_0;
            elseif y(jj)>=606.8*10(-9);
                m_star(ii,jj)=0.073*m_0;
        end;
    end;
end;

```

```

        end;
    end;
end;

%the loop calculates the effective mass coefficients
m_star1=zeros(length(x),length(y));
for ii=1:length(x)
    for jj=1:length(y)
        m_star(ii,jj)=1/0.0795*m_0;
        if y(jj)<20*10^-9
            m_star(ii,jj)=1/0.073*m_0;
        elseif y(jj)>=77.6*10^-9 && y(jj)<90.2*10^-9
            m_star(ii,jj)=1/0.043*m_0;
        elseif y(jj)>=100.8*10^-9 && y(jj)<116.8*10^-9
            m_star(ii,jj)=1/0.043*m_0;
        end;
    end;
end;

end;

% this loop calculates the donor concentration
N_A = zeros(length(x),length(y));
for ii = 1:length(x)
    for jj = 1:length(y)
        N_A(ii,jj)=0;

```

```

    end;

end;

%Using an initial analytical expression for electrostatic potential
phi(x,y,z)=hbar^2/(2*q*m(z))^2*d/dz*(m(z)*d/dz(psi)/psi)-lambda/q...
-(lambdal*L^2*m(z)^2)/q;

%L is device length, d/dz is the derivative, m(z) is the effective mass in
%the z-direction and psi is the wave function.
%.

%Next determine Fermi-Dirac approximation using series representations as
%no closed form exists.

function[DiracFermi]=Dirac(x)%x is the electrostatic potential
%which can be a function.
P=(x.^2+pi^2);
Q=(x.^2+9*pi^2);
DiracFermi=-23.51121+2.8356*x+0.05585*x.^2+0.000713*x.^3-0.000022*x.^4+...
(8*pi)^(1/2)*((sqrt(P)-x).^ (1/2)+(sqrt(Q)-x).^ (1/2));
%.

function[ElectroP]=Electro(eps1,N_A,a,b,c,d,e)
m1=(0.19^2/0.98)*9.1095*10^(-34);%kg (a)
m2=(0.19*9.1095*10^(-34));%kg (b)
m3=(0.19*9.1095*10^(-34));%kg (c)
c_1=1/pi*((2*m1*B*T)/hbar^2)^(1/2);

```

```

alph1=-(sqrt(2)*sqrt(m2*m1-sqrt(2)*sqrt(m1*m2)*sqrt(m2*m3)))/2;
alph2=(sqrt(2)*sqrt(m2*m3-sqrt(2)*sqrt(m1*m2)*sqrt(m2*m3)))/2;
alph3=-(sqrt(2)*sqrt(m1*m3-sqrt(2)*sqrt(m1*m2)*sqrt(m1*m3)))/2;
alph4=(sqrt(2)*sqrt(m1*m3-sqrt(2)*sqrt(m1*m2)*sqrt(m1*m3)))/2;
alph5=-(sqrt(2)*sqrt(m1*m2-sqrt(2)*sqrt(m1*m2)*sqrt(m2*m3)))/2;
alph6=(sqrt(2)*sqrt(m1*m2-sqrt(2)*sqrt(m1*m2)*sqrt(m2*m3)))/2;

```

```

F=@(x,z)-q/eps1*tanh(x-sqrt(2)*z).*(c_1*abs(96124*exp(alph1*(x+z))...
.*(tanh(sqrt(m2*m3)*x-sqrt(2)*sqrt(m1*m2).*z-alph1*sqrt(m2*m3)/(m2*m3)))...
.^2.*frenchDirac2((E_F-lambda1)/(B*T))+...
c_1*abs(-96124*exp(alph2*(x+z)).*(tanh(sqrt(m2*m3)*x-sqrt(2)*sqrt(m1*m2)...
.*z-alph2*sqrt(m2*m3)/(m2*m3))))).^2.*frenchDirac2((E_F-lambda1)/(B*T))+...
c_1*abs(50715.1*exp(alph3*(x+z)).*(tanh(sqrt(m1*m3)*x-sqrt(2)*sqrt(m1*m2)...
.*z-alph3*sqrt(m1*m3)/(m1*m3))))).^2.*frenchDirac2((E_F-lambda2)/(B*T))+...
c_1*abs(-50715.1*exp(alph4*(x+z)).*(tanh(sqrt(m1*m3)*x-sqrt(2)*sqrt(m1*m2)...
.*z-alph4*sqrt(m1*m3)/(m1*m3))))).^2.*frenchDirac2((E_F-lambda2)/(B*T))+...
c_1*abs(108620.4*exp(alph5*(x+z)).*(tanh(sqrt(m1*m2)*x-sqrt(2)*sqrt(m2*m3)...
.*z-alph5*sqrt(m1*m2)/(m1*m2))))).^2.*frenchDirac2((E_F-lambda3)/(B*T))+...
c_1*abs(-108620.4*exp(alph6*(x+z)).*(tanh(sqrt(m1*m2)*x-sqrt(2)*sqrt(m2*m3)...
.*z-alph6*sqrt(m1*m2)/(m1*m2))))).^2.*frenchDirac2((E_F-lambda3)/(B*T)));
I=dblquad(F,a,b,a,c);%a,b,e,f in X & c,d in Y. x=0-76 & 264-340, y=19-208

```

```

F1=@(x,z)-q/eps1*tanh(x-sqrt(2)*z).*(c_1*abs(96124*exp(alph1*(x+z))...
.*(tanh(sqrt(m2*m3)*x-sqrt(2)*sqrt(m1*m2).*z-alph1*sqrt(m2*m3)/(m2*m3)))...
.^2.*frenchDirac2((E_F-lambda1)/(B*T))+...

```

```

c_1*abs(-96124*exp(alpha2*(x+z)).*(tanh(sqrt(m2*m3)*x-sqrt(2)*sqrt(m1*m2)...
.*z-alpha2*sqrt(m2*m3)/(m2*m3))))).^2.*frenchDirac2((E_F-lambda1)/(B*T))+...
c_1*abs(50715.1*exp(alpha3*(x+z)).*(tanh(sqrt(m1*m3)*x-sqrt(2)*sqrt(m1*m2)...
.*z-alpha3*sqrt(m1*m3)/(m1*m3))))).^2.*frenchDirac2((E_F-lambda2)/(B*T))+...
c_1*abs(-50715.1*exp(alpha4*(x+z)).*(tanh(sqrt(m1*m3)*x-sqrt(2)*sqrt(m1*m2)...
.*z-alpha4*sqrt(m1*m3)/(m1*m3))))).^2.*frenchDirac2((E_F-lambda2)/(B*T))+...
c_1*abs(108620.4*exp(alpha5*(x+z)).*(tanh(sqrt(m1*m2)*x-sqrt(2)*sqrt(m2*m3)...
.*z-alpha5*sqrt(m1*m2)/(m1*m2))))).^2.*frenchDirac2((E_F-lambda3)/(B*T))+...
c_1*abs(-108620.4*exp(alpha6*(x+z)).*(tanh(sqrt(m1*m2)*x-sqrt(2)*sqrt(m2*m3)...
.*z-alpha6*sqrt(m1*m2)/(m1*m2))))).^2.*frenchDirac2((E_F-lambda3)/(B*T)));
I2=dblquad(F1,b,d,a,c);

```

```

F2=@(x,z)-q/eps1*tanh(x-sqrt(2)*z).*(c_1*abs(96124*exp(alpha1*(x+z))...
.*(tanh(sqrt(m2*m3)*x-sqrt(2)*sqrt(m1*m2).*z-alpha1*sqrt(m2*m3)/(m2*m3))))...
).^2.*frenchDirac2((E_F-lambda1)/(B*T))+...
c_1*abs(-96124*exp(alpha2*(x+z)).*(tanh(sqrt(m2*m3)*x-sqrt(2)*sqrt(m1*m2)...
.*z-alpha2*sqrt(m2*m3)/(m2*m3))))).^2.*frenchDirac2((E_F-lambda1)/(B*T))+...
c_1*abs(50715.1*exp(alpha3*(x+z)).*(tanh(sqrt(m1*m3)*x-sqrt(2)*sqrt(m1*m2)...
.*z-alpha3*sqrt(m1*m3)/(m1*m3))))).^2.*frenchDirac2((E_F-lambda2)/(B*T))+...
c_1*abs(-50715.1*exp(alpha4*(x+z)).*(tanh(sqrt(m1*m3)*x-sqrt(2)*sqrt(m1*m2)...
.*z-alpha4*sqrt(m1*m3)/(m1*m3))))).^2.*frenchDirac2((E_F-lambda2)/(B*T))+...
c_1*abs(108620.4*exp(alpha5*(x+z)).*(tanh(sqrt(m1*m2)*x-sqrt(2)*sqrt(m2*m3)...
.*z-alpha5*sqrt(m1*m2)/(m1*m2))))).^2.*frenchDirac2((E_F-lambda3)/(B*T))+...
c_1*abs(-108620.4*exp(alpha6*(x+z)).*(tanh(sqrt(m1*m2)*x-sqrt(2)*sqrt(m2*m3)...
.*z-alpha6*sqrt(m1*m2)/(m1*m2))))).^2.*frenchDirac2((E_F-lambda3)/(B*T)));

```

```
I3=dblquad(F2,d,e,a,c);
```

```
F3=@(x,z)q/eps1*tanh(x-sqrt(2)*z).*N_A;
```

```
I4=dblquad(F3,a,b,a,c);
```

```
F4=@(x,z)q/eps1*tanh(x-sqrt(2)*z).*N_A;
```

```
I5=dblquad(F4,d,e,a,d);
```

```
ElectroP=I+I2+I3+I4+I5;
```

```
%.....  
%.....Calculating eigenvalues via the Evans function.....  
Evans=[-2/9*(2*mstar(ii,jj)/hbar^2).^5 2/9*(2*mstar(ii,jj)/hbar^2).^4  
(2*mstar(ii,jj)/hbar^2).^3.*(798699*N_A(ii,jj).*(2*mstar(ii,jj)/hbar^2)...  
+10^(24)*(50001*N_D(ii,jj).*(2*mstar(ii,jj)/hbar^2)...  
+39*(2*mstar(ii,jj)/hbar^2).*(65641*eps(ii,jj)+14664)-125000*eps(ii,jj))...  
./(2.25*10^(30)*eps(ii,jj)) -(2*mstar(ii,jj)/hbar^2).^2.*(266233*N_A(ii,jj)...  
.*(2*mstar(ii,jj)/hbar^2)+10^(24)*(166667*N_D(ii,jj).*(2*mstar(ii,jj)/hbar^2)...  
+13*(2*mstar(ii,jj)/hbar^2).*(65641*eps(ii,jj)+14664)+10^6*eps(ii,jj))...  
./(1.5*10^(30)*eps(ii,jj)) -(2*mstar(ii,jj)/hbar^2).*(212640030867*N_A(ii,jj).^2...  
.*(2*mstar(ii,jj)/hbar^2).^2+(1.597398*10^(30))*N_A(ii,jj).*(2*mstar(ii,jj)/hbar...  
.*(166667*N_D(ii,jj)+13*(65641*eps(ii,jj)+14664))...  
+10^(48)*(83333666667*N_D(ii,jj).^2.*(2*mstar(ii,jj)/hbar^2).^2+13000026*N_D(ii...  
.*(2*mstar(ii,jj)/hbar^2).^2.*(65641*eps(ii,jj)+14664)+507*(2*mstar(ii,jj)/hbar...  
.*(65641*eps(ii,jj)+14664).^2-(5*10^(11))*eps(ii,jj).^2))...]
```

```

./(1.5*10^(60)*eps(ii,jj).^2) (2*mstar(ii,jj)/hbar^2).*(266233*N_A(ii,jj)...
+10^(24)*(166667*N_D(ii,jj)+13*(65641*eps(ii,jj)+14664)))./(5*10^(29)*eps(ii,jj)
format long
for n=length(Evans)-1;
A = diag(ones(n-1,1),-1);
A(1,:)=-Evans(2:n+1)./Evans(1);
end;
f=[-0.177212109;-0.25561201;0.25341210;0.30471234;1.26882121];%normalisation
%constants
Ladder1 = 1000*f.*eig(A);
u =(0.4:.1:.8);

plot(u,Ladder1,'-*'),xlabel('gate voltage [v]'),ylabel('Energy(meV)'),...
title('Eigenvalue-ladder1 vs Gate voltage');

```